5-27-1955

A Shock Tube for Transonic and Supersonic Aerodynamic Research

John Hopkins Atkinson

A

SHOCK

TUBE

ATKINSON

A SHOCK TUBE FOR TRANSONIC AND SUPERSONIC AERODYNAMIC RESEARCH

A Thesis

Presented to

the Faculty of the College of Engineering

The University of New Mexico

In Partial Fulfillment

of the Requirements for the Degree

Master of Science in Mechanical Engineering

---

by

John Hopkins Atkinson

June 1955

This thesis, directed and approved by the candidate's committee, has been accepted by the Graduate Committee of the University of New Mexico in partial fulfillment of the requirements for the degree of

MASTER OF SCIENCE

E. A. Castetter
DEAN

5/27/1955
DATE

Thesis committee

A. D. Ford
CHAIRMAN

Edward C. Rightley

Victor J. Hoglund

TABLE OF CONTENTS

TABLE OF CONTENTS

CHAPTER PAGE

LIST OF TABLES

LIST OF TABLES

LIST OF FIGURES

FIGURE PAGE

FIGURES

FIGURE PAGE

FIGURE PAGE

FIGURE PAGE

CHAPTER I

INTRODUCTION TO THE PROBLEM

The shock tube as known today consists essentially of a constant cross section tube divided into two chambers by a breakable membrane. The chambers may be filled with like or different gases at various pressures. It was first used by Vielle[1] in France in 1899 about the time the first wind tunnels appeared. Vielle's shock tube consisted of a tube 22 mm. in diameter and 20 feet long which he filled with air to a pressure of about 400 psi. Vielle measured shock velocities up to about twice the velocity of sound. In spite of his success with these experiments the method was completely abandoned until about 1940.

Little was done toward the study of pressure waves released by a bursting diaphragm until Payman and Shepherd[2] conducted a series of experiments to study the air flow following the bursting of a diaphragm in a shock tube. They used copper-foil diaphragms to sustain high air pressures in the compression chamber of the tube.

---

[1] W. Payman and W. C. F. Sheppard, "Explosion and Shock Waves, VI, The Disturbance Produced by Bursting Diaphragms with Compressed Air," Proceedings Royal Society, Series A, 186:294, 1946.

[2] Ibid., p. 293.

In 1943 Reynolds[3] used the shock tube to produce shock waves of known strength for the calibration of piezo-electric pressure gages which were to be used in blast wave measurements.

In 1943 Smith[4] made an extensive study of the reflection of shock waves, in which the shock waves were allowed to strike an inclined plate. His purpose was to study the conditions for the onset of Mach reflection.

Since 1950, both in the United States and Canada, interest has increased in the use of the shock tube as an aerodynamic wind tunnel.[5]

Bleakney[6] and his co-workers are continuing the study of Mach reflection, using a shock tube equipped with a Mach-Zehender interferometer.

Previous studies have been made of the shock wave following the breaking of a diaphragm in a shock tube. This paper is concerned with an investigation of the transonic flow following the shock wave and contact surface rather than with the shock wave itself, with the

---

[3] J. Lukasiewicz, "Shock Tube Theory and Applications," National Aeronautical Establishment, Canada, Report 15, 1952, p. 7.

[4] Ibid., p. 7.

[5] Ibid., p. 7.

[6] Walker Bleakney, D. K. Weimer, and C. H. Fletcher, "Shock Tube: A Facility for Investigations of Fluid Dynamics," Review of Scientific Instruments, 20:807, 1949.

purpose in view that the shock tube might be used as an intermittent wind tunnel in the mechanical engineering laboratory.

A study of shock tube theory indicates that the shock tube as an intermittent wind tunnel has both advantages and disadvantages when compared to the standard wind tunnel. The principal advantage is the ease in producing various flow Mach numbers by setting the pressure ratio of the chambers for the desired Mach number flow within the range available. A second advantage is the fact that the flow at any particular station in the shock tube starts instantaneously. Thus, steady flow patterns may be studied in the process of formation. Principal disadvantages are the difficulty of measuring forces and torques on models, the lack of time for establishment of a desired flow in some cases, and the limit of the Mach number flow to a value less than 1.89 following the primary shock wave.

Purpose of the study. The purpose of building a shock tube was to give the University another research tool and demonstration instrument for aerodynamic studies since the present wind tunnel is not suitable for high velocity research. It was hoped that the shock tube might, when calibrated against theoretical flow data,

prove suitable as a test facility. To determine its usefulness as such a facility it was necessary to devise a method for measuring local velocities, investigate size effects of models in the flow and provide a check against standard wind tunnel data. The shock tube was to be built as simply and cheaply as possible.

Shock tube flow consists of a steady flow period following the primary shock wave developed at the bursting of the diaphragm, and a second steady flow period following passage of the discontinuity or contact surface between the high and low pressure gases. Preliminary investigation indicated that it might be possible to measure, by the use of wedges and airfoils, the flow in the cold gas following the contact surface. After the diaphragm is broken this region moves toward the low pressure end of the shock tube followed by a period of steady flow. The duration of steady flow is dependent on the shock tube length, the pressure ratio of the two gases, and the location of the test stations.

In this study the high pressure section of the shock tube is referred to as the chamber, and the low pressure section as the channel. Using air as the gas in both the chamber and the channel, and pressure ratios up to 60, it was considered likely that flow Mach numbers of

1.5 to 2.0 could be measured in the channel section.

Shock tube theory predicts a region of steady flow preceding the passage of the contact surface. This flow region follows the primary shock wave developed when the diaphragm is broken. A greater pressure ratio is necessary here for a given Mach number than in the flow following the contact surface, and there is a much shorter period of steady flow. The upper limit in Mach number is 1.89. Using air as the gas in both the chamber and channel, it appeared feasible to obtain flow Mach numbers up to 1.20 with a pressure ratio of 150.

After a workable shock tube is accomplished it is necessary to calibrate it for use as a test facility. Rather than go to the expense of an electronic method of calibration of the flow velocity between two points in the channel, which would only indicate the velocity of the passage of the primary shock wave, plans were made to measure the angle of the bow wave on a wedge from shadowgraph pictures. This meant that only supersonic flows could be measured. It was felt, however, that if these measured flows were consistent the curve could be extrapolated into the region below Mach 1.00.

It also appeared feasible to measure the Mach wavelet angle at striations on a wedge, if sufficient density were available, as a check against this bow wave

measurement. If the striation angles were visible it would be possible to measure local velocity on an airfoil or other object in the flow stream.

Wedges of different cross sectional areas might also be installed in the test section of the tube in order to observe the effect on the air flow.

Following the cailbration of the shock tube with measured velocities plotted against the pressure ratio, a standard NACA airfoil for which wind tunnel information was available might then be installed in the shock tube and the critical Mach number determined.

CHAPTER II

THE THEORY OF THE IDEAL SHOCK TUBE

Shock tube notation. Figure 1 illustrates schematically the shock tube after the diaphragm has been broken. It shows the tube of uniform cross section, closed at one end, this a gas-tight diaphragm and indicates the pressures, velocities and speed of sound expected in each part of the shock tube.

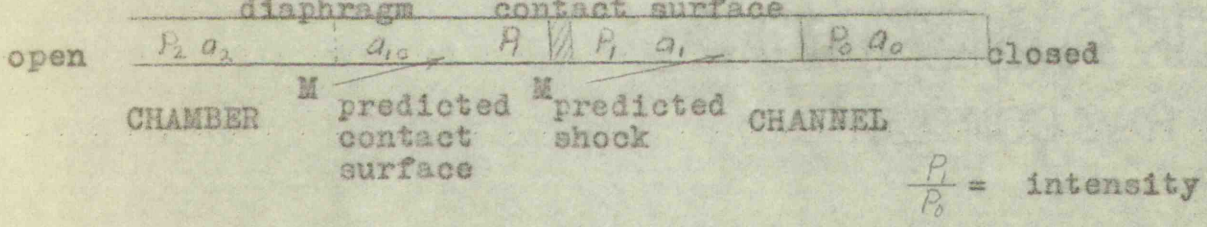

Figure 1. Shock Tube after the Diaphragm has been Ruptured

P_0- gas pressure in the low pressure region of the shock tube

P_1- gas pressure following the primary shock wave

P_2- gas pressure in the chamber or high pressure region of the shock tube after rupture of the diaphragm (Atmospheric pressure for all tests in this paper)

a_0- velocity of sound in the stationary gas

a_1- velocity of sound in the gas following the primary shock wave

a_{1c}- velocity of sound in the gas following the contact surface

a_2- velocity of sound in the high pressure air before the diaphragm is ruptured

U- velocity of propagation of the primary shock wave

Contact surface - The contact surface is the region of mixing gases at the diaphragm that moves down the channel following rupture of the diaphragm. The density and consequently the temperature is different although the pressure remains the same in this region. The gases following the passage of this contact surface are cooled.

The process following the rupture of the diaphragm.

In analyzing the process following the rupture of the diaphragm, the assumptions are made that the diaphragm is a plane barrier which disappears instantaneously, and that the gases in the chamber and channel obey the ideal gas laws.

When the diaphragm is suddenly broken a shock wave is formed in the channel, or low pressure portion of the tube, advancing along the tube away from the diaphragm. The shock wave is eventually reflected from the closed end of the tube. The breaking of the diaphragm also causes a rarefaction wave to be formed in the high pressure section of the tube, and moves back in the high pressure gas until it is reflected at the end of the compression chamber. The sequence of events may be shown

in the following way:[1]

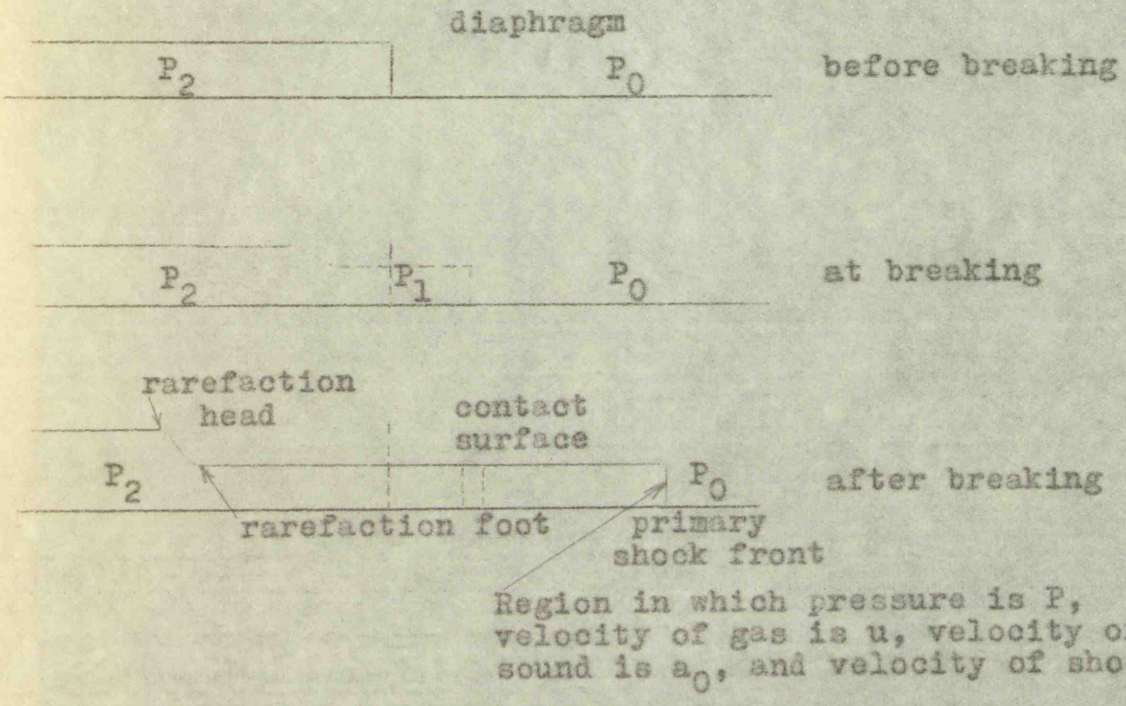

Figure 2. Development of Flows following the breaking of the Diaphragm

From the Rankine-Hugoniot equations we have the relationship between the particle velocity following the shock front and the pressure ratio $\frac{P_1}{P_0}$ at the shock front. This is:

$$\frac{u^2}{a_0^2} = \frac{2}{\gamma} \frac{(\gamma-1)^2}{\gamma-1+(\gamma+1)\gamma} \qquad \text{(II - 1)}$$

where $\gamma = \frac{P_1}{P_0}$, $a_0 = \sqrt{\frac{\gamma P_0}{\rho_0}}$ and u = particle velocity following the shock front.

---

[1] C. W. Lampson, "Resume' of the Theory of Plane Shock and Adiabatic Waves with Applications to the Theory of the Shock Tube," Ballistics Research Laboratory, Technical Note, No. 139:26-29, Aberdeen, Maryland, 1950.

The high pressure region in the chamber behind the diaphragm is propagating a rarefaction wave because of the relief of pressure by the bursting of the diaphragm. The velocity of the particles in the rarefaction wave where the pressure is P is given by

$$u = \pm \int_{\rho}^{\rho_c} \sqrt{\frac{dP}{d\rho}}\, \frac{d\rho}{\rho} \qquad u = \pm \frac{2}{\gamma - 1} a_2 \left[1 - \left(\frac{P_1}{P_2} \right)^{\frac{\gamma - 1}{2\gamma}} \right]$$

where P_2 is the pressure of the region into which the wave advances and a_2 is the velocity of sound in this region.

Now $$P = P_0 \frac{P}{P_0} = P_0 \gamma$$

so the equation becomes

$$u = \pm \frac{2}{\gamma - 1} a_2 \left[1 - \left(\gamma \frac{P_0}{P_2} \right)^{\frac{\gamma - 1}{2\gamma}} \right] \qquad \text{(II - 2)}$$

These two particle velocities must be equal at the diaphragm after breaking; otherwise a local region of vacuum or high pressure will develop in time. The area and particle velocity is the same on each side of the diaphragm but the density of the gases is different causing a discontinuity in both temperature and density but holding the same pressure. So, equating the two particle velocities we have

$$\frac{2 a_0^2 (\gamma - 1)^2}{\gamma [\gamma - 1 + (\gamma + 1)\gamma]} = \frac{4 a_1}{(\gamma - 1)^2} \left[1 - \left(\gamma \frac{P_0}{P_2} \right)^{\frac{\gamma - 1}{2\gamma}} \right]^2$$

Assume $a_0 = a_2$ which means that sufficient time must elapse after adjusting the chamber pressures for the temperature to equalize. Taking the square root of each side of the above equation we have

$$\frac{\sqrt{2}(y-1)}{\sqrt{\gamma\,[\gamma-1+(\gamma+1)y]}} = \frac{2}{\gamma-1}\left[1-\left(y\,\frac{P_0}{P_2}\right)^{\frac{\gamma-1}{2\gamma}}\right] \qquad \text{(II - 3)}$$

Assume $\gamma = 1.4$, then

$$\frac{y-1}{\sqrt{7(1+6y)}} = 1-\left(y\,\frac{P_0}{P_2}\right)^{\frac{1}{7}} \qquad \text{(II - 4)}$$

or $$\frac{P_2}{P_0} = \frac{y}{\left[1-\frac{y-1}{\sqrt{7(1+6y)}}\right]^7}$$

This equation then gives the ratio of pressures in the chamber and channel, before the diaphragm is broken, necessary to establish a shock wave of pressure P traveling down the tube. This relationship is plotted in Figure 3. See Table I.

The pressure distribution in the tube following the breaking of the diaphragm is indicated in Figure 4. The rarefaction has a head pressure or leading point at the chamber pressure while the foot of the rarefaction is at the primary shock pressure of P . Figure 4 shows the rarefaction both as to pressure and position with R as the head, and F as the foot. The foot of the rarefaction moves into the chamber with the speed of sound a_2 .

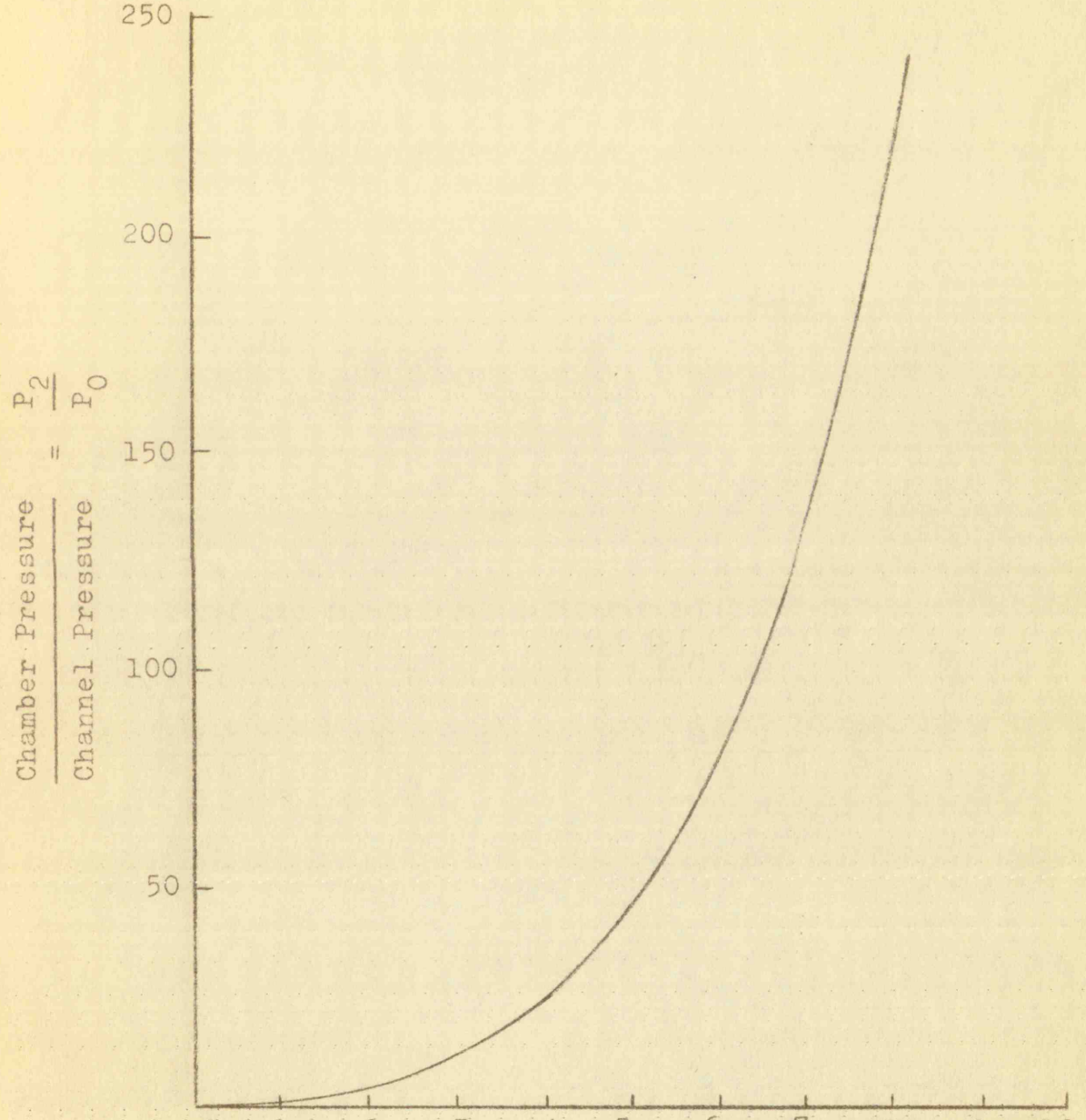

FIGURE 3

EFFECT OF PRESSURE RATIO ON SHOCK STRENGTH

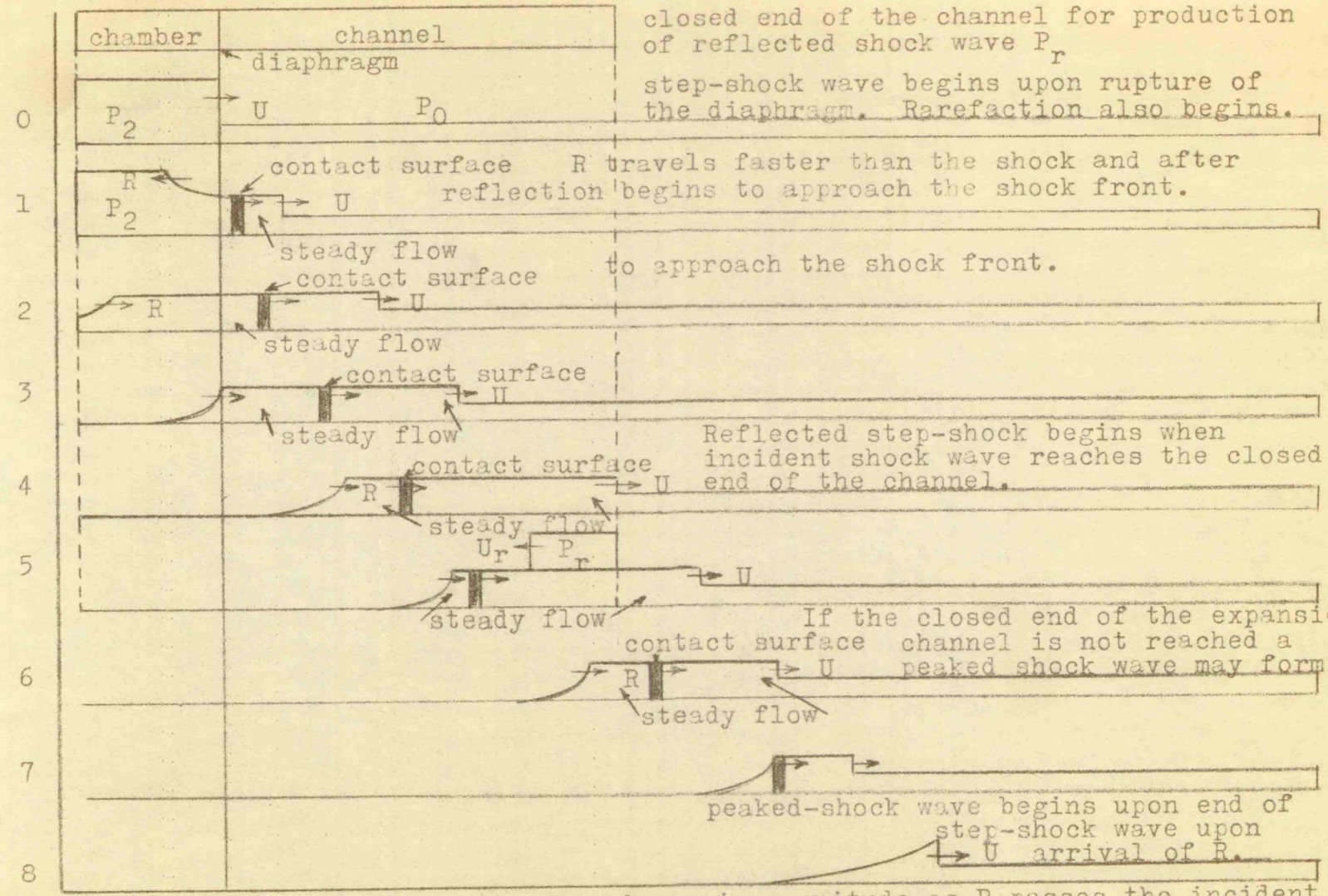

FIGURE 4

PRESSURE PHENOMENA IN THE SHOCK TUBE

The region between the foot of the rarefaction and the contact surface is also one of uniform flow.

The critical pressure of the gas determines whether the flow will be supersonic, sonic, or subsonic.[2] This is determined from

$$P_{CR} = P_2 \left(\frac{2}{\gamma+1}\right)^{\frac{2\gamma}{\gamma-1}} \qquad \text{(II - 5)}$$

where $\gamma = 1.4$ for air $P_{CR} = P_2 \times \left(\frac{2}{2.4}\right)^7 = P_2 \times 0.279$

if $P_2 = 25''Hg$ then $P_{CR} = 6.98''Hg.$

From this then the foot of the rarefaction may move upstream, remain stationary, or move downstream, depending upon whether the pressure is greater than, equal to, or less than the critical pressure.

Figure 5a shows the pressure distribution when the pressure is less than the critical and Figure 5b when the pressure is greater than the critical pressure. In Figures 5c and 5d, the movements of the rarefaction, contact surface, and shock wave are shown.

---

[2] F. W. Geiger and C. W. Mautz, "The Shock Tube as an Instrument for the Investigation of Transonic and Supersonic Flow Patterns," Engineering Research Institute University of Michigan, Ann Arbor, June, 1949, pp. 15-17.

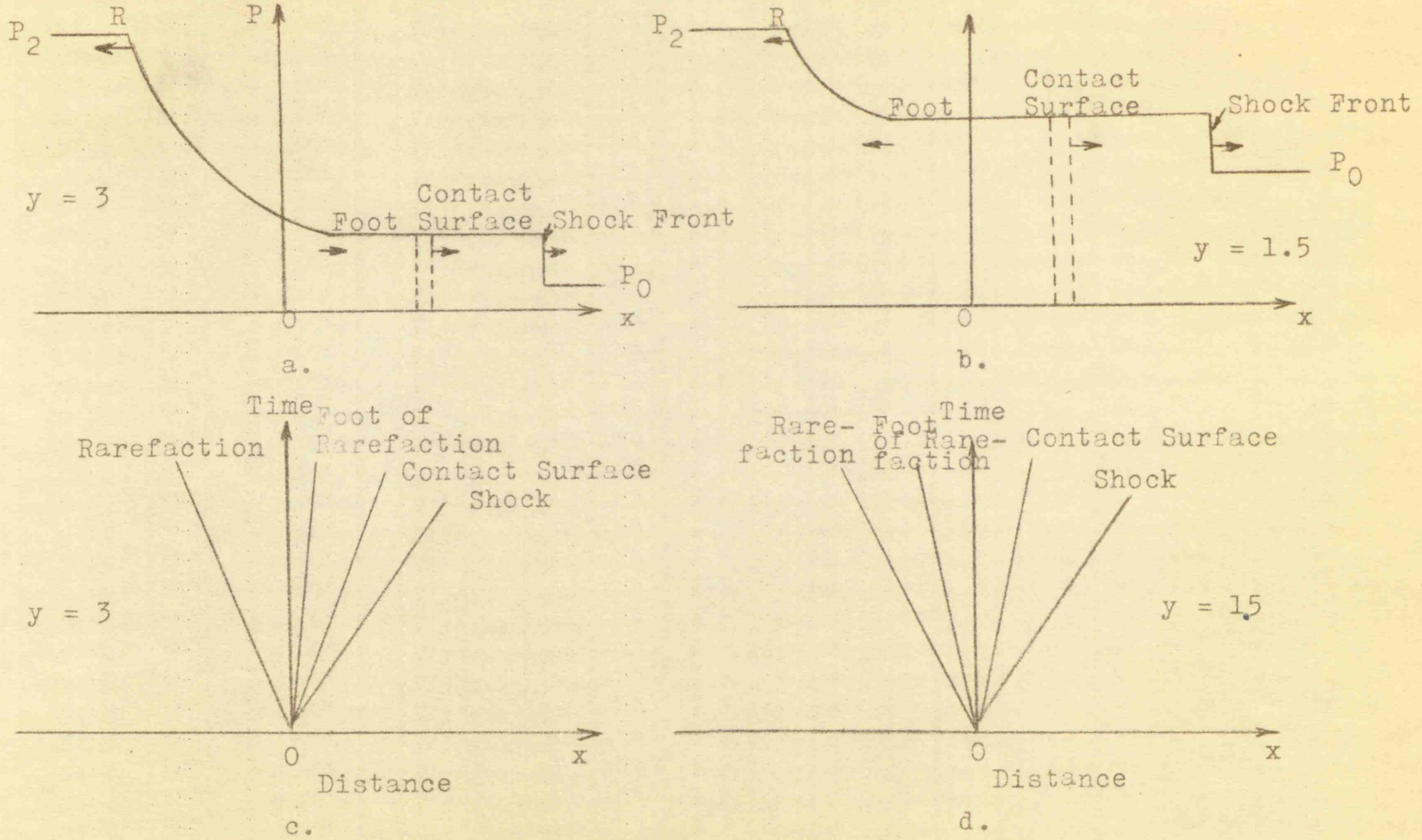

FIGURE 5

FLOW PRODUCED BY BURSTING DIAPHRAGM

Figure 6 shows, through a double exposure, the complete flow in the shock tube. The air flows over a 3-degree steel wedge and the primary shock wave may be seen about one third of the way down the wedge from the leading edge. A detached bow wave may also be seen about one-eighth inch in front of the leading edge of the wedge. The detached wave is caused by the flow Mach number being just under the speed of sound 0.98. From the second exposure an attached shock wave may be seen at the leading edge of the wedge. The measured Mach flow was 1.3. The second exposure was taken in the flow region following the contact surface. The wake and expansion waves at the corners are due to be flow following the contact surface also.

The flow field produced by a plane shock. The pressures, P_0 and P_1, and the corresponding flow speeds, V_0 and V_1, on either side of the shock wave are related by the Rankine-Hugoniot relation

$$\frac{V_0}{V_1} = \frac{\frac{\gamma+1}{\gamma-1} + \frac{P_0}{P_1}}{1 + \left(\frac{\gamma+1}{\gamma-1}\right)\left(\frac{P_0}{P_1}\right)} \qquad \text{(II - 6)}$$

where V_0 and V_1 are measured with respect to the shock front, and γ is the ratio of the specific heats of the gas. In the case of the shock wave proceeding into a stationary gas a transformation of the equation gives

Figure 6 shows, through a double exposure, the complete flow in the shock tube. The air flows over a 3-degree steel wedge and the primary shock wave may be seen about one third of the way down the wedge from the leading edge. A detached bow wave may also be seen about one-eighth inch in front of the leading edge of the wedge. The detached wave is caused by the flow Mach number being just under the speed of sound 0.95. From the second exposure an attached shock wave may be seen at the leading edge of the wedge. The measured Mach flow was 1.5. The second exposure was taken in the flow region following the contact surface. The wake and expansion waves at the corners are due to be flow following the contact surface also.

The flow field produced by a plane shock. The pressures, P_0 and P_1, and the corresponding flow speeds, V_0 and V_1, on either side of the shock wave are related by the Rankine-Hugoniot relation

$$\frac{V_0}{V_1} = \frac{\frac{\gamma+1}{\gamma-1} + \frac{P_0}{P_1}}{1 + \left(\frac{\gamma+1}{\gamma-1}\right)\left(\frac{P_0}{P_1}\right)} \qquad (II - 6)$$

where V_0 and V_1 are measured with respect to the shock front, and γ is the ratio of the specific heats of the gas. In the case of the shock wave proceeding into a stationary gas a transformation of the equation gives

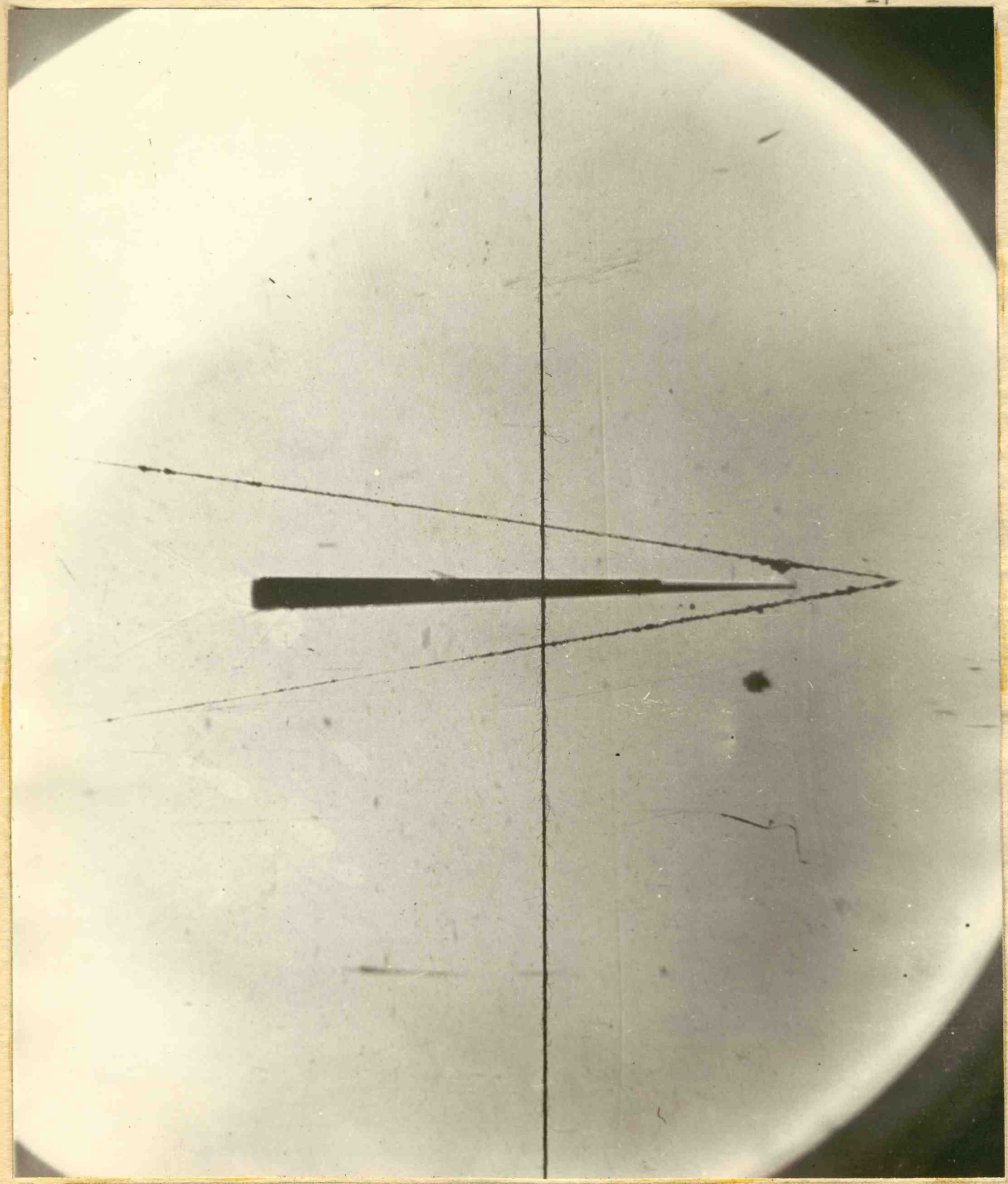

FIGURE 6

DOUBLE EXPOSURE M_{PS} 0.98, M_{PC} 1.3

FIGURE 6

DOUBLE EXPOSURE M_{PS} 0.78, M_{PO} 1.5

of the equation gives

$$\frac{U}{U-u} = \frac{\frac{\gamma+1}{\gamma-1} + \frac{P_0}{P_1}}{1 + \left(\frac{\gamma+1}{\gamma-1}\right)\left(\frac{P_0}{P_1}\right)} \qquad \text{(II - 7)}$$

where P_0 is the pressure in the stationary medium, and P_1 is the pressure behind the shock wave. Adopting the notation

$$y = \frac{P_1}{P_0} \quad 0 < y < \infty; \quad \nu = \frac{\gamma+1}{\gamma-1};$$

the equation becomes

$$\frac{U}{U-u} \qquad \frac{\nu + \frac{1}{y}}{1 + \frac{\nu}{y}} \qquad \text{(II - 8)}$$

The relation between the shock speed, U, and the pressure ratio y, is (Appendix A, III - 5)

$$U = a_0 \sqrt{\frac{6y+1}{7}} \qquad \text{(II - 9)}$$

The calculated data is shown in Table II and a plot of data may be seen in Figure 7.

Equations (II - 8) and II - 9) and the expression for the ratio of the sound speeds a_0 and a_1 are combined in Appendix IV to give

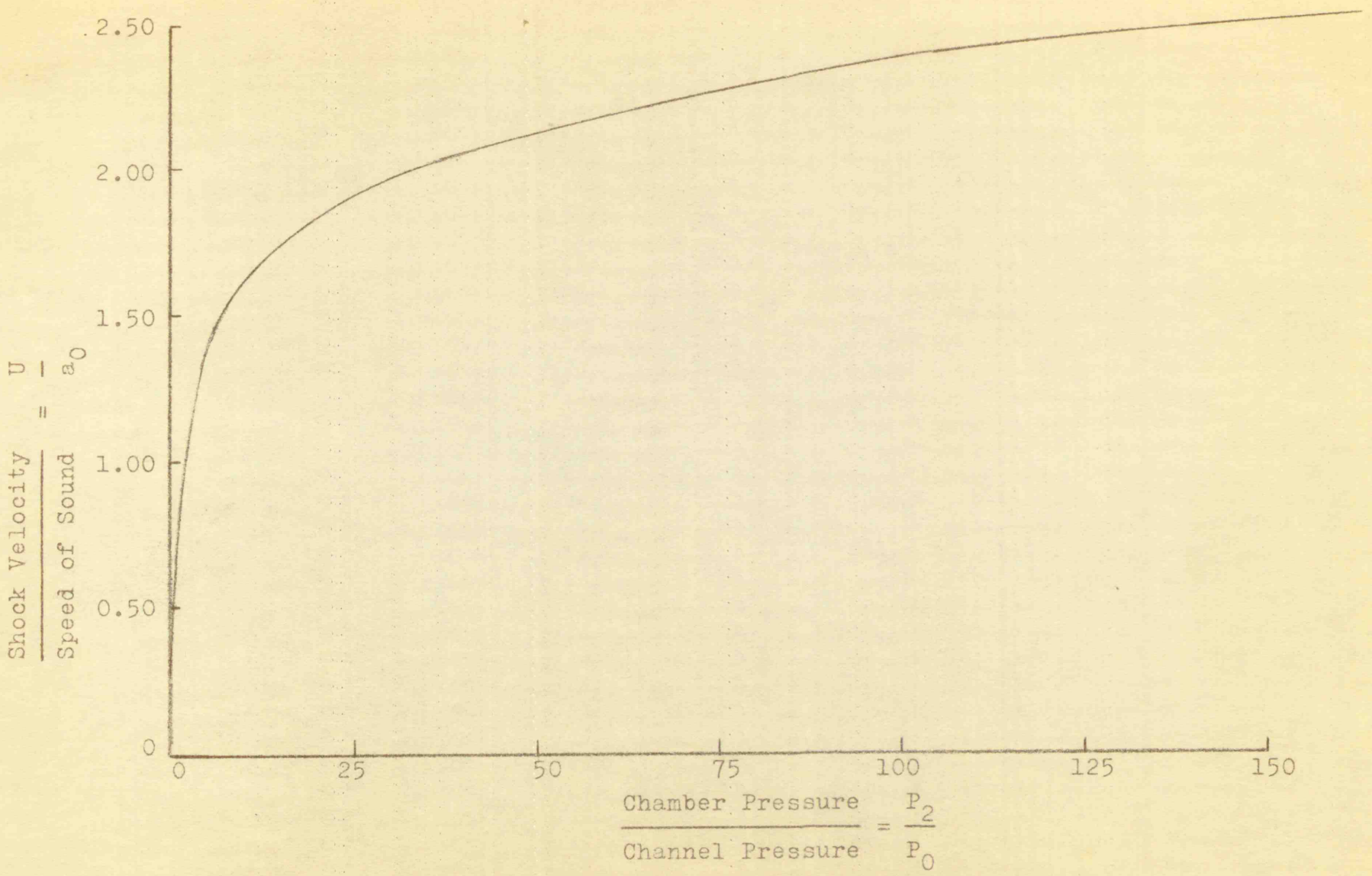

FIGURE 7

COMPARISON OF PRIMARY SHOCK VELOCITY TO
SHOCK TUBE PRESSURE RATIO

$$M_{PS} = \frac{U}{a_o} = \frac{2(\gamma-1)}{\sqrt{2\gamma\gamma[\gamma(\gamma-1)+\gamma+1]}} \qquad \text{(II - 10)}$$

where M_{PS} is the Mach number of the flow. If the ratio of the specific heats is taken as 1.4 which is very nearly true for air, equation (II - 10) becomes

$$M_{PS} = \frac{5(\gamma-1)}{\sqrt{7\gamma(\gamma+6)}} \qquad \text{(II - 11)}$$

The data has been calculated for Table III and a plot of the data may be seen in Figure 8.

The flow following the contact surface has a Mach number controlled by the speed of sound in the cooled gas. The derivation may be found in Appendix V.

$$M_{PC} = \frac{U}{a_{1C}} = \frac{\frac{2}{\gamma-1}(\gamma-1)}{\sqrt{\frac{2\gamma}{\gamma-1}[\gamma(\gamma+1)+1]-(\gamma-1)}} \qquad \text{(II - 12)}$$

where M_{PC} is the Mach number of the flow. If the ratio of the specific heats is taken as 1.4 for air (II - 12) becomes

$$M_{PC} = \frac{5(\gamma-1)}{\sqrt{7(6\gamma+1)}-(\gamma-1)} \qquad \text{(II - 13)}$$

The data has been calculated for Table IV and a plot of

CORRELATION OF MEASURED MACH FLOW TO PREDICTED MACH FLOW
FOLLOWING THE PRIMARY SHOCK FRONT

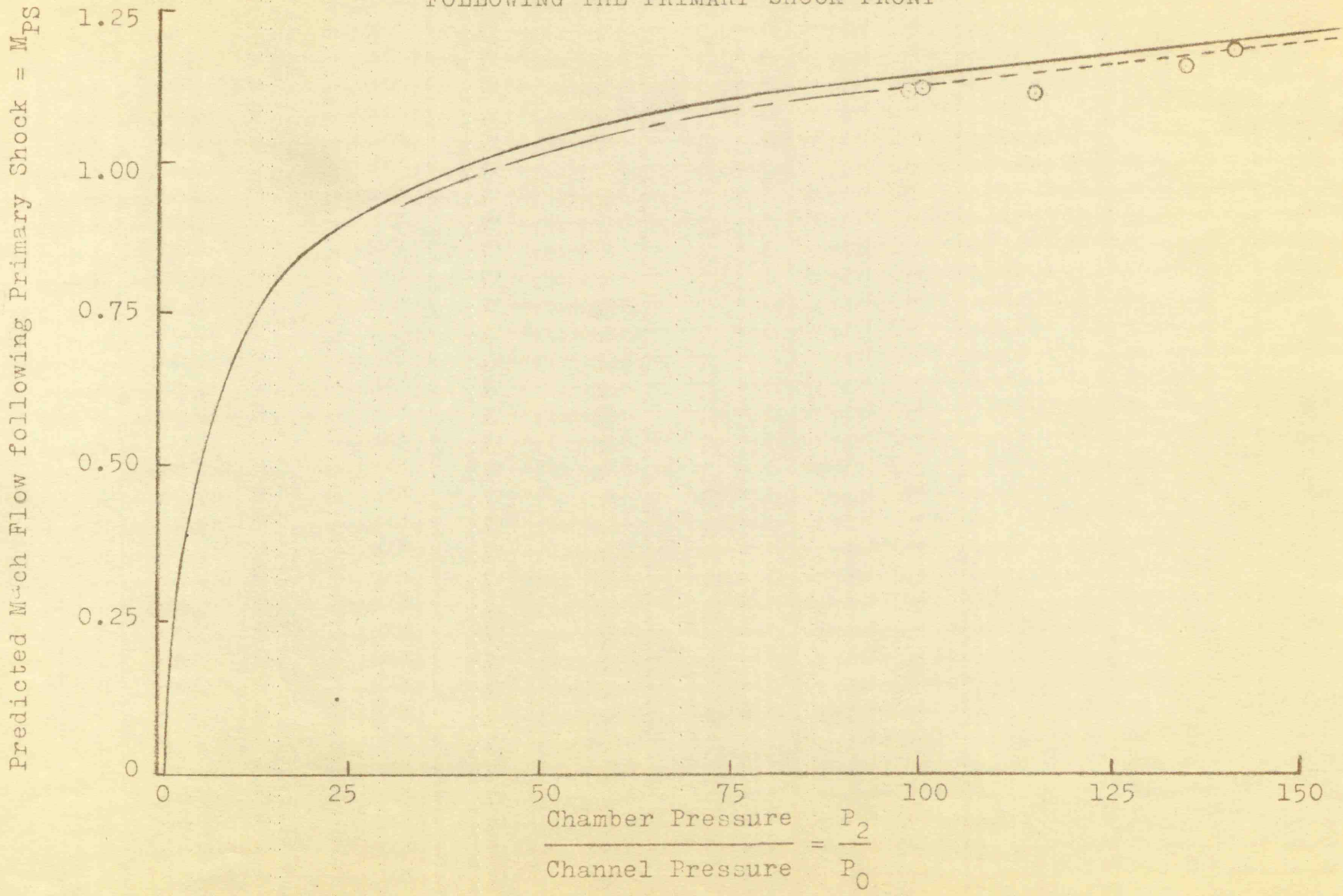

FIGURE 8

the data may be seen in Figure 9.

Reflections at the ends of the shock tube. C. W. Lampson[3] shows that if a shock wave of pressure ratio γ is reflected from a rigid wall, the pressure ratio γ_r of the reflected shock is given by

$$\gamma_r = \frac{\gamma\rho + 2\gamma - 1}{\gamma + \rho} \qquad \text{(II - 14)}$$

The velocity, U_r, of this shock wave with respect to the wall, in this case the end of the channel, is given by

$$U_r = a_o \frac{(2\gamma + \rho - 1)}{\sqrt{(\rho + 1)(\rho\gamma + 1)}} \qquad \text{(II - 15)}$$

where a_o is the sound speed in the undisturbed gas. For air, with $\rho = 6$ equation (II - 15) becomes

$$U_r = a_o \frac{2\gamma + 5}{\sqrt{7(6\gamma + 1)}} \qquad \text{(II - 16)}$$

---

[3] Lampson, op. cit., pp. 24-26.

CORRELATION OF MEASURED MACH FLOW TO PREDICTED MACH FLOW FOLLOWING THE CONTACT SURFACE

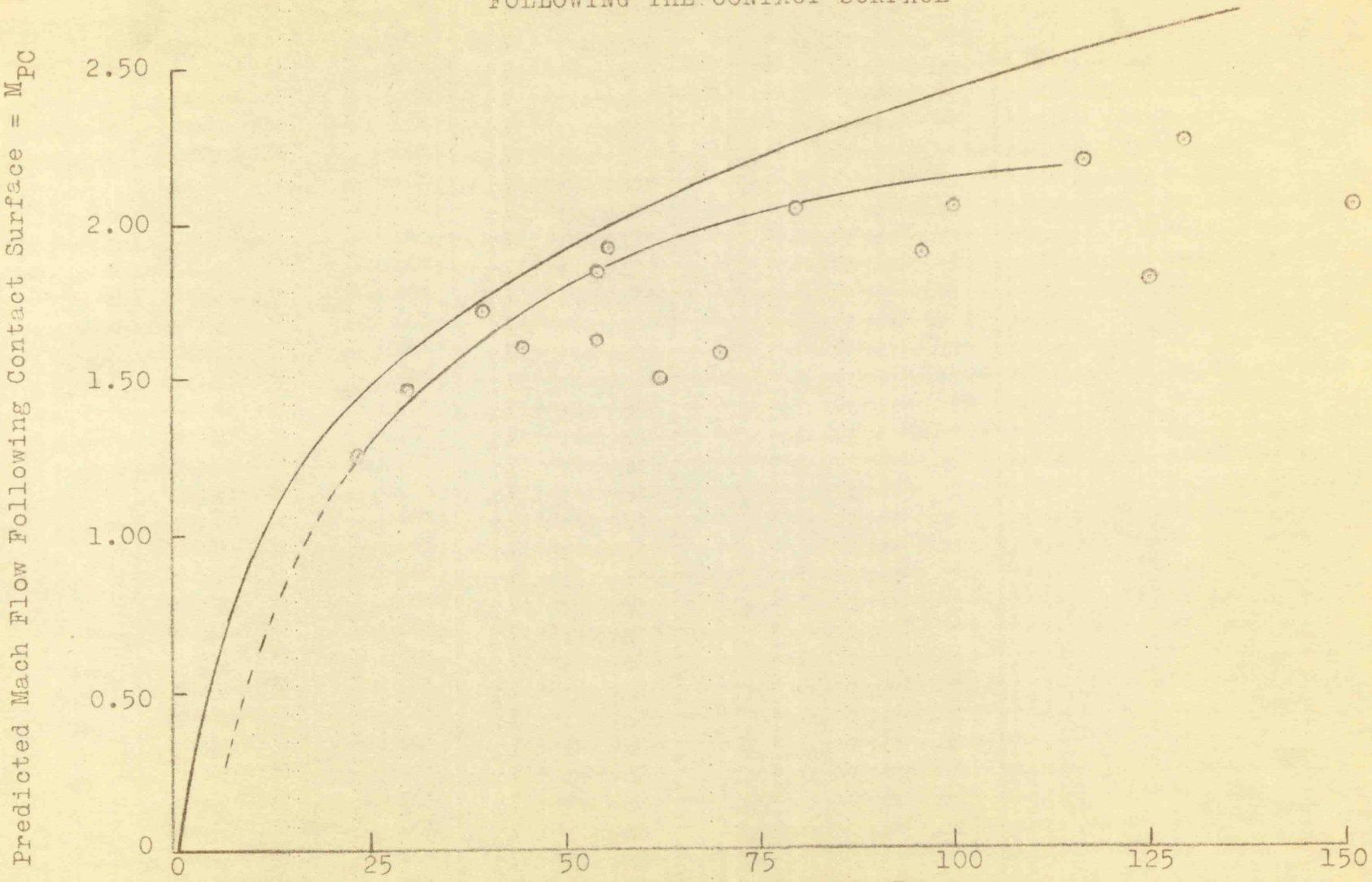

FIGURE 9

CHAPTER III

DESIGN AND CONSTRUCTION OF THE APPARATUS

The apparatus, see Figure 10, required for this study consisted essentially of (1) a tube divided into two parts consisting of a high pressure chamber and low pressure channel; (2) vacuum pumps for obtaining the necessary pressure differentials between these parts; (3) devices for measuring these pressure differences including a barometer, mercurial manometer, and a thermometer; (4) a diaphragm for maintaining these pressure differences; (5) a device for breaking the diaphragm to initiate the flow of gases into the channel; (6) the photographic apparatus for recording this flow; (7) the synchronizing mechanism for triggering the light source.

The tube. A wooden tube was first constructed out of one inch plywood, with 2 x 8 inch inside dimensions and adjustable up to 24 feet in length. This proved unsatisfactory since the leakage was excessive through the wood which resulted in inaccurate pressure readings.

A rectangular steel tube of 4 foot flanged sections was then made of 7 inch standard steel channel with a 1/4 inch steel plate welded over the open side. This tube

CHAPTER III

DESIGN AND CONSTRUCTION OF THE APPARATUS

The apparatus, see Figure 10, required for this study consisted essentially of (1) a tube divided into two parts consisting of a high pressure chamber and low pressure channel; (2) vacuum pumps for obtaining the necessary pressure differentials between these parts; (3) devices for measuring these pressure differences including a barometer, mercurial manometer, and a thermometer; (4) a diaphragm for maintaining these pressure differences; (5) a device for bursting the diaphragm to initiate the flow of gases into the channel; (6) the photographic apparatus for recording this flow; (7) the synchronizing mechanism for triggering the light source.

The tube. A wooden tube was first constructed out of one inch plywood, with 2 x 8 inch inside dimensions and adjustable up to 24 feet in length. This proved unsatisfactory since the leakage was excessive through the wood which resulted in inaccurate pressure readings.

A rectangular steel tube of 4 foot flanged sections was then made of 7 inch standard steel channel with a 1/4 inch steel plate welded over the open side. This tube

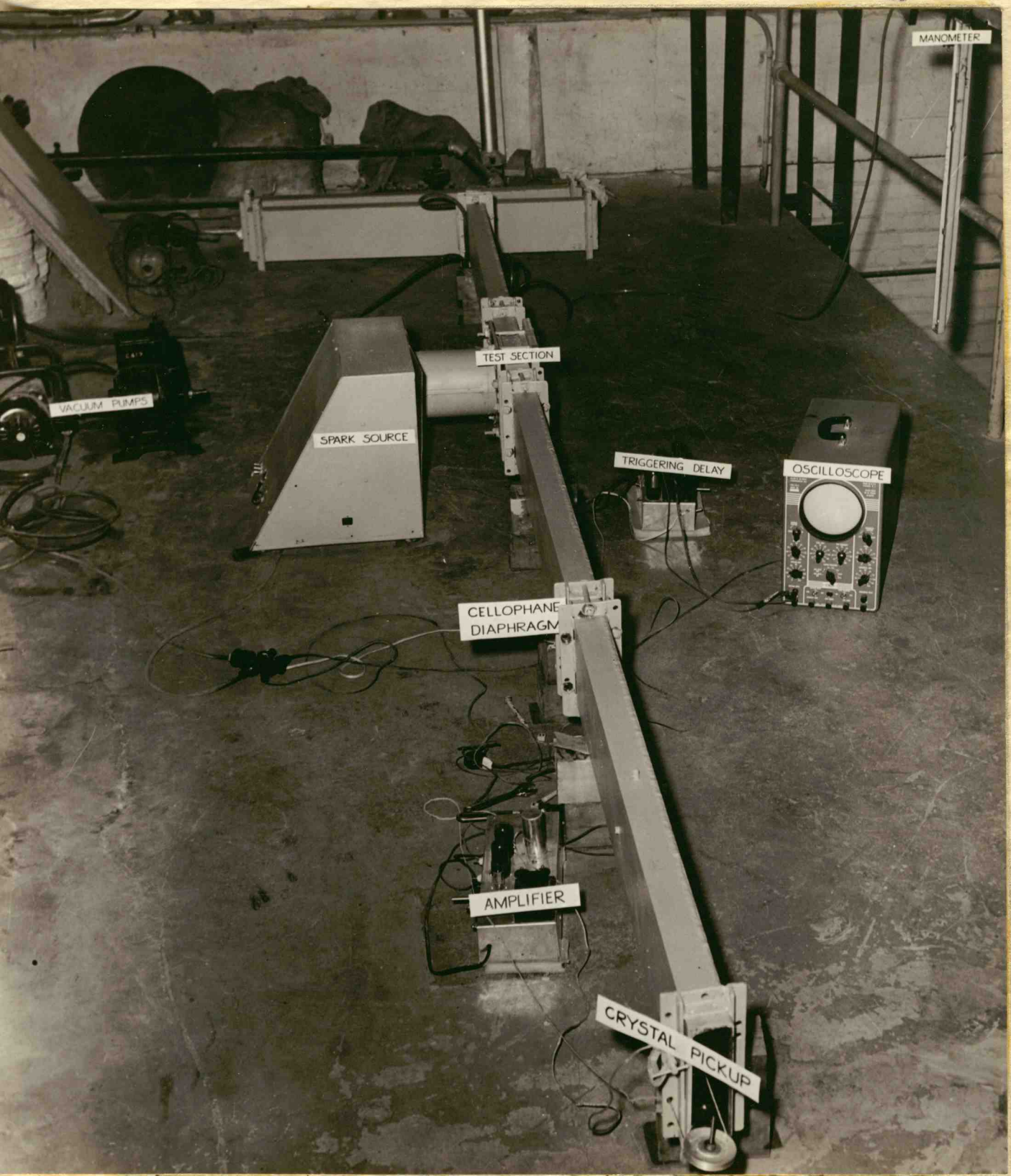

FIGURE 10

THE EXPERIMENTAL APPARATUS

2

4c-19

7-19 - 4

was adjustable in length up to 22 feet. The channel region of the tube included a two-foot test section at which point data was recorded. Two extra four-foot sections were available for use if needed. The vacuum seal at the section junctions was obtained by installing a 1/16 inch Victorite gasket packing greased with cup grease. The sections were fastened together with six 3/8 inch bolts, two on each side and one each on the top and bottom.

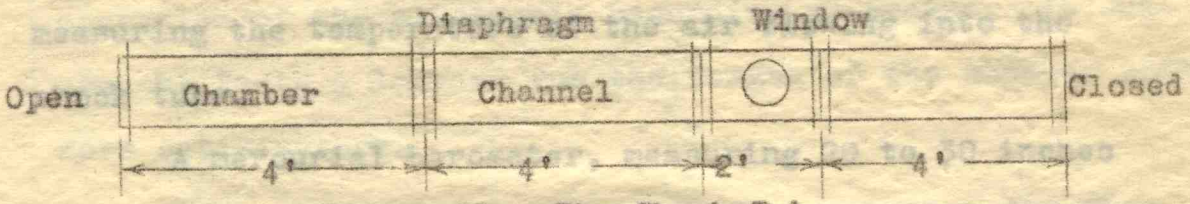

Figure 11. The Shock Tube

The vacuum system. Connections to the tube from the vacuum pump and manometer were made through the end plate of the channel to preserve the interchangeability of the sections of the tube. Non-collapsing 1/4 inch neoprene was connected with Schrader fittings to two holes in the end plate. One tube was connected to the mercurial manometer and one to the vacuum pumps. Pinch cocks on the neoprene tubing were used to seal off the shock tube. No screens were used over the openings in the end plate although a double filter filled with spun glass was installed to prevent particles of cellophane from clogging the vacuum pumps and entering the manometer.

Two vacuum pumps were used, a USAF rotary pump oil-sealed and with an air-oil separator for low pressure rapid evacuation, and a Cenco Hi-Vac two stage oil-sealed pump. The first drew a vacuum down to about 2 inches of mercury absolute. The second drew a vacuum down to about 0.1 inches of mercury absolute.

Devices for measuring temperatures and pressures

A standard Taylor mercurial thermometer was used for measuring the temperature of the air flowing into the shock tube.

A mercurial barometer, measuring 20 to 30 inches of mercury, absolute, was read for pressure measurements on the chamber.

A mercurial manometer, measuring 30 inches of mercury, was connected to the end plate of the channel section of the shock tube to measure the difference between the atmospheric pressure in the chamber and the pressure in the channel.

The diaphragm. The diaphragm consisted of 4 thicknesses of 0.001 inch cellophane wound on an aluminum frame and inserted between the gasketed ends of the chamber and channel. It was found by experiment that 4 thicknesses of the cellophane would withstand any pressure used even if allowed to maintain high pressure differentials for several hours.

Device for breaking the diaphragm. The device for breaking the diaphragm consisted of an "Exacto" blade mounted on an arm of 1/8 inch welding rod 3 1/2 inches in length. This arm pivoted on a stand mounted inside the shock tube chamber and moved through an arc to pierce the diaphragm when actuated. During early tests the diaphragm-breaking device was actuated by a small solenoid but it was found that the voltage surges interfered with the operation of the electronic recording apparatus. In subsequent tests a lanyard run the length of the chamber proved more satisfactory.

The photographic apparatus for recording the flow. Since the air flow in the shock tube takes place in less than 0.1 seconds, recording of the flow data by mechanical or electronic means is necessary. Thus a photographic device was needed to study the flow phenomena. The shadowgraph was chosen as the simplest and cheapest type of photographic apparatus. The flow in the tube was directed over wedges and other air foil models mounted in the test section in line with the shadowgraph light source and film. Figure 12 shows a block diagram of the triggering system.

The schematic diagram of the light source can be seen in Figure 13. The circuit consisted essentially of

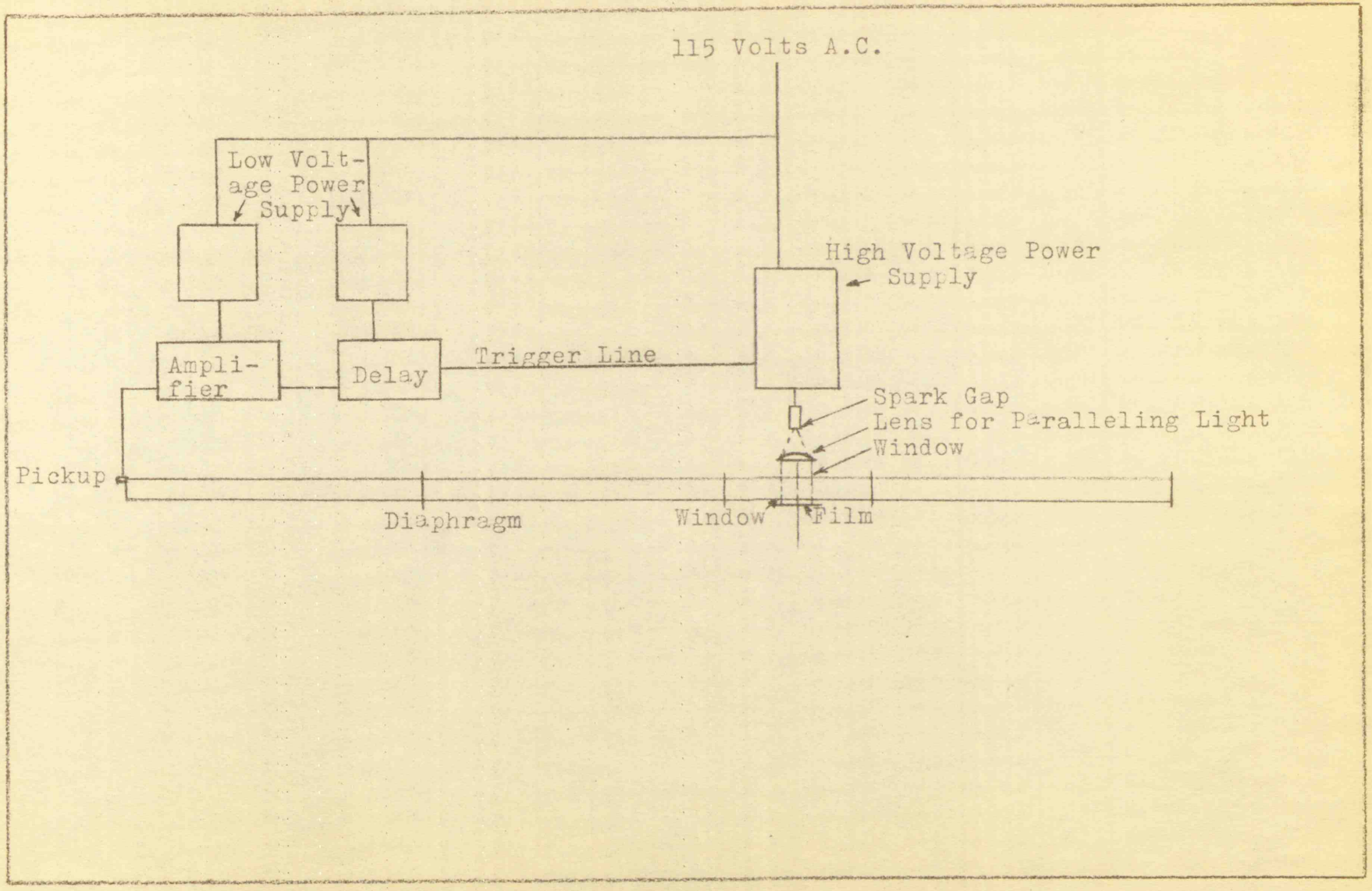

FIGURE 12

SCHEMATIC FOR APPARATUS FOR SHADOWGRAPH PHOTOGRAPHY

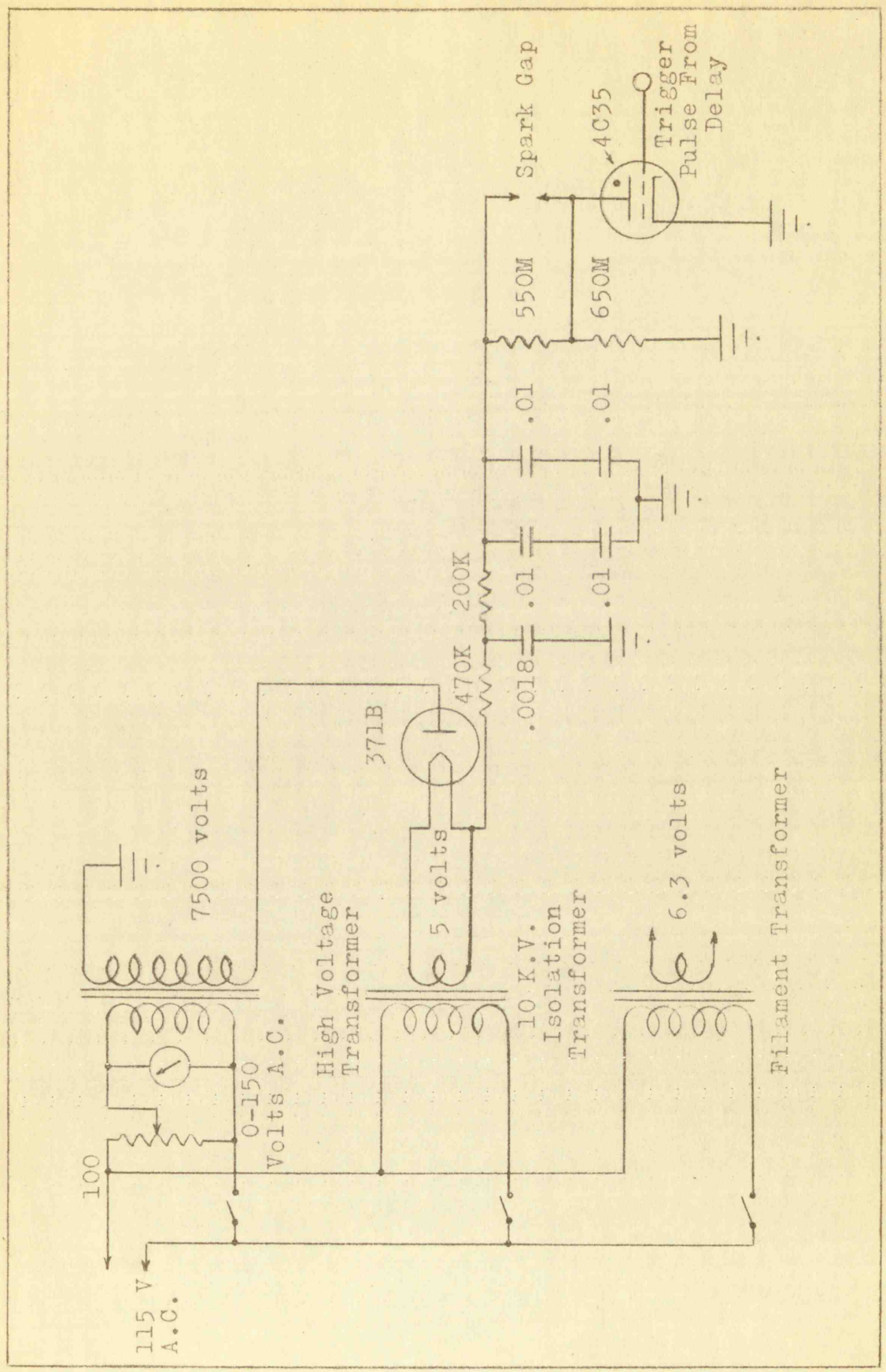

FIGURE 13

THE SPARK CIRCUIT

a high voltage power supply, a condenser to hold the electrical charge, and a discharge vacuum tube for triggering the spark.

The power supply used a 371 B rectifier. The bank of capacitors equal in capacity to 0.01 microfarads was available for 6 kilovolts. As a safety precaution resistors were installed across the spark gap and trigger tube to bleed off the system when not in use.

The trigger tube, a 4035 hydrogen thyratron, is designed to carry a current flow of 90 amperes. Although the capacitor bank probably discharges several times that current through the tube, the flow has a duration of about 0.1 microseconds and no tube damage has resulted from these brief overload currents. The duration of the spark has been checked by a rotating mirror as on the order of 0.1 microseconds.

The spark head is a "Mycalex" block machined for mounting and for the installation of tungsten tips to carry the discharging amperage from the capacitor bank. Figure 14 shows the dimensions of the spark head as used for this investigation. The block is mounted sufficiently far away from the chassis and components to prevent arcover. The voltage could be varied from zero to about 6000 volts. The operating voltage, however, was about 5000 volts for most pictures in this investigation.

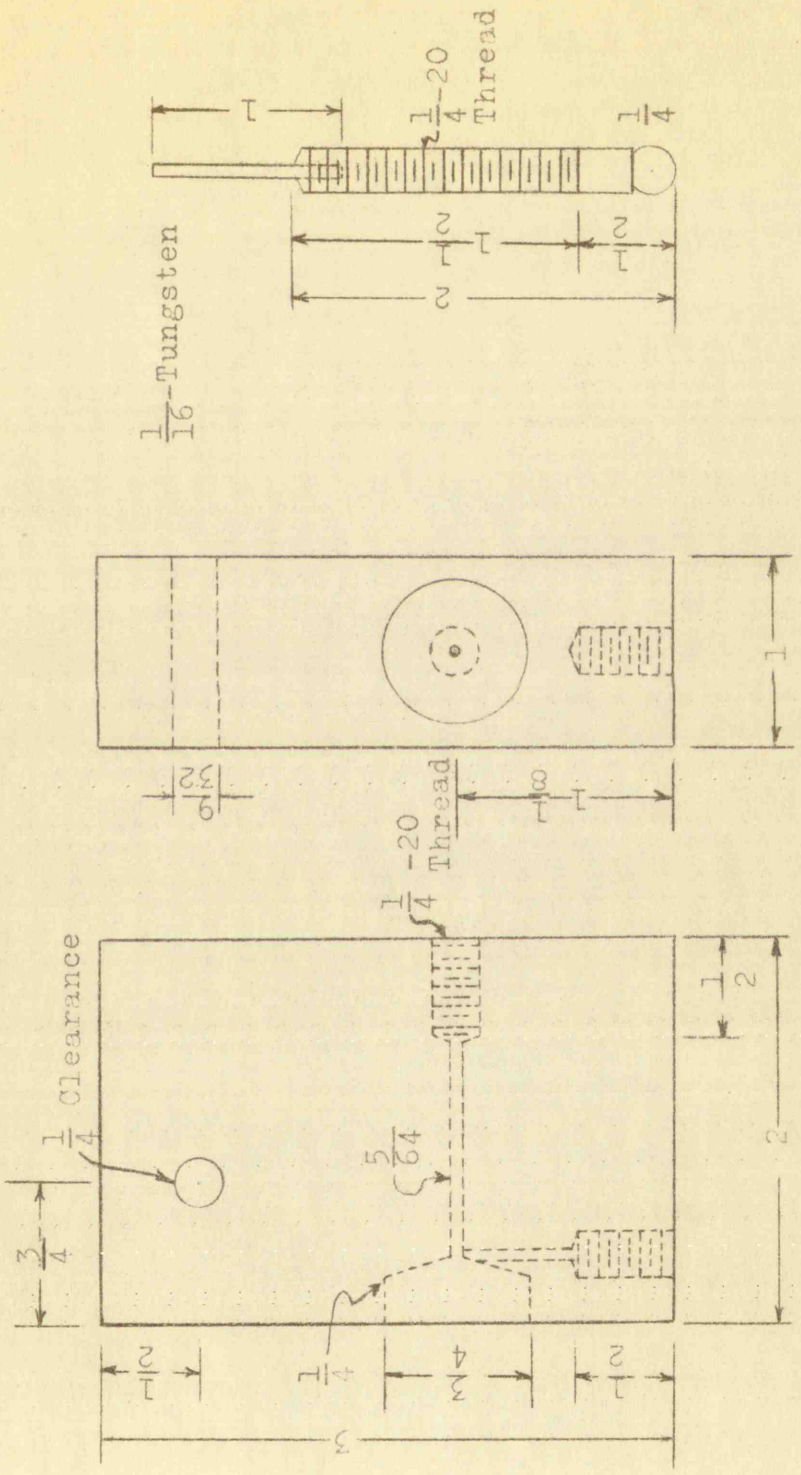

FIGURE 14

THE SPARK GAP

The paralleling lens was a plano-convex 6-inch diameter lens with a focal length of 9 1/2 inches. The lens was mounted in a 6-inch stovepipe with a focal point at the forward electrode of the spark gap.

The windows of the shock tube test section were of 1/2 inch plate glass, 6 7/8 inches by 6 15/32 inches, mounted flush with the inside walls. The windows were supported by the top and bottom of the shock tube, and the test model which was mounted between them. To provide a vacuum seal the glass was fitted into a recessed area and sealed with "Permatex" No. 2 in a semi-plastic state, and a rubberized fabric gasket.

The test section of the shock tube was 2 feet long with an inside width of 1.840 inches. The wedge or airfoil model, machined to 1.840 $^{+.000}_{-.003}$ inches in width, was held by the pressure of the glass windows after being set in place with clear cellophane tape inserted between the glass and the model.

The entire photographic system was light-tight from the light source to the film. Sheet film, 4 x 5, was held in a standard holder set outside the glass opposite the light source. The spark exposed the film. Eastman Super-Panchro Press Type B and Royal Pan film were used, followed by normal development in D-19 developer. Figure 15 shows a diagram of the light path for shadowgraph photography.

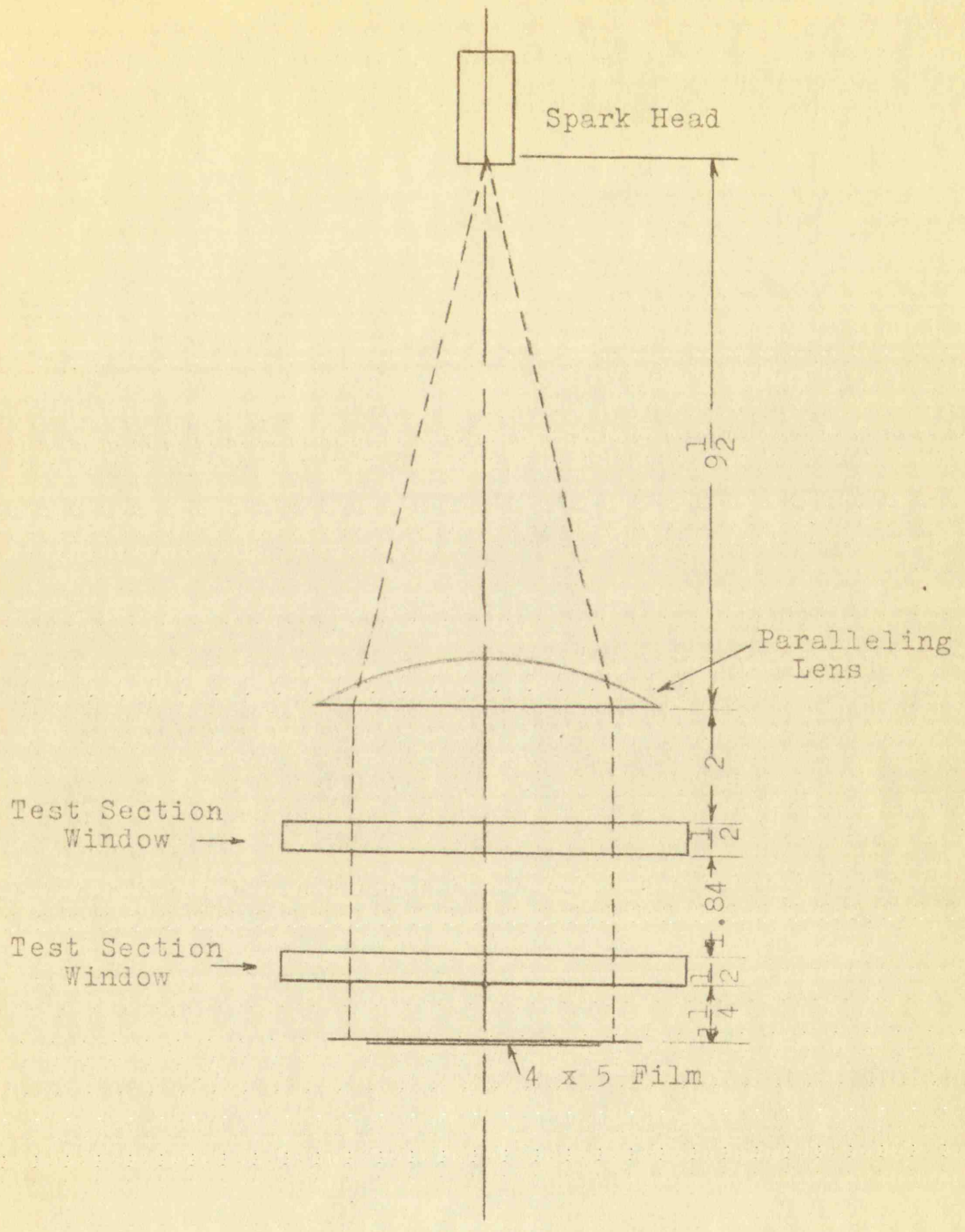

The system was enclosed and light tight

FIGURE 15

DIAGRAM OF LIGHT PATH FOR SHADOWGRAPH PHOTOGRAPHY

The synchronizing mechanism for triggering the light source. A crystal pickup with amplifier and delay system proved to be the simplest and least expensive synchronizing mechanism for the triggering of the shadowgraph light with the time of flow.

Figure 12 shows the place of the pickup in the system. In first trials an earphone pickup was used but because of its erratic behavior it was discarded. A small loudspeaker was then used with no better results. For this study a barium-titinate crystal 1/2 inch in diameter and 1/4 inch thick was used. The crystal was silvered on both flat surfaces and was fastened to the open end of the chamber with glue.

The amplifier is shown in the block diagram Figure 12. Figure 16 shows the schematic diagram of the resistance-coupled amplifier used to amplify the sound pulse from the barium-titinate crystal. The circuit was simple in that it used two stages of amplification with a single 6SN7. The 2D21 thyratron was used for two reasons. First, a sharp negative pulse of at least 22 1/2 volts was needed to trigger the delay. This pulse was possible with the action of the thyratron which provided a sharp voltage rise when the flow began. Second, isolation was needed for the delay unit. When triggered, the thyratron continued to conduct until reset, therefore, a single pulse

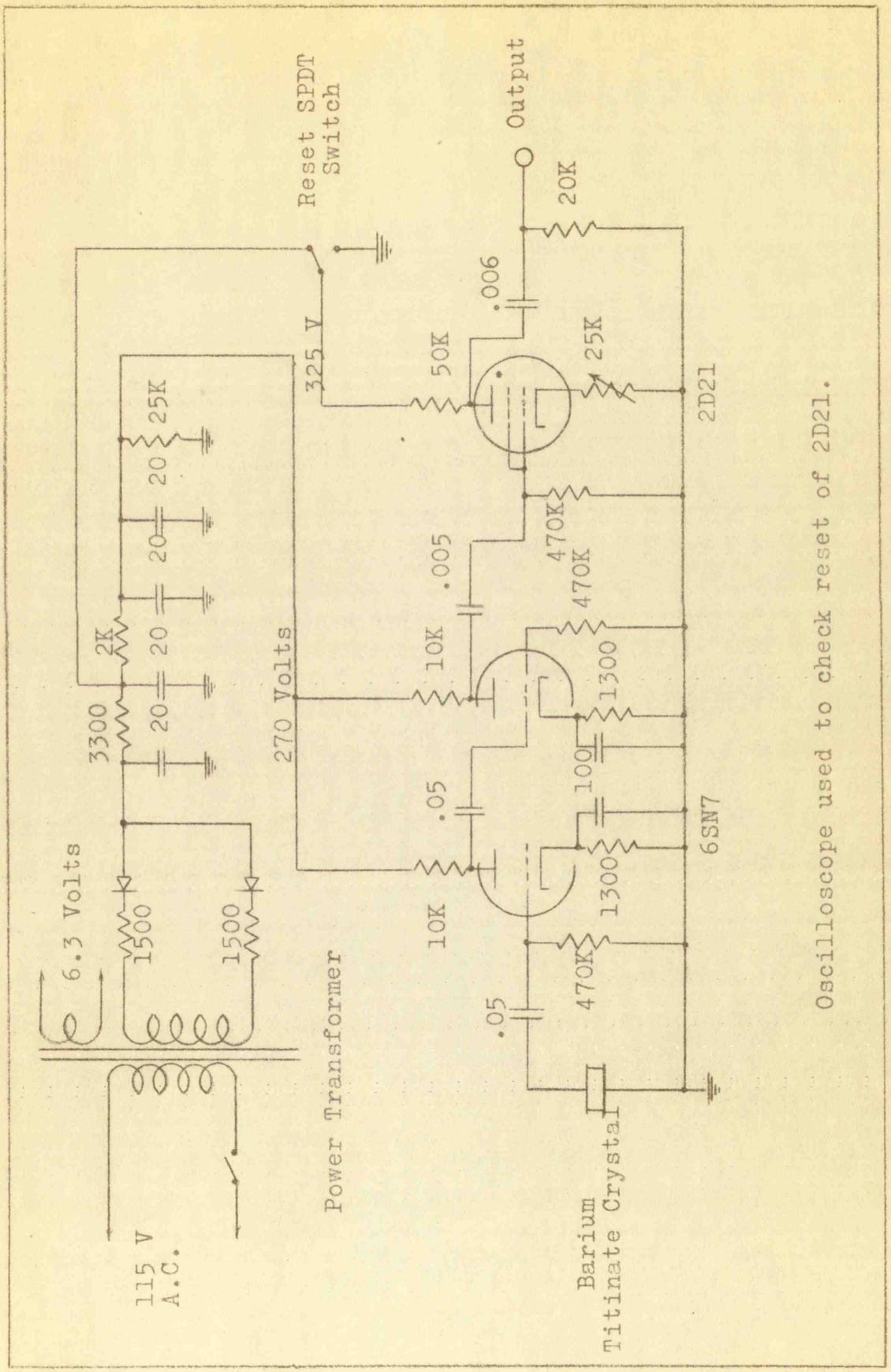

Oscilloscope used to check reset of 2D21.

FIGURE 16

RESISTANCE - COUPLED AMPLIFIER

resulted from the amplifier regardless of the number of pulses received from the crystal pickup.

The schematic diagram of the delay circuit is shown in Figure 17. The pulse from the thyratron was received on the cathode of 1/2 of the 6SN7 used as a diode. The voltage was adjusted to a fixed level by the 25K ohm helipot. The adjustment of this voltage was critical in that it determined the delay time. The voltage was adjusted from 36 to 228 volts for full coverage of the delay. Flow travels in one direction only through the diode, therefore, all positive pulses are rejected. The negative pulse caused the 6SA7 to cutoff and at the same time cut off the other half of the 6SN7. The delay RC network of the 3920 $\mu\mu fd$ capacitor and 1.8 megohm resistor determined the time of voltage buildup until the 6SA7 conducted. The plate voltage of this tube was determined by the helipot setting. The delayed pulse was taken from the cathode of the 6SA7 and amplified by the two-stage amplifier of the 12AU7. Two stages were necessary in order to give a positive pulse on the grid of the output thyratron. The 2D21 thyratron was equipped with an indicator to show when it was conducting. It triggered only once but kept conducting until reset. The voltages were critical and the power supply for the delay circuit was regulated only

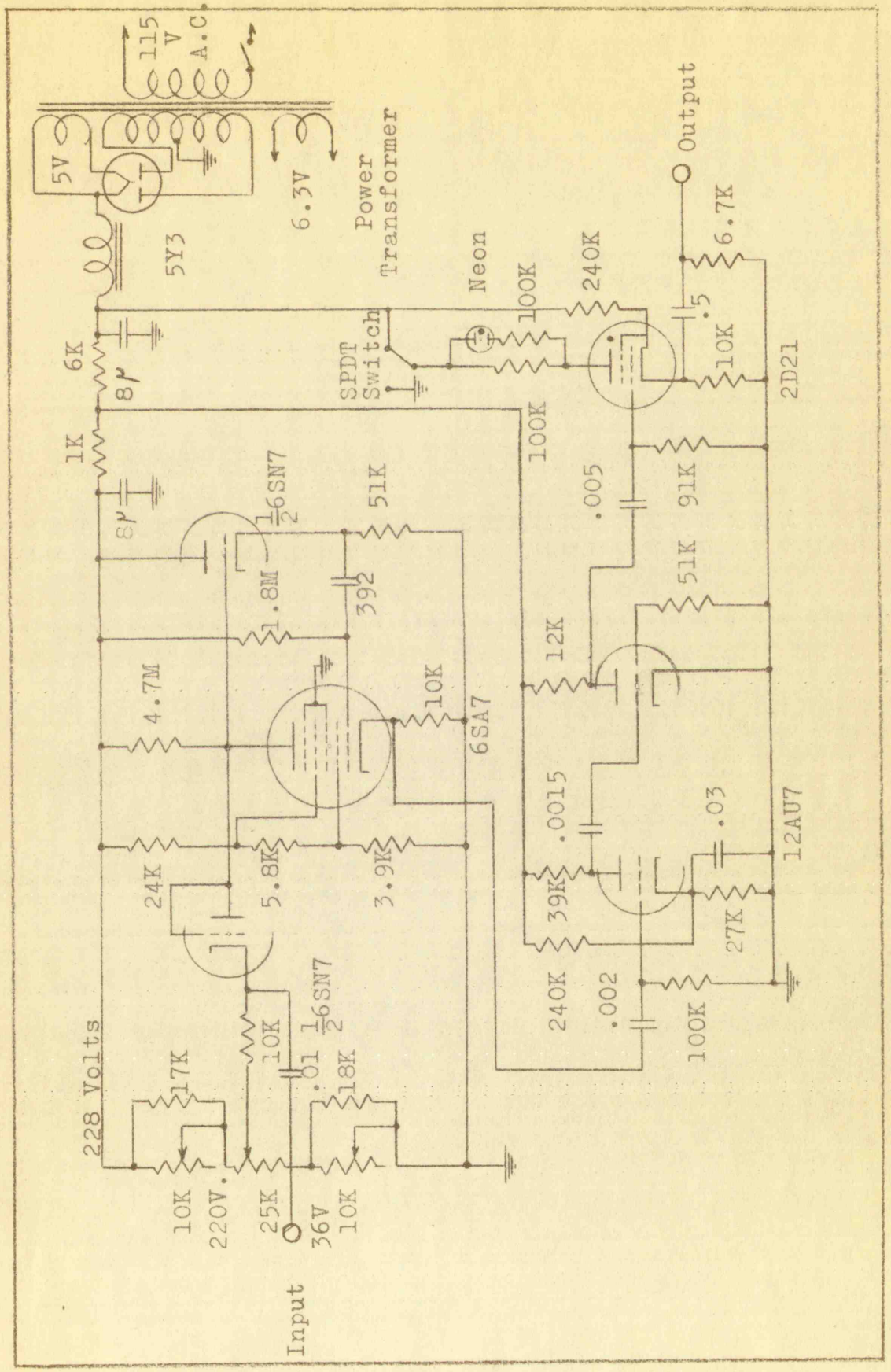

FIGURE 17

THE DELAY CIRCUIT

by load. A positive voltage pulse was taken off to trigger the 4C35 hydrogen thyratron in the light source.

CHAPTER IV

TEST PROCEDURE

Assembly of the shock tube. The sections of the shock tube were lined up and bolted together. The test section was checked with a square with respect to both the floor and the spark light source.

Assembly of the cellophane diaphragm. The cellophane was cut and wound around the aluminum frame to give 4 thicknesses, and the frame inserted between the chamber and channel of the shock tube. The top and bottom bolts were snugged down and the alignment of the two sections observed. The side bolts were then drawn down and tightened followed by the final tightening of all bolts. Improper adjustment of the gaskets or bolts caused the cellophane to be strained and to break.

Calculations made for data desired. The barometer was read and corrections made for the temperature. From this corrected reading a value was calculated for the pressure needed in the channel and the delay setting needed in order to obtain the desired results.

Vacuum drawn. The low-vacuum pump was started and vacuum was drawn on the channel section until about 22

CHAPTER IV

TEST PROCEDURE

Assembly of the shock tube. The two halves of the shock tube were lined up and bolted together. The test section was checked with a square with respect to both the floor and the spark light source.

Assembly of the orifice diaphragm. The cellophane was cut and wound around the aluminum frame to give 4 thicknesses, and was then inserted between the shock tube and channel of the shock tube. The two end bolts were snugged down and the alignment of the two sections observed. The side bolts were then drawn up and tightened followed by the final tightening of the end bolts. The proper adjustment of the spindle of the valve caused the cellophane to be stretched out to the orifice.

Calculations made for data reduction. The barometer was read and corrections made for the temperature. Data this corrected recording a weight was calculated for the pressure needed in the channel and the unit weight needed in order to obtain the desired results.

Vacuum pump. The low-vacuum pump was started and vacuum was drawn on the driver section until about

inches of mercury was shown on the manometer. If further vacuum was needed for the pressure ratio desired the small Hi-Vac pump was put into operation. The two pumps were not operated at the same time. When the pressure was within about 1/2 inch of the desired pressure in the channel, the amplifier, delay unit, and spark light source were turned on. When the desired pressure had been reached in the channel the vacuum pump was switched off and the high voltage applied to the spark gap to ready it for triggering.

Triggering operation. A test triggering pulse was applied to the amplifier to make certain that it would operate satisfactorily. The amplifier and delay were then reset ready for the trigger pulse. The manometer was sealed off from the shock tube after a final reading. The film was installed in the holder, and the cover slide on the film pack raised. The lanyard operating the diaphragm-breaking device was then pulled to break the cellophane. The sound from the breaking operation traveled down the steel tube to the barium-titinate crystal pickup, was amplified, delayed the amount calculated, and the spark discharged exposing the film. The slide was immediately closed over the film. The time involved between rounds varied from 20 to 30 minutes. If during the triggering

inches of mercury was shown on the manometer. A better
vacuum was needed for the experiments described here and a
Hi-Vac pump was put into operation. The two pumps were
not operated at the same time. When the pressure had
within about 1/3 inch of the desired pressure in the
channel, the amplifier, delay unit, and spark light sources
were turned on. When the desired pressure had been reached
in the channel the vacuum pump was switched off and the
high voltage applied to the spark gap to start
triggering.

Triggering operation. A
applied to the amplifier to make certain that it would
operate satisfactorily. The amplifier was then kept turned
reset ready for the trigger pulse. The
sealed off from the shock tube after a final cleaning. The
film was installed in the holder, and the cover slide on
the film pack raised. The lowered over the light-
breaking device was then put in place over the orifices.
The sound from the breaking operation
steel tube to the beam-splitter
amplified, delayed the
discharged exposing the film. The
closed over the film. The
varied from 20 to

cycle an unexpected voltage surge took place the delay system might be unreliable and that round rejected.

Maintenance. Between test runs the tubing to the filter for the vacuum pumps had to be blown clear of shattered cellophane. After from between 20 to 25 rounds the back plate of the tube had to be taken off and the packed cellophane removed. Also, the test section had to be dismantled and the plate glass windows cleaned. The entire tube was not purged of cellophane particles except at this time and frequently bits of cellophane may be seen in the flow stream in the shadowgraph pictures.

After approximately 100 rounds had been fired the spark head had to be disassembled and cleaned. A 5/64 inch drill was run down the passage in order to clean it of tungsten particles.

CHAPTER V

CALIBRATION OF THE APPARATUS

Delay unit calibration. The delay unit was calibrated by the use of a Textronic 514 D Oscilloscope, with a Krohn-Hite push button oscillator Model 440-A used to calibrate the oscilloscope sweep. The delay unit and the oscilloscope were triggered with a 22 1/2 volt battery. Figure 18 shows a plot of the calibration curve with the voltages used at the high and low ends of the helipot. See Figure 17 for the schematic diagram on the delay unit.

Velocity measurements in the shock tube. Since the shock tube was designed to be used for aerodynamic investigations, it was of first importance that the flow become stabilized at any desired Mach number. The usefulness of the tube was determined by the duration of constant flow.

Shock tube theory predicts a constant flow following the primary shock wave of 800 microseconds at Mach 1.15 with a pressure ratio of 100. The theory also predicts a constant flow for approximately 2900 microseconds following the contact surface. Steady flow following the

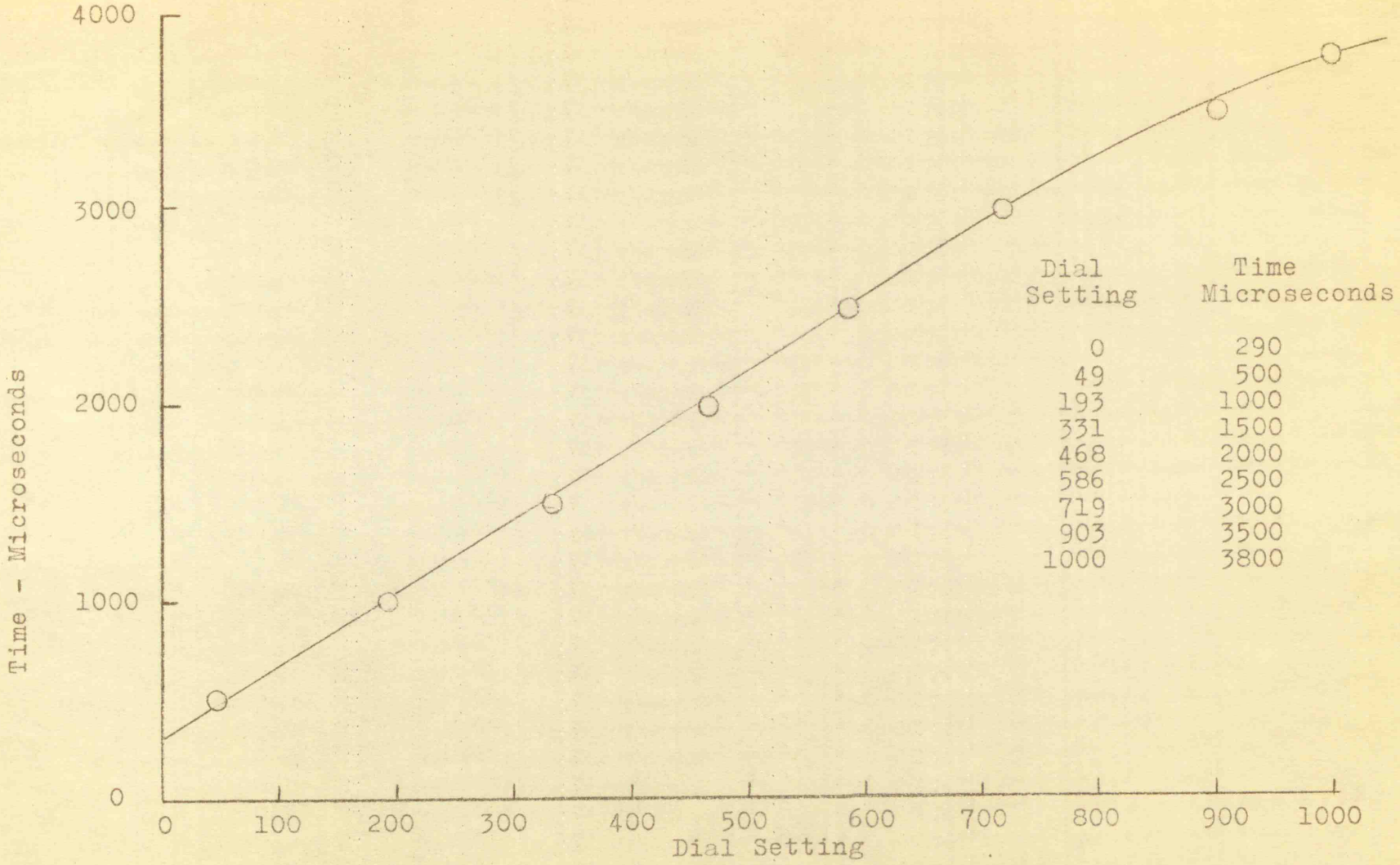

Dial Setting	Time Microseconds
0	290
49	500
193	1000
331	1500
468	2000
586	2500
719	3000
903	3500
1000	3800

FIGURE 18

CALIBRATION OF THE DELAY CIRCUIT

primary shock wave was about 300 microseconds as shown in Figure 19 and Table VI. A steady flow following the contact surface did not actually occur although velocity measurements could be made up to about 2000 microseconds after passage of the contact surface. The delay unit was designed to provide for a maximum delay time of 3800 microseconds, and about 1900 microseconds were required from the pickup trigger until the contact surface had passed the test window. After the contact surface had passed the test section, the measured flow velocities dropped off as the delay time was increased. At this pressure ratio either the flow velocity decreased with longer time delay or the flow could not stabilize because the test section was too close to the diaphragm.

According to the ideal shock tube theory, steady flow of about 2100 microseconds was predicted following the primary shock wave, and a steady flow of 3300 microseconds was predicted following the contact surface at a pressure ratio of about 40. The flow Mach following the primary shock wave was found to be about 1.00. The flow Mach following the contact surface was found to be about 1.75 and it did not seem to attenuate with time as had the flow Mach following the contact surface at a pressure ratio of 100.

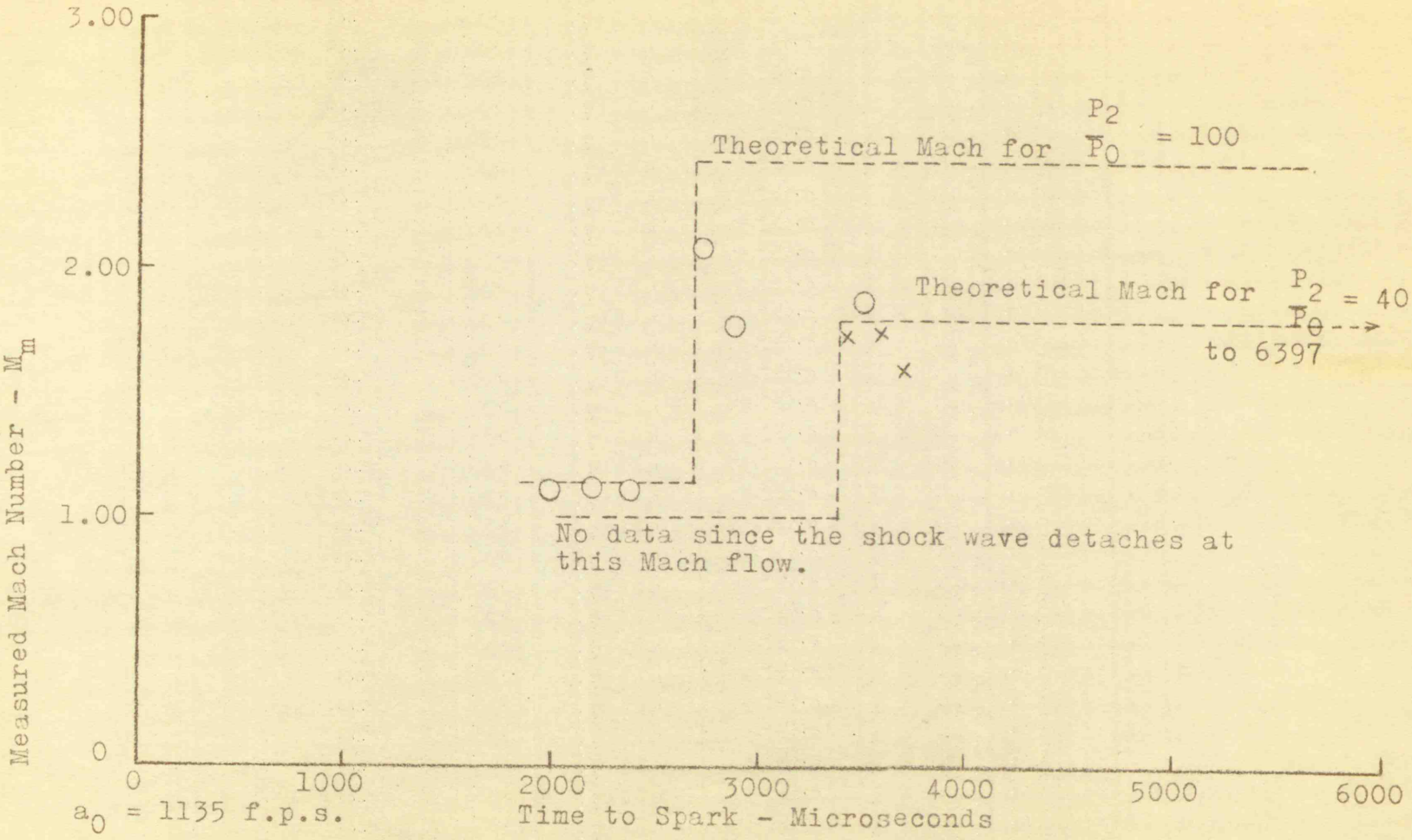

FIGURE 19

COMPARISON BETWEEN THEORETICAL MACH FLOW AND MEASURED MACH FLOW AT PRESSURE RATIOS OF 100 AND 40

The predicted Mach number was obtained from the original shock tube pressure ratio, and was calculated by use of the ideal shock tube theory.

The measured Mach number was calculated from the attached shock wave angle and in this paper is designated as Mm. Nonviscous flow was assumed in the calculation.

When the wedge of half-angle θ was placed in the flow stream, the measured Mach number for steady flow was obtained by[1]

$$\frac{1}{M_m^2} = \sin^2\beta - \frac{\gamma+1}{2}\,\frac{\sin\beta\sin\theta}{\cos(\beta-\theta)} \qquad (V-1)$$

where β was the inclination of the bow-wave in the direction of the flow as indicated in Figure 20.

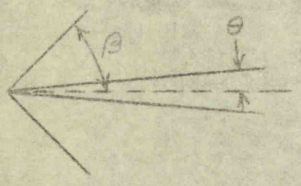

Figure 20. Shock Wave Attached to Wedge

Several wedges with different total angles were used in early experiments. A soft wood wedge became battered immediately. A hardwood wedge was used for some time but eventually became battered from cellophane particles. An aluminum wedge of 18 1/2 degrees included angle

---

[1] H. W. Liepmann and A. E. Puckett, Introduction of Aerodynamics of a Compressible Fluid, (New York: John Wiley and Sons, Inc., 1947), pp. 51-58.

was also used but the leading edge became rough and had to be resharpened several times. For final velocity measurements a hardened steel wedge was accurately ground to a total angle of 3 degrees. Using this wedge, and with the assumption that 1.400 for air, equation (V-1) can be written

$$M_m = \frac{1}{\sqrt{\sin^2\beta - \frac{0.0314 \sin\beta}{\cos(\beta - 1.5)}}} \qquad (V - 2)$$

This equation was plotted and the graph used to read M_m. Figure 21 shows this graph. This graph shows that the lower the measured angle the higher the Mach number. Note that the steepness of the curve decreases with decreasing Mach number until at 77 degrees the curve again swings upward. At that point the Mach number was 1.098. No measurement of the Mach number was possible below 1.098 since the bow wave detached at any lower Mach flow. After the leading edge of the wedge became slightly roughened from the battering of cellophane particles the shock detached at Mach 1.12 and measurement of the angle becomes difficult.

In order to obtain the shock wave angle as a function of time, it was necessary to take a series of pictures, using the same pressure ratio. The spark delay was varied for each picture. The resulting shadowgrams might be compared to a high-speed motion picture of a single shock wave.

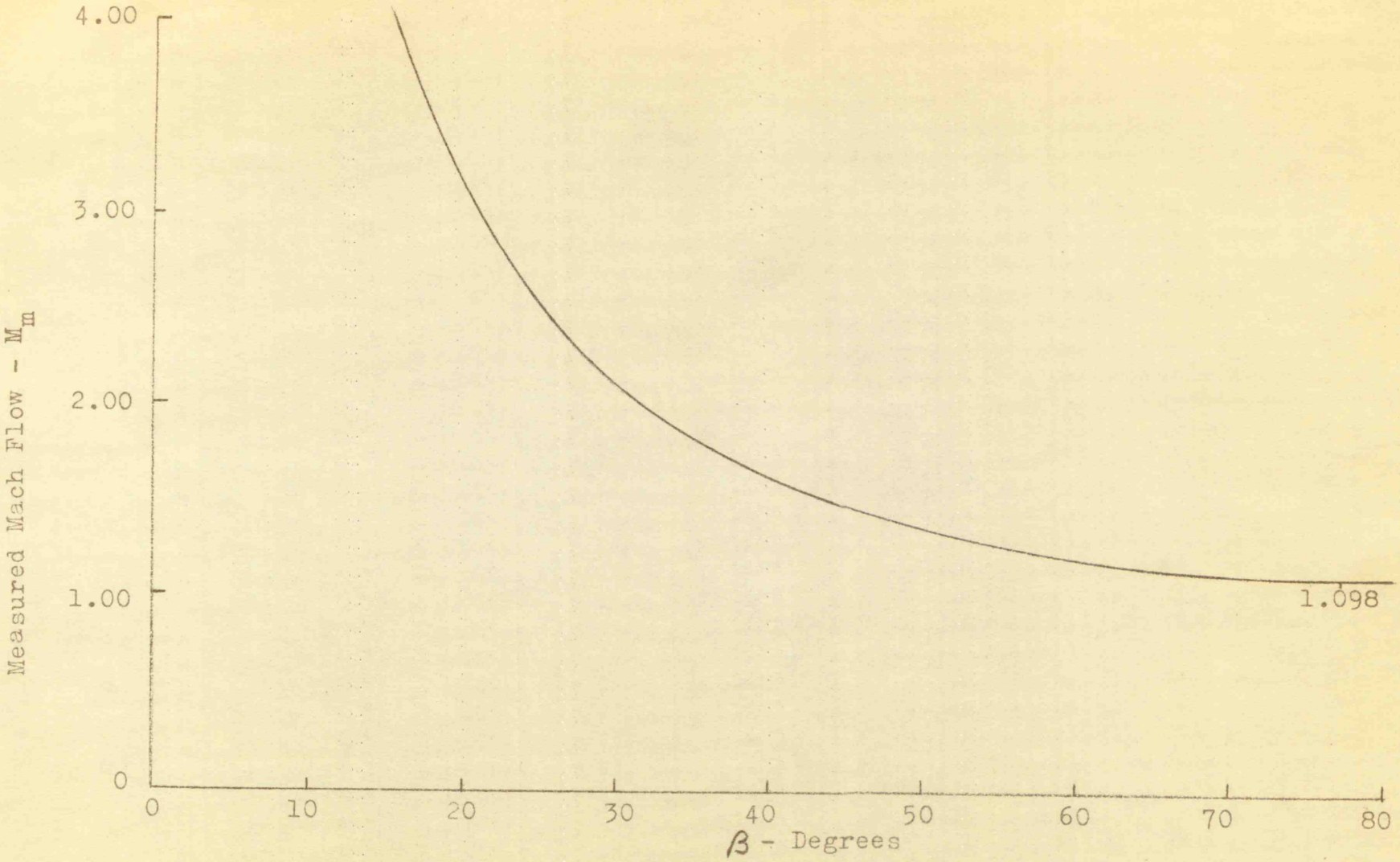

FIGURE 21

ONE-HALF BOW WAVE ANGLE PLOTTED AGAINST MEASURED MACH FLOW FOR A THREE-DEGREE WEDGE

The variation between the measured Mach number of the flow following the primary shock wave and the predicted Mach flow may be seen in Figure 8. It was found that the Mach flow closely followed that predicted by the theory between 1.10 and 1.18. This region was of little use, however, since the duration of flow was only about 300 microseconds. Above Mach 1.18 the density of air was not sufficient for the use of shadowgraph pictures.

The variation between the measured Mach number of the flow following the contact surface and the predicted Mach flow may be seen in Figure 9. The flow can not be predicted accurately at pressure ratios greater than 40 or with Mach numbers greater than 1.75. Below a pressure ratio of 25, results are not obtainable because of the limitations of the present electronic delay system to 3800 microseconds.

Measurement of the shock wave angle. The angle formed by the attached shock wave, $2/\beta$, was measured directly from the photographic film. The method followed was to measure the largest included angle to nearest half degree. The error involved in one-half degree measurement of $2/\beta$ varies with the Mach number as can be seen in Figure 21. The higher the Mach number the steeper the slope and the greater the error. The measurement

was difficult both when the Mach number was small and when the shock tube and spark source were not perfectly aligned. When the Mach number was low the bow waves were ragged, curved, and sometimes double.

Figures 22 and 23 show the three-degree wedge with the attached shock wave at two different Mach numbers. Here the wake as well as the wavering shock lines are visible.

It may be concluded from the data taken at points between 1.10 and 1.18 Mach flow that the actual flow Mach number was slightly low due to energy lost in shattering the cellophane diaphragm[2] or from boundary losses[3] due to the walls of the shock tube.

---

[2]F. W. Geiger, C. W. Mautz, The Shock Tube as an Instrument for Investigation of Transonic and Supersonic Flow Patterns, (Engineering Research Institute, University of Michigan, Ann Arbor, June 1949), pp. 86-88.

[3]R. J. Emrich, C. W. Curtis, "Dissipation of a Shock Traveling in a Tube," The Physical Review, 77:573, Feb., 1950.

was difficult both when the Mach number was small and when the shock tube and spark source were not perfectly aligned. When the Mach number was low the bow waves were ragged, curved, and sometimes double.

Figures 22 and 23 show the three-degree wedge with the attached shock wave at two different Mach numbers. Here the waves as well as the wavering shock lines are visible.

It may be concluded from the data taken at points between 1.10 and 1.18 Mach flow that the actual flow Mach number was slightly low due to energy lost in shattering the cellophane diaphragm[2] or from boundary losses[3] due to the walls of the shock tube.

---

[2] F. W. Geiger, C. W. Kuntz, "The Shock Tube as an Instrument for Investigation of Transonic and Supersonic Flow Patterns," (Engine Testing Research Institute, University of Michigan, Ann Arbor, June 1949), pp. 86-88.

[3] R. J. Emrich, G. W. Curtis, "Diaphragm Location of a Shock Traveling in a Tube," The Physical Review, 77:573, Feb., 1950.

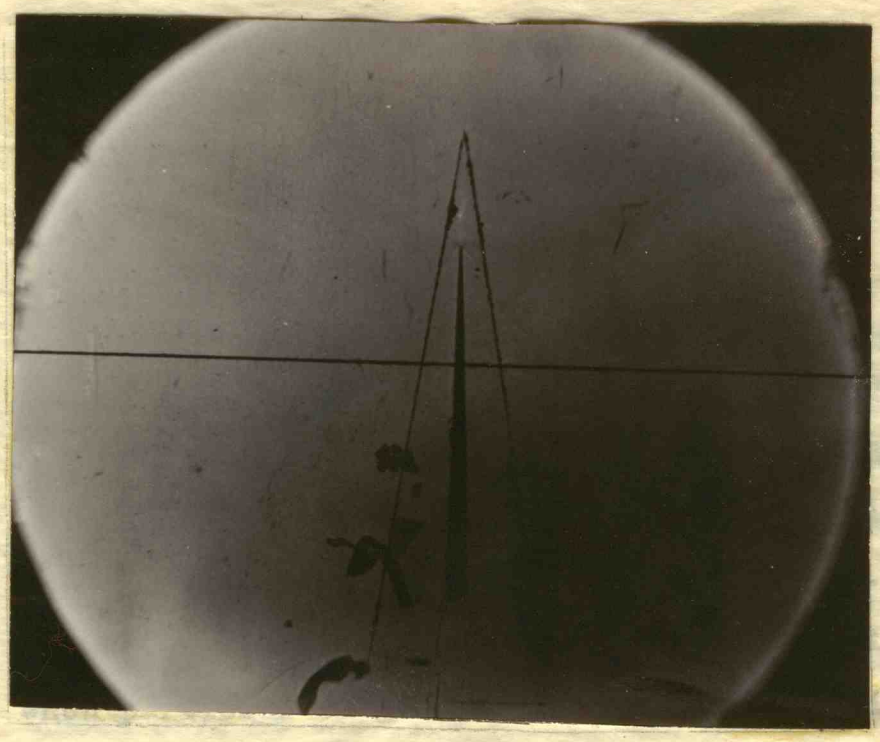

FIGURE 23
Round Number 245
ATTACHED BOW WAVE
M_m = 2.07, 3° Wedge

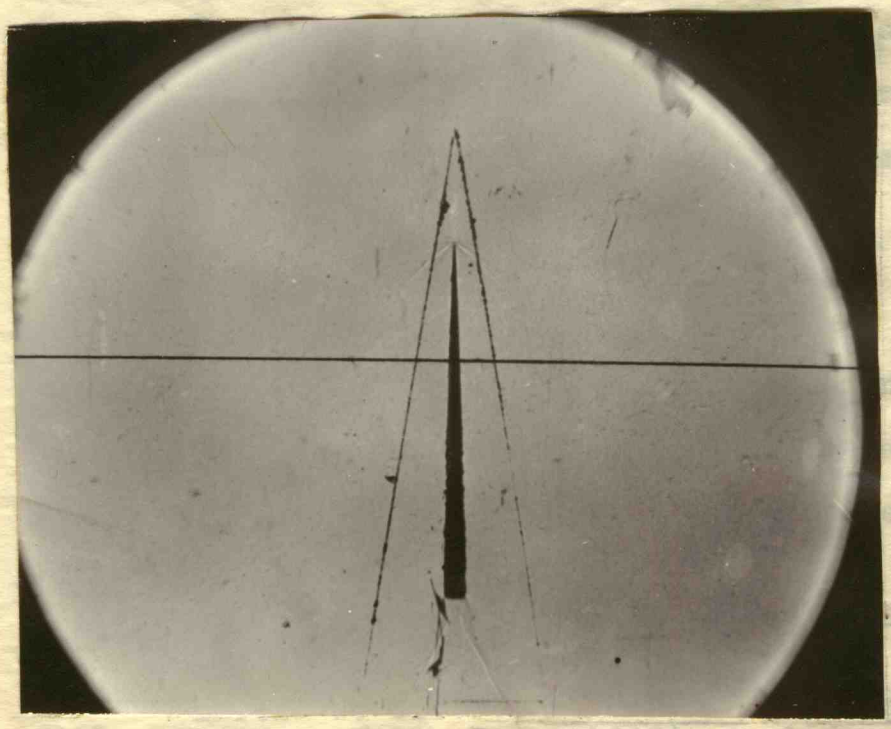

FIGURE 22
Round Number 247
ATTACHED BOW WAVE
M_m = 1.58, 3° Wedge

13

27

CHAPTER VI

AERODYNAMIC STUDIES

Velocity measurements on models from striation Mach waves. During preliminary testing it was noted that the saw marks on one face of the wooden wedge caused Mach wavelets to be developed. It seemed feasible that velocity might be measured from these wavelet angles.

Dwinnell[1] points out that a Mach angle is formed when particles of gas at supersonic velocities strike surface roughnesses in passing over an object in the flow path. The Mach wavelet may be seen in some shadowgraph and schlieren pictures when the density is sufficient. Dwinnell used the following equation to show the relationship between Mach wavelet angle and Mach number:

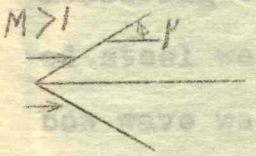

$$\mu = \sin^{-1}\frac{1}{M_{local}} \qquad (VI - 1)$$

$$M_{local} = \frac{1}{\sin\mu}$$

Sibert[2] says that one way of determining the Mach number is to measure the angle between a weak shock and the direction of motion along a body surface and then

---

[1] James H. Dwinnell, Principles of Aerodynamics, (New York: McGraw-Hill Book Company, Inc., 1949), p. 185.

[2] Harold W. Sibert, High-Speed Aerodynamics, (New York: Prentice-Hall, Inc., 1948), p. 160.

CHAPTER VI

AERODYNAMIC STUDIES

Velocity measurements on models from **Mach waves.** During preliminary testing it was noted that the saw marks on one face of the wooden wedge caused Mach wavelets to be developed. It seemed feasible that velocity might be measured from these wavelet angles.

Dwinnell[1] points out that a Mach angle is formed when particles of gas at supersonic velocities strike surface roughnesses in passing over an object in the flow path. The Mach wavelet may be seen in some shadowgraph and schlieren pictures when the density is sufficient. Dwinnell used the following equation to show the relationship between Mach wavelet angle and Mach number:

$$\mu = \sin^{-1}\frac{1}{M_{local}} \qquad (VI - 1)$$

$$M_{local} = \frac{1}{\sin\mu}$$

Sibert[2] says that one way of determining the Mach number is to measure the angle between a weak shock and the direction of motion along a body surface and then

---

[1] James H. Dwinnell, Principles of Aerodynamics, (New York: McGraw-Hill Book Company, Inc., 1949), p. 185.

[2] Harold W. Sibert, High-Speed Aerodynamics, (New York: Prentice-Hall, Inc., 1948), p. 150.

find the Mach number from the above equation. This necessitates laying off a tangent at the point of flow measurement except in the case of a wedge.

The chance striations caused by the saw cuts in preliminary experiments were too close together to form clearcut wavelet angles. Table VII gives data taken from the four pictures in which this occurs. Two of these pictures are shown in Figures 24 and 25. They show correlation between the measured Mach flow and the measured striated angles. The other two pictures show a detached shock wave at the flow velocities measured. The distortion of the shock waves in all four pictures seems to indicate that they are near the detaching point.

A later series of pictures shows the possibilities of accurate local velocity measurement on a model by measuring the Mach wavelet angle. The three-degree hardened steel wedge used in the velocity calibration from the bow wave was used.

First the wedge was scored on one face to a depth of about 0.005 inches at a distance of 1/2 inch from the leading edge and also to the same depth at a distance of 1 inch from the leading edge on the other face. No satisfactory data were obtained. The 1 inch striation gave some indication of Mach angle but the 1/2 inch striation showed none. This was attributed to the rougher scoring

find the Mach number from the above equation. This necessitates laying off a tangent at the point of flow measurement except in the case of a wedge.

The obvious striations caused by the saw cuts in preliminary experiments were too close together to form clearcut wavelet angles. Table VII gives data taken from the four pictures in which this occurs. Two of these pictures are shown in Figures 24 and 25. They show correlation between the measured Mach flow and the measured striated angles. The other two pictures show a detached shock wave at the flow velocities measured. The distortion of the shock waves in all four pictures seems to indicate that they are near the detaching point.

A later series of pictures shows the possibilities of accurate local velocity measurement on a model by measuring the Mach wavelet angle. The three-degree beveled steel wedge used in the velocity calibration from the bow wave was used.

First the wedge was scored on one face to a depth of about 0.005 inches at a distance of 1/2 inch from the leading edge and also to the same depth at a distance of 1 inch from the leading edge on the other face. No satisfactory data were obtained. The 1 inch striation gave some indication of Mach angle but the 1/2 inch striation showed none. This was attributed to the rougher scoring

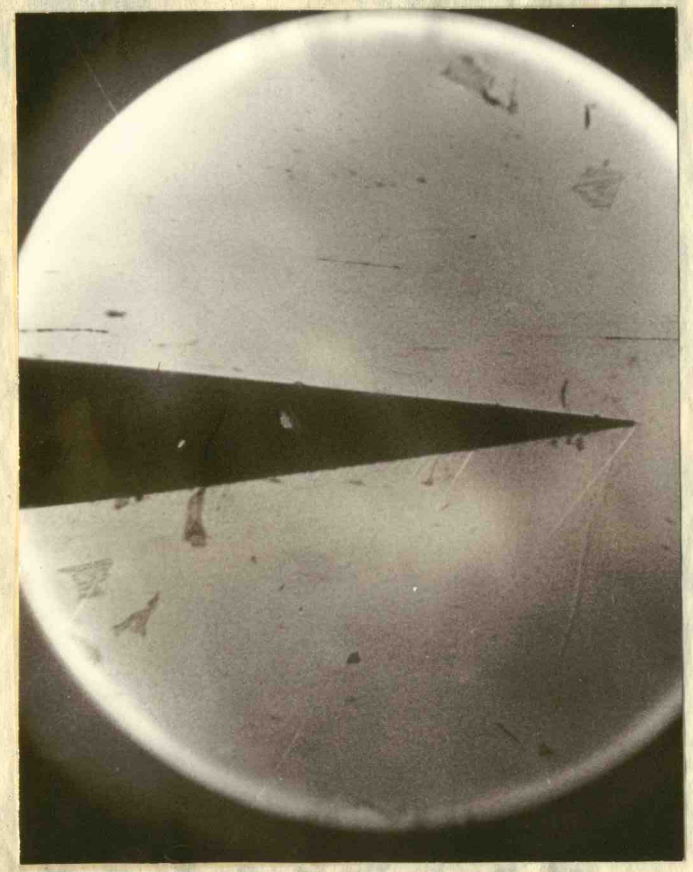

FIGURE 24

Bow Wave M_m = 1.42
Striation M_m = 1.39 to 1.31

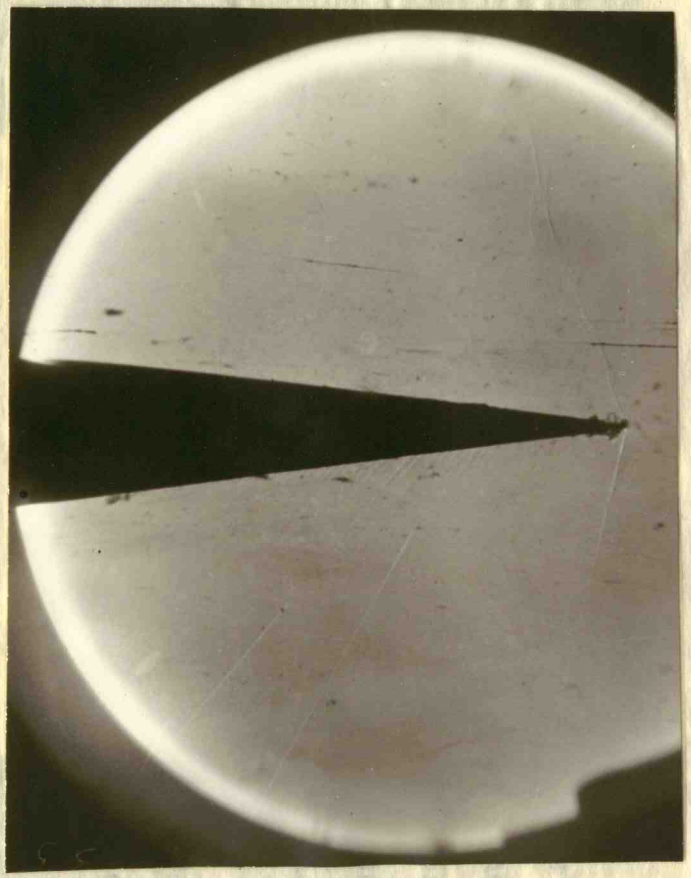

FIGURE 25

Bow Wave M_m = 1.34
Striation M_m = 1.44 to 1.27

Mean Value (%)

Saturation M^m = 1.44 to 1.54

Dew Wave M^m = 1.42

Saturation M^m = 1.38 to 1.51

Dew Wave M^m = 1.45

Mean Value (%)

at the 1 inch striation.

Following the unsatisfactory results from notching the wedge, a strip of 0.0015 inch cellophane tape was applied to the wedge as a striation to interrupt the flow. This proved satisfactory and excellent agreement resulted from measurements made on the striations and on the bow wave. The tape striation, while temporary, proved satisfactory for a series of 30 pictures. See Table IX for the tabulated results. Figures 26, 27, 28 and 29 show representative results.

From this series of pictures it appears that local velocities can be satisfactorily measured on models by a striation across the model at any point local velocity is desired in the supersonic range.

Size effect of models on shock tube flow. In wind tunnels as the flow velocity increases the tunnel finally reaches a chocked condition where the boundary layers of air build up in thickness and obscure the observed flow, distorting force measurements on the models. The shock tube on the other hand has a slow build up of these boundary layers, and data may be obtained before choking occurs. Figures 30, 31, 32, and 33 show the build up to this choking condition. Sibert[3] shows that the choking Mach flow

---

[3] Sibert, op. cit., pp. 85-86.

at the 1 inch stretch.

Following the unsatisfactory results from notching the wedge, a strip of 0.0015 inch cellophane tape was applied to the wedge as a stretch to interrupt the flow. This proved satisfactory and excellent agreement resulted from measurements made on the stretches and on the bow wave. The tape stretch, while temporary, proved satisfactory for a series of 30 pictures. See Table IX for the tabulated results. Figures 26, 27, 28 and 29 show representative results.

From this series of pictures it appears that local velocities can be satisfactorily measured on models by a stretch across the model at any point local velocity is desired in the supersonic range.

Size effect of models on shock tube flow. In wind tunnels as the flow velocity increases the tunnel finally reaches a choked condition where the boundary layers of air build up in thickness and obscure the observed flow, distorting force measurements on the models. The shock tube on the other hand has a slow build up of these boundary layers, and data may be obtained before choking occurs. Figures 30, 31, 32, and 33 show the build up to this choking condition. Sibert[3] shows that the choking Mach flow

---

[3] Sibert, op. cit., pp. 85-86.

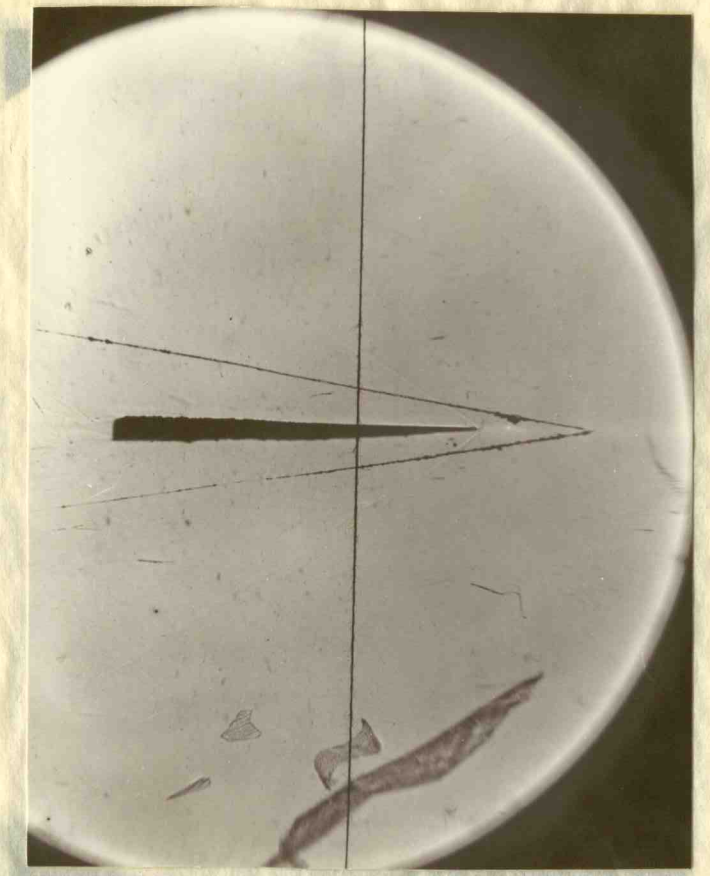

FIGURE 26
Round Number 257

Bow Wave M_m = 2.28
Mach Wave M_m = 2.28
Delay Time - 3850 Microseconds

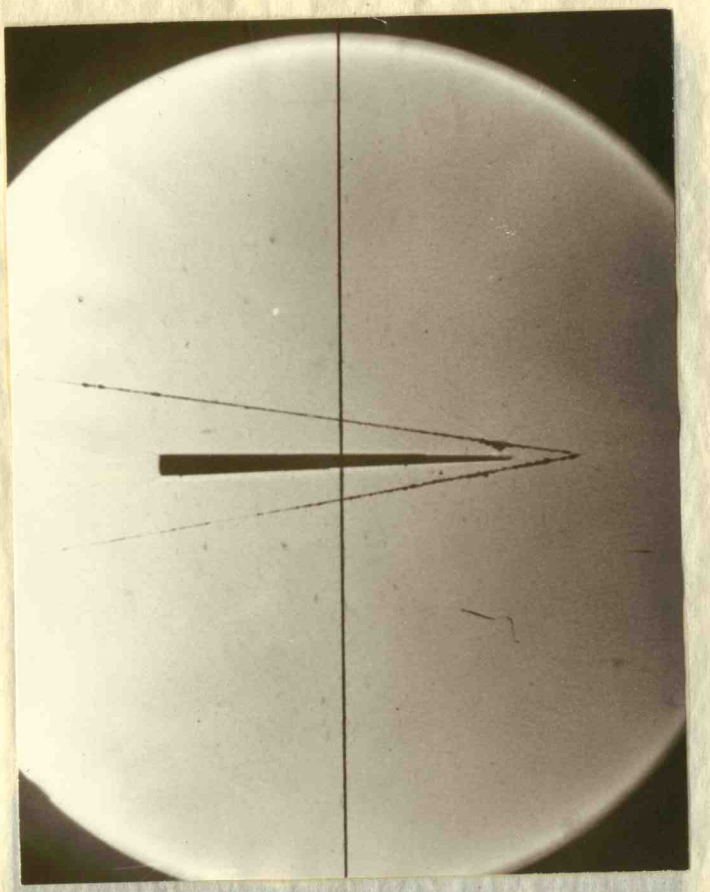

FIGURE 27
Round Number 262

Bow Wave M_m = 2.03
Mach Wave M_m = 2.03 and 2.00
Delay Time - 3300 Microseconds

FIGURE 26

Round Number 257

Bow Wave $M_{\infty} = 5.28$

Mach Wave $M_{\infty} = 5.28$

Delay Time - 2520 Microseconds

FIGURE 27

Round Number 258

Bow Wave $M_{\infty} = 5.03$ and 5.00

Mach Wave $M_{\infty} = 5.03$ and 5.00

Delay Time - 2520 Microseconds

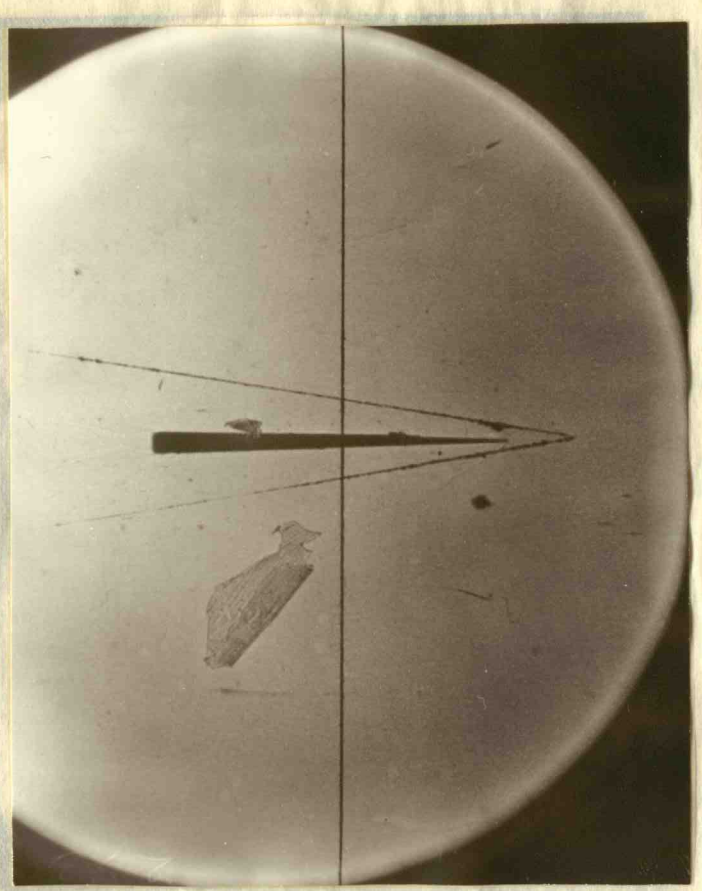

FIGURE 28
Round Number 282

Bow Wave M_m = 2.10
Mach Wave M_m = 2.10
Delay Time - 2640 Microseconds

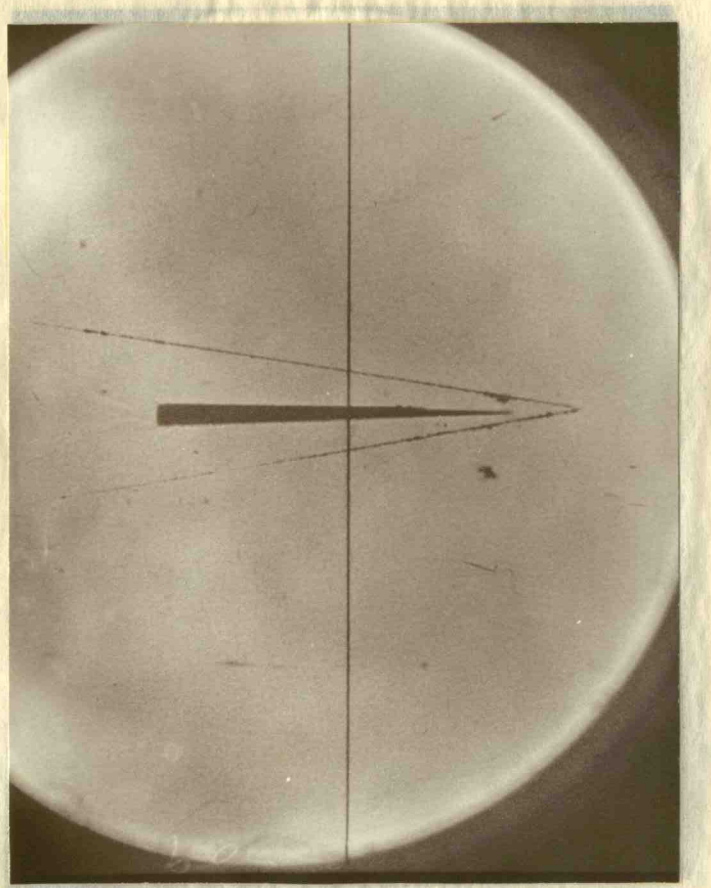

FIGURE 29
Round Number 289

Bow Wave M_m = 1.60
Mach Wave M_m = 1.60
Delay Time - 3675 Microseconds

Data Type - 32-bit Microcomputer

Word Number 32

Most Sig. Byte M_{n+3} = 7.50

Next Most Sig. Byte M_{n+2} = 7.50

Next Least Sig. Byte M_{n+1} = 7.50

Least Sig. Byte M_n = 7.50

Data Type - 32-bit Microcomputer

Word Number 32

Most Sig. Byte M_{n+3} = 7.50

Next Most Sig. Byte M_{n+2} = 7.50

Next Least Sig. Byte M_{n+1} = 7.50

Least Sig. Byte M_n = 7.50

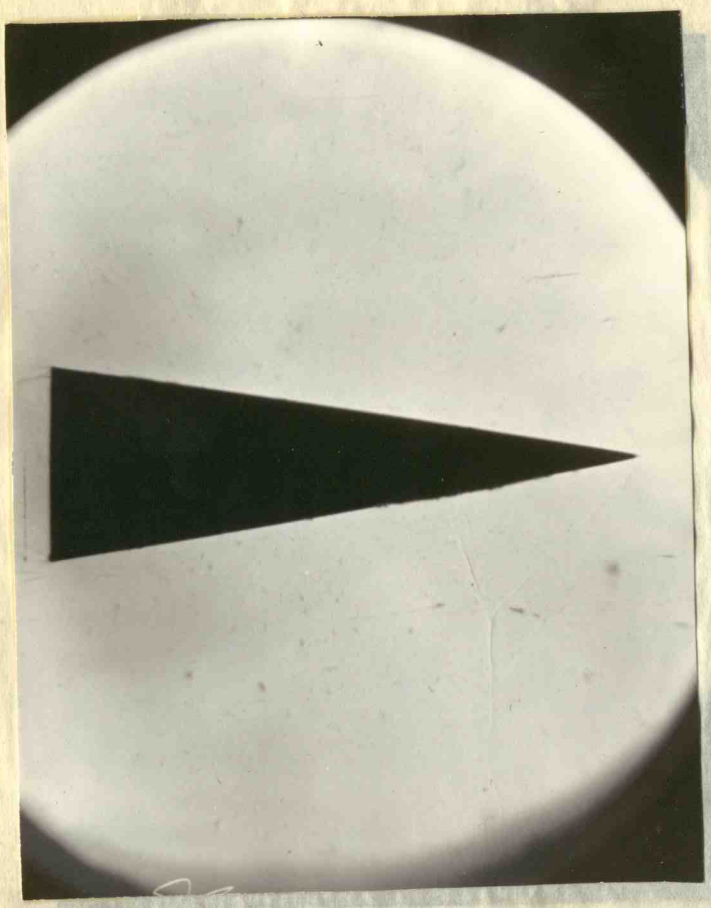

FIGURE 30
Round Number 33

Aluminum Wedge 18 1/2-degrees
M_{PS} = 1.12
Time after Primary Shock
Wave Passage = 300 Microseconds

FIGURE 31
Round Number 34

Aluminum Wedge 18 1/2-degrees
M_{PS} = 1.12
Time after Primary Shock
Wave Passage = 500 Microseconds

FIGURE 30
Round Number 23

Aluminum Wedge 1B 1/2-degree
Mps = 1.15
Time effect Symmetry Check
Mesh Spacing = 500 Microseconds

FIGURE 31
Round Number 24

Aluminum Wedge 1B 1/2-degree
Mps = 1.15
Time effect Symmetry Check
Mesh Spacing = 500 Microseconds

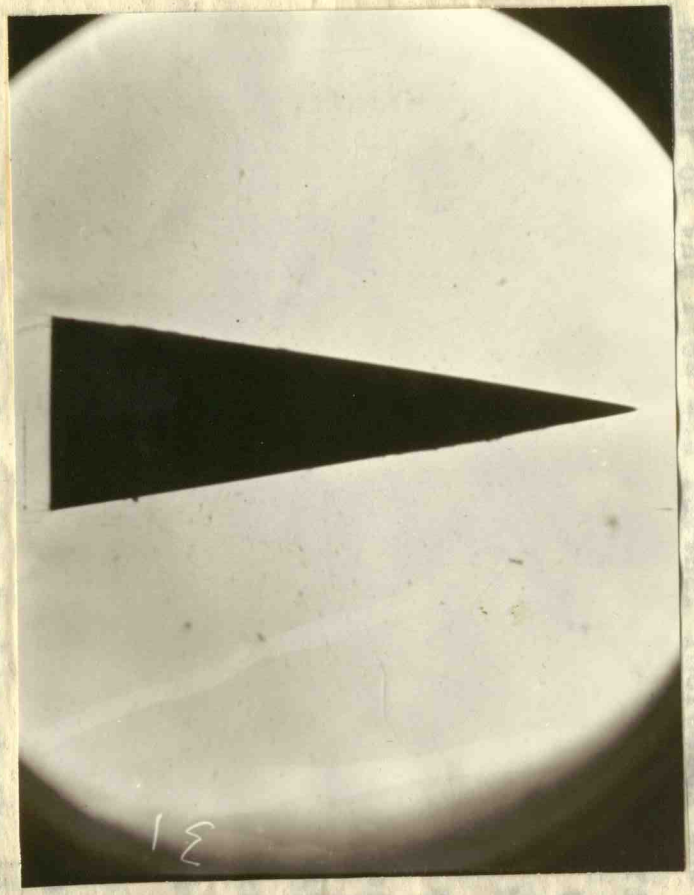

FIGURE 32
Round Number 31
Aluminum Wedge 18 1/2-Degrees
M_{PS} = 1.12
Time After Primary Shock
Wave Passage = 700 Microseconds

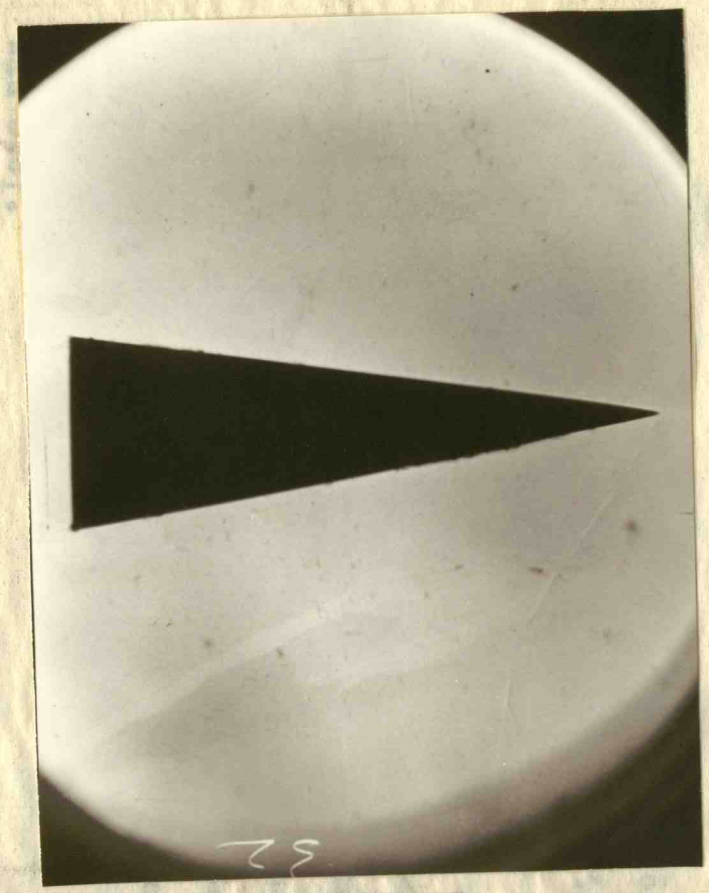

FIGURE 33
Round Number 32
Aluminum Wedge 18 1/2-Degrees
M_{PS} = 1.12
Time after Primary Shock
Wave Passage = 900 Microseconds

FIGURE 23
Bound Number 23
Aluminum Weld Splatters-Defects
Time after Etch
Knoop Microhardness - 200 Kg
Ave Response = 0.0

FIGURE 24
Bound Number 24
Aluminum Weld Splatters-Defects
Time After Etch
Knoop Microhardness - 200 Kg
Ave Response = 0.0

can be determined from the following equation if the area at the model location is known and if the presented area of the model is known.

$$\frac{A_{model}}{A_{throat}} = 1 - \frac{1.728\,M_{CH}}{(1+0.2M_{CH}^2)^3} \qquad \text{(VI - 2)}$$

A derivation of the equation may be found in Appendix VI. The wedge used for these experiments had a presented area in cross section of 1.840 square inches. The shock tube cross sectional area was 11.270 square inches. The indicated Mach number at which choking occurred in this duct was 0.67.

When the critical speed, Mach 0.67 of the model, is exceeded a shock wave formed on the model. As the Mach number of the flow was further increased the shock extended from the model through the flow stream and finally reached the top and bottom walls of the tube. M_{ch}, the wind tunnel choking Mach number, is defined as the flow Mach number at which the shock wave extended completely across the tunnel at the model. When this occurred, essentially sonic speed existed at the model location. At velocities above the choking Mach number the tunnel acted like a nozzle rather than a wind tunnel and any aerodynamic data taken in this range were questionable.

Figure 30 shows a lambda shock wave attached to the model. Figure 31 shows the lambda shocks slightly more

can be determined from the following equation if the area at the model location is known and if the presented area of the model is known.

$$\frac{A_{model}}{A_{throat}} = 1 - \frac{1.728\,M_{ch}}{(1+0.2M_{ch}^2)^3} \qquad (VI - 2)$$

A derivation of the equation may be found in Appendix VI. The wedge used for these experiments had a presented area in cross section of 1.340 square inches. The shock tube cross sectional area was 11.270 square inches. The indicated Mach number at which choking occurred in this duct was 0.67.

When the critical speed, Mach 0.67 of the model, is exceeded a shock wave formed on the model. As the Mach number of the flow was further increased the shock extended from the model through the flow stream and finally reached the top and bottom walls of the tube. M_{ch}, the wind tunnel choking Mach number, is defined as the flow Mach number at which the shock wave extended completely across the tunnel at the model. When this occurred, sonic speed existed at the model location. At velocities above the choking Mach number the tunnel acted like a nozzle rather than a wind tunnel and any aerodynamic data taken in this range were questionable.

Figure 30 shows a lambda shock wave attached to the model. Figure 31 shows the lambda shocks slightly more

developed. Figure 32 shows the lambda shocks fully developed, and with Figure 33 the shocks have widened out further to reach the top and bottom walls of the shock tube. The bow wave will probably detach from the leading edge of the wedge. If the glassed sides of the tube could be viewed from top to bottom this could easily be seen in its entirety. In all of these pictures the expansion region at the corners of the wedge can be seen.

Observation of rapid choking of the shock tube. Several shadowgraph pictures were made of a large wedge with 90 degrees included angle. Figure 34 shows the primary shock wave just past the tip of the wedge and the reflection taking place from this blunt object. In Figure 35 the primary shock wave has passed and the reflected and detached wave is well along toward choking the shock tube. The wake trailing out from the rear of the wedge can also be seen. With this wedge the shock tube will choke at about Mach 0.35.

Aerodynamic experiments with the NACA 0009 airfoil. An NACA 0009 airfoil model of aluminum 3 inches long was mounted in the test section. Rubber gaskets were used between the model and the glass. It was hoped that the critical flow Mach number might be found but due to the limitations of shadowgraph photography it could not be

developed. Figure 32 shows the lambda shocks fully develop-
ed, and with Figure 33 the shocks have widened out further
to reach the top and bottom walls of the shock tube. The
bow wave will probably detach from the leading edge of
the wedge. If the glassed sides of the tube could be
viewed from top to bottom this could easily be seen in
its entirety. In all of these pictures the expansion
region at the corners of the wedge can be seen.

Observation of rapid choking of the shock tube.

Several shadowgraph pictures were made of a large wedge
with 90 degrees included angle. Figure 34 shows the pri-
mary shock wave just past the tip of the wedge and the
reflection taking place from this blunt object. In Figure
35 the primary shock wave has passed and the reflected
and detached wave is well along toward choking the shock
tube. The mole trailing out from the rear of the wedge
can also be seen. With this wedge the shock tube will
choke at about Mach 0.35.

Aerodynamic experiments with the NACA 0009 airfoil.

An NACA 0009 airfoil model of aluminum 3 inches long was
mounted in the test section. Rubber gaskets were used
between the model and the glass. It was hoped that the
critical flow Mach number might be found but due to the
limitations of shadowgraph photography it could not be

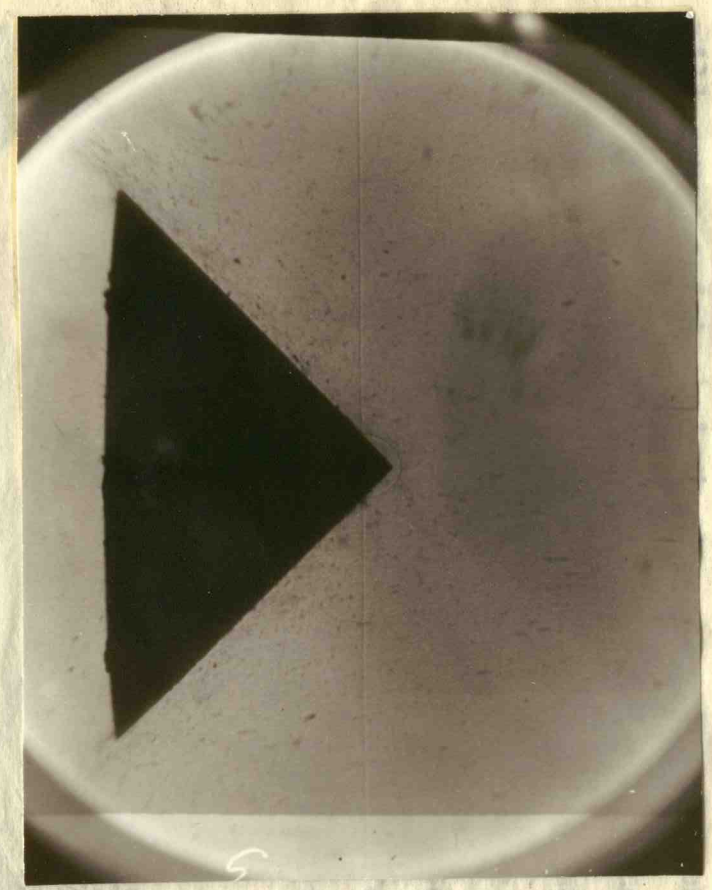

FIGURE 34
Round Number 3

M = 1.20
Primary Shockwave

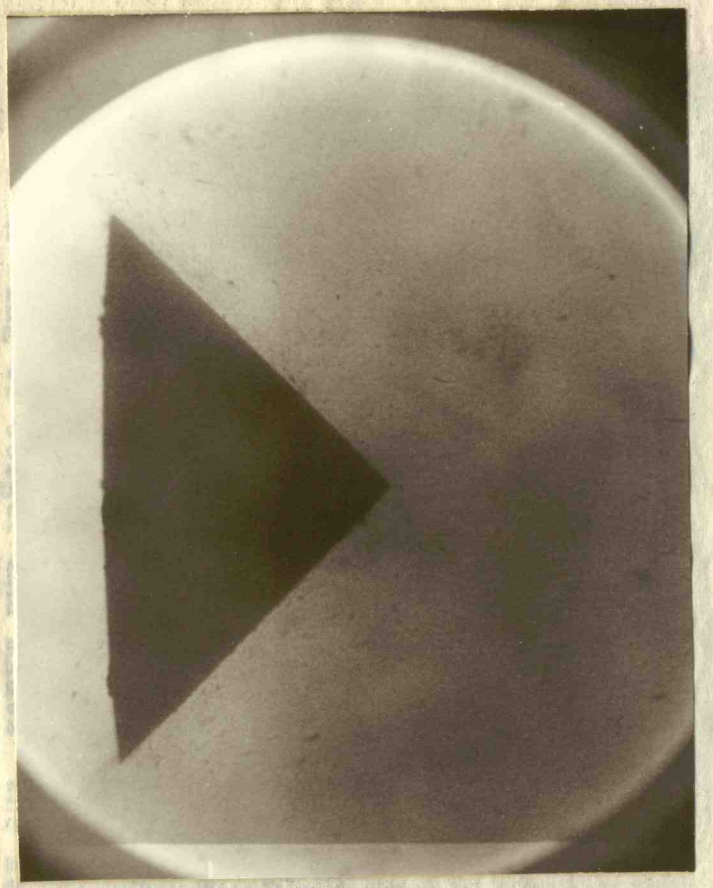

FIGURE 35
Round Number 4

M = 1.20
100 Microseconds after the
Primary Shockwave

FIGURE 14
Round Number 3
M = 1.50
Primary Shockwave

FIGURE 15
Round Number 4
M = 1.50
700 Microseconds after the Primary Shockwave

determined.

The continual changing of conditions due to flow disturbances in the shock tube make it necessary to make all angle measurements as close as possible to the model where the flow has stabilized. Figures 36 and 37 show the relatively fixed position of the detached shock wave and the changing position and shape of the shock wave further out from the model. Experimental tests were made at both subsonic and supersonic flow velocities to view effects on the model.

According to Geiger and Mautz[4] the study of the detached shock wave can be put on a quantitative basis. For Mach numbers greater than unity a blunt-nosed model will cause a detached shock wave. The detached shock wave in the shock tube originates at the time when the primary shock wave reaches the nose of the model and proceeds against the flow reaching a stationary limiting position. This is true providing that the tube does not become choked. The distance from the most forward part of the wave to the model can be measured on the film and plotted as a function of time.

---

[4] F. W. Geiger and C. W. Mautz, The Shock Tube as An Instrument for the Investigation of Transonic and Supersonic Flow Patterns, (Engineering Research Institute, University of Michigan, Ann Arbor, Mich.) pp. 110-116.

determined.

The continual changing of conditions due to flow disturbances in the shock tube make it necessary to make all angle measurements as close as possible to the model where the flow has stabilized. Figures 36 and 37 show the relatively fixed position of the detached shock wave and the changing position and shape of the shock wave further out from the model. Experimental tests were made at both subsonic and supersonic flow velocities to view effects on the model.

According to Geiger and Mautz[4] the study of the detached shock wave can be put on a quantitative basis. For Mach numbers greater than unity a blunt-nosed model will cause a detached shock wave. The detached shock wave in the shock tube originates at the time when the primary shock wave reaches the nose of the model and proceeds against the flow reaching a stationary limiting position. This is true providing that the tube does not become choked. The distance from the most forward part of the wave to the model can be measured on the film and plotted as a function of time.

---

[4] W. Geiger and C. W. Mautz, The Shock Tube as An Instrument for the Investigation of Transonic and Supersonic Flow Patterns, (Engineering Research Institute, University of Michigan, Ann Arbor, Mich.) pp. 110-116.

FIGURE 36
Round Number 207
M = 1.20
Angle of Attack - 0°
Delay Time - 2175 Microseconds

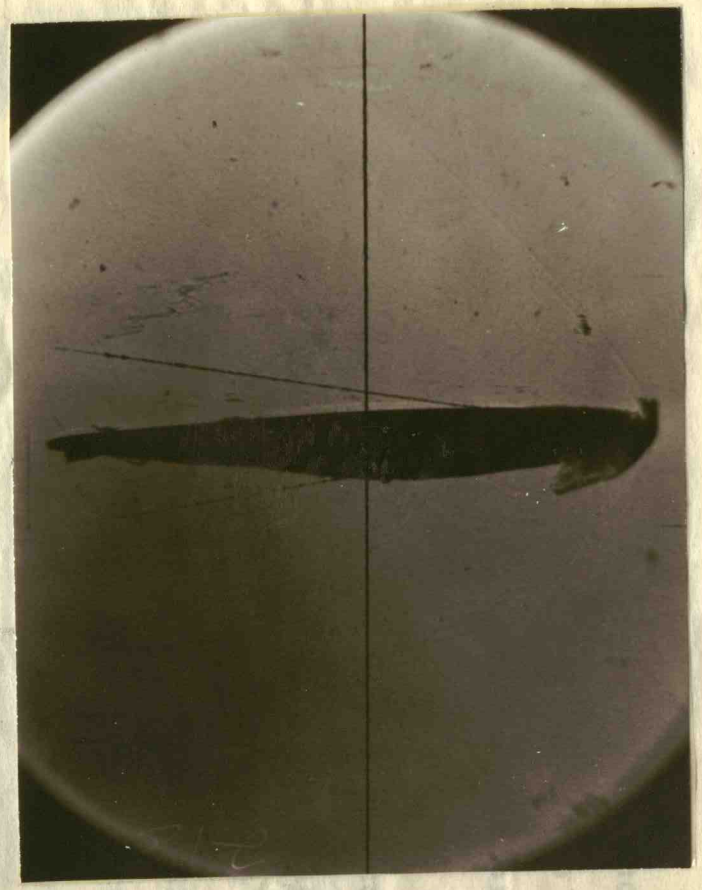

FIGURE 37
Round Number 213
M = 1.15
Angle of Attack - 0°
Delay Time - 2540 Microseconds

FIGURE 37
Mach Number 1.75
M = 1.75
Angle of Attack - 0°
Delay Time - 2540 Microseconds

FIGURE 38
Mach Number 1.50
M = 1.50
Angle of Attack - 0°
Delay Time - 2175 Microseconds

A detached wave also occurs in the shock tube when flow is subsonic. Then it moves against the flow, becoming weaker as it moves. In this case no equilibrium position is reached.

Figures 38 and 39 show a detached shock wave in a supersonic flow. Figure 38 shows the detached shock wave at 2175 microseconds and Figure 39 shows the detached shock at 2540 microseconds. The pictures were taken about 365 microseconds apart. The detached shock wave is stable.

Figures 40 and 41 show the 0009 airfoil at zero degrees angle of attack. The primary shock wave has passed in both pictures. Figure 40 was taken about 100 microseconds after passage of the primary shock wave and Figure 41 about 365 microseconds after the primary shock wave had passed. Both shadowgraphs were taken at Mach 0.98. The wake can be seen as well as the detached shock waves. In all of the above figures considerable distortion may be seen around the airfoil due to the pressure forcing the rubber gasket to work out around the edges of the model. Cellophane also became lodged against the rubber gaskets and satisfactory measurements of the detached shock wave were not possible. This method of mounting the model was abandoned following this series of pictures. Figure 42 shows the 0009 airfoil with an angle of attack of 4 degrees. The shock was moving against the flow at a flow Mach of

A detached wave also occurs in the shock tube when flow is subsonic. Then it moves against the flow, becoming weaker as it moves. In this case no equilibrium position is reached.

Figures 38 and 39 show a detached shock wave in a supersonic flow. Figure 38 shows the detached shock wave at 2175 microseconds and Figure 39 shows the detached shock at 2540 microseconds. The pictures were taken about 365 microseconds apart. The detached shock wave is stable.

Figures 40 and 41 show the 0009 airfoil at zero degrees angle of attack. The primary shock wave has passed in both pictures. Figure 40 was taken about 100 microseconds after passage of the primary shock wave and Figure 41 about 365 microseconds after the primary shock wave had passed. Both shadowgraphs were taken at Mach 0.98. The wake can be seen as well as the detached shock waves. In all of the above figures considerable distortion may be seen around the airfoil due to the pressure forcing the rubber gasket to work out around the edges of the model. Oscillophone also became lodged against the rubber gaskets and satisfactory measurements of the detached shock wave were not possible. This method of mounting the model was abandoned following this series of pictures. Figure 42 shows the 0009 airfoil with an angle of attack of 4 degrees. The shock was moving against the flow at a flow Mach of

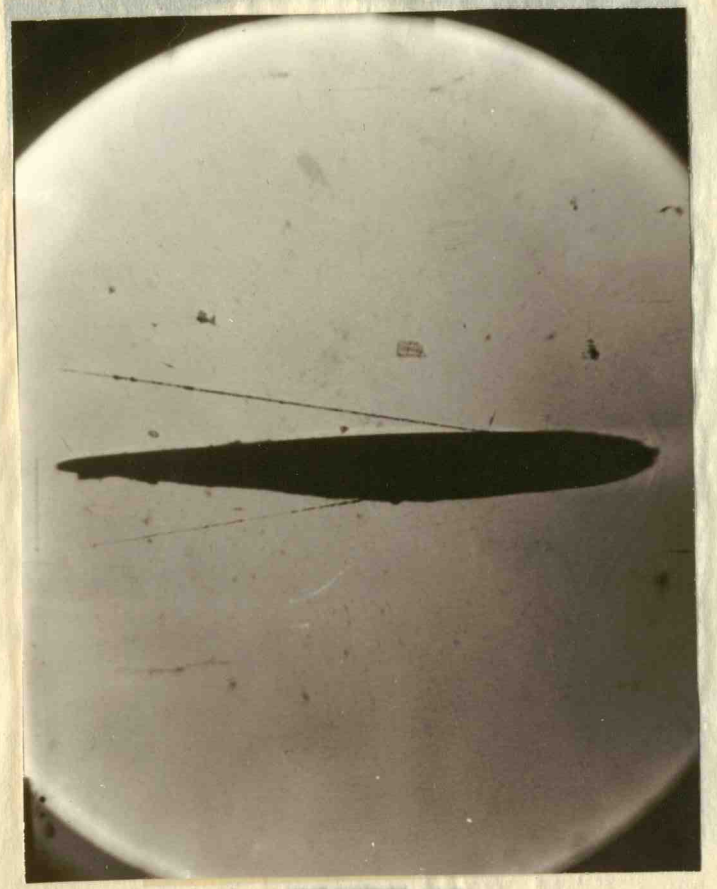

FIGURE 38
Round Number 210
M = 1.10
Angle of Attack = 0°
Delay Time - 2175 Microseconds

FIGURE 39
Round Number 214
M = 1.10
Angle of Attack = 0°
Delay Time - 2540 Microseconds

FIGURE 38
Round Number 210
M = 1.70
Angle of Attack = 0°
Delay Time - 2575 Microseconds

FIGURE 39
Round Number 574
M = 1.70
Angle of Attack = 0°
Delay Time - 3240 Microseconds

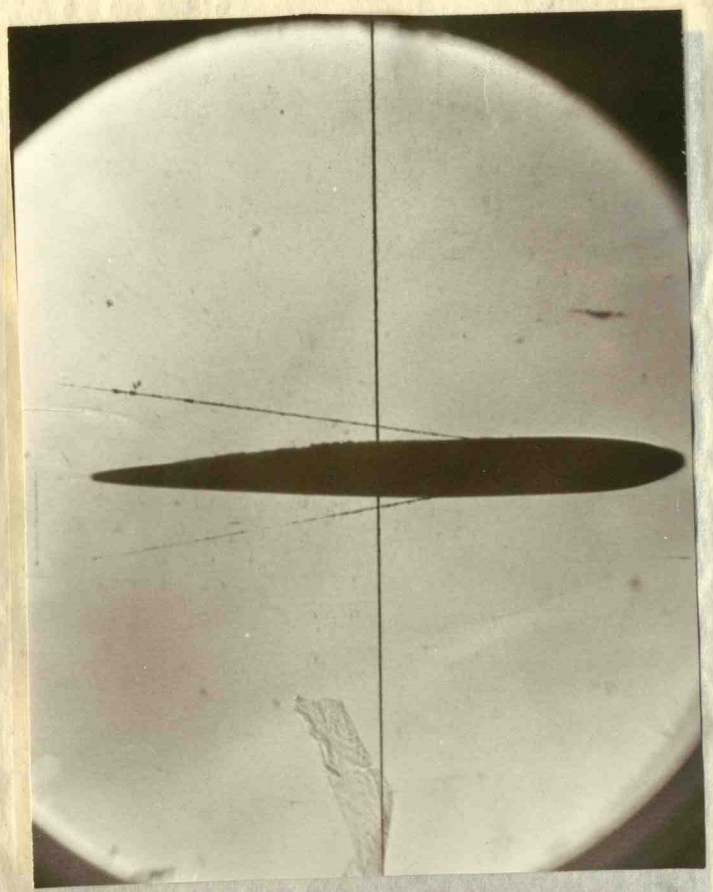

FIGURE 40
Round Number 219
M = 0.98
Angle of Attack = 0°
Delay Time - 2175 Microseconds

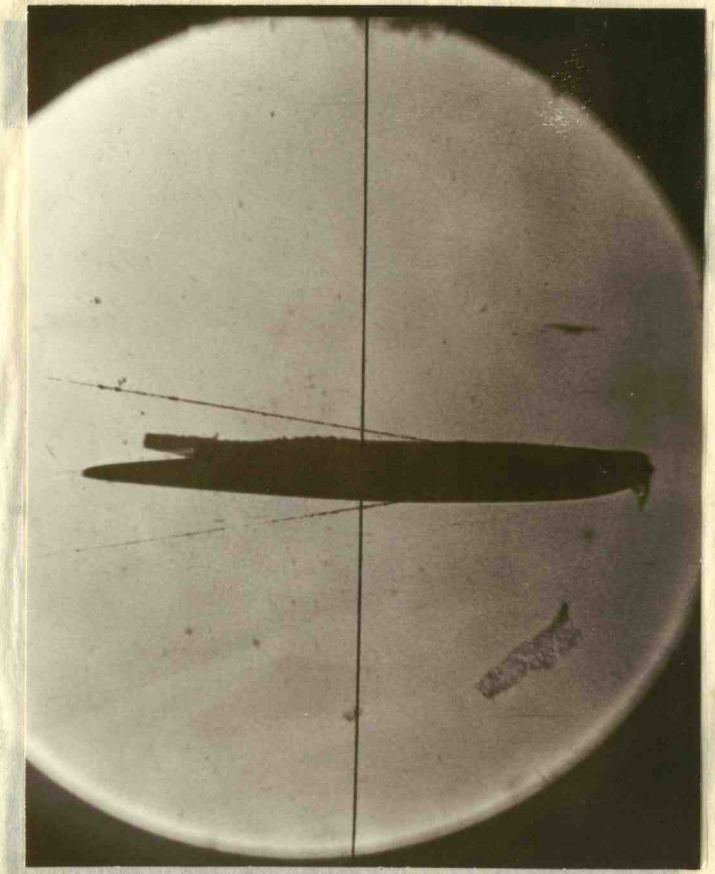

FIGURE 41
Round Number 224
M = 0.98
Angle of Attack = 0°
Delay Time - 2540 Microseconds

FIGURE 43

Boundary Number 554

M = 0.80

Angle of Attack = 0°

Delta Time - 0.5 Microseconds

FIGURE 44

Boundary Number 555

M = 0.80

Angle of Attack = 0°

Delta Time - 0.5 Microseconds

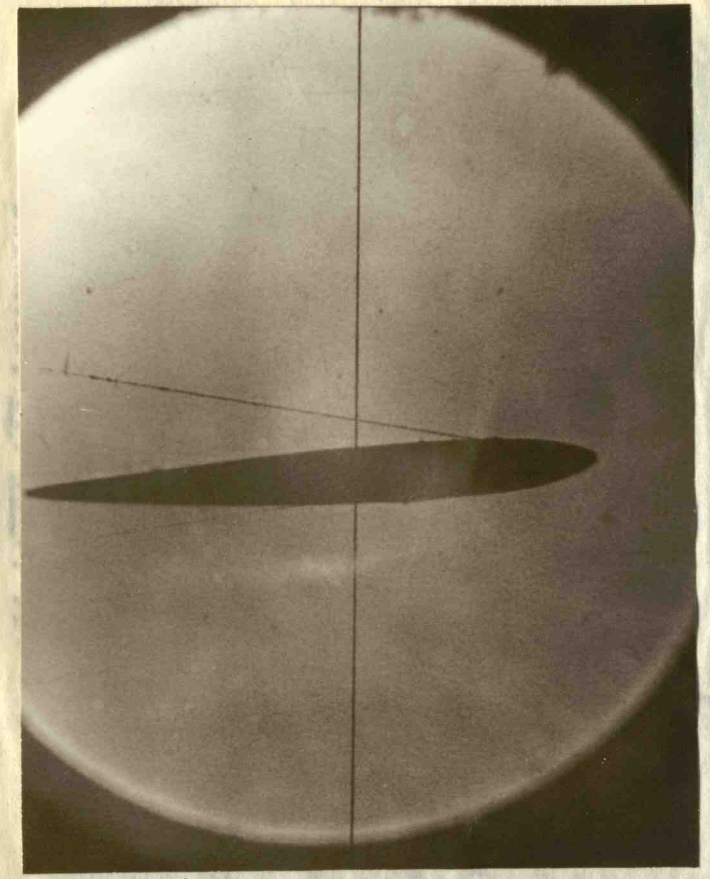

FIGURE 42
Round Number 229
M = 0.87
Angle of Attack = 4°
Delay Time - 3100 Microseconds

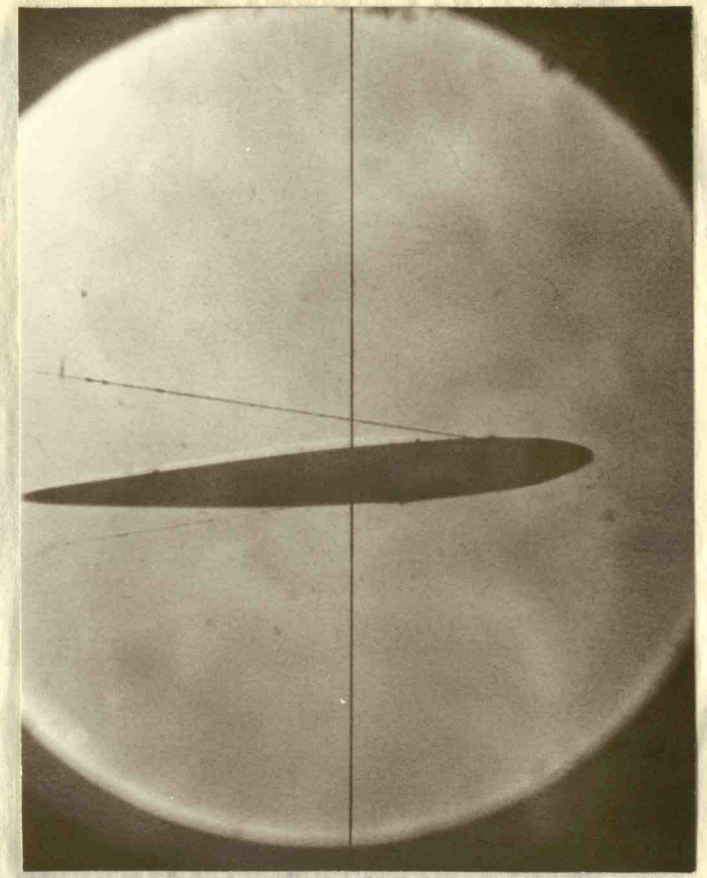

FIGURE 43
Round Number 227
M = 1.02
Angle of Attack = 4°
Delay Time - 2540 Microseconds

FIGURE 43

Round Number 152

M = 7.05

Angle of Attack = 4°

Delay Time - 2560 Microseconds

FIGURE 44

Round Number 250

M = 0.87

Angle of Attack = 4°

Delay Time - 3700 Microseconds

0.87. Figure 43 shows the 0009 airfoil with an angle of attack of 4 degrees and a flow Mach of about 1.02. The detached shock wave became stabilized at its position after 500 microseconds flow.

Transonic flow around an airfoil.[5] The transonic region of airflow is between the subsonic and supersonic regions. It begins when some point on the airfoil surface attains supersonic speed, and ends when the complete flow pattern is supersonic.

Figure 44 is a shadowgraph of flow at about Mach .81 and there should have been some indication of a supersonic region on the upper surface of the airfoil since there was a 4 degree angle of attack. The density of the air, however, may not have been sufficient to photograph satisfactorily.

Figure 45 shows the flow at about Mach 0.90 and although there is no indication on the upper surface, a shock can be seen extending from the lower surface near the rear of the airfoil. Probably most of the upper surface is subjected to supersonic flow.

Figure 46 shows the effect of supersonic flow. The flow Mach is 1.05 at zero degrees angle of attack and a

---

[5] Dwinnell, op. cit., pp. 190-195.

0.87. Figure 43 shows the 0009 airfoil with an angle of attack of 4 degrees and a flow Mach of about 1.02. The detached shock wave became stabilized at its position after 500 microseconds flow.

Transonic flow around an airfoil.[5] The transonic region of airflow is between the subsonic and supersonic regions. It begins when some point on the airfoil surface attains supersonic speed, and ends when the complete flow pattern is supersonic.

Figure 44 is a shadowgraph of flow at about Mach .81 and there should have been some indication of a supersonic region on the upper surface of the airfoil since there was a 4 degree angle of attack. The density of the air, however, may not have been sufficient to photograph satisfactorily.

Figure 45 shows the flow at about Mach 0.90 and although there is no indication on the upper surface, a shock can be seen extending from the lower surface near the rear of the airfoil. Probably most of the upper surface is subjected to supersonic flow.

Figure 46 shows the effect of supersonic flow. The flow Mach is 1.05 at zero degree angle of attack and a

---

[5] Dwinnell, op. cit., pp. 190-192.

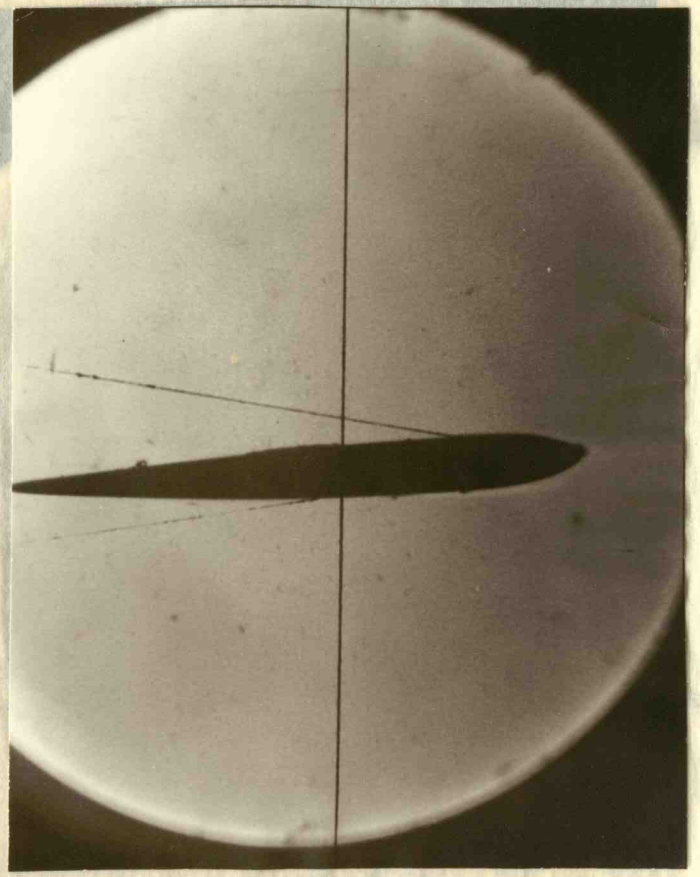

FIGURE 44
Round Number 236
Mach 0.81
Angle of Attack = 4°
Delay Time - 2740
Microseconds

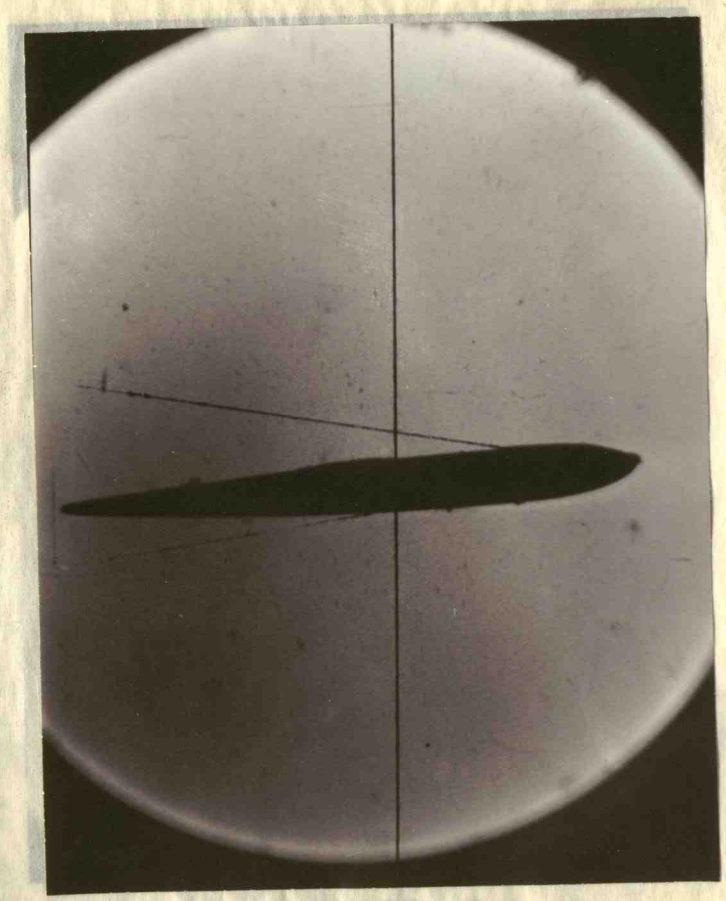

FIGURE 45
Round Number 237
Mach 0.90
Angle of Attack = 4°
Delay Time - 2920 Microseconds

FIGURE 45
Bounce Number 251
Mach 0.80
Angle of Attack = 4°
Delay Time - 3360 Microseconds

FIGURE 46
Bounce Number 252
Mach 0.81
Angle of Attack = 4°
Delay Time - 3340 Microseconds

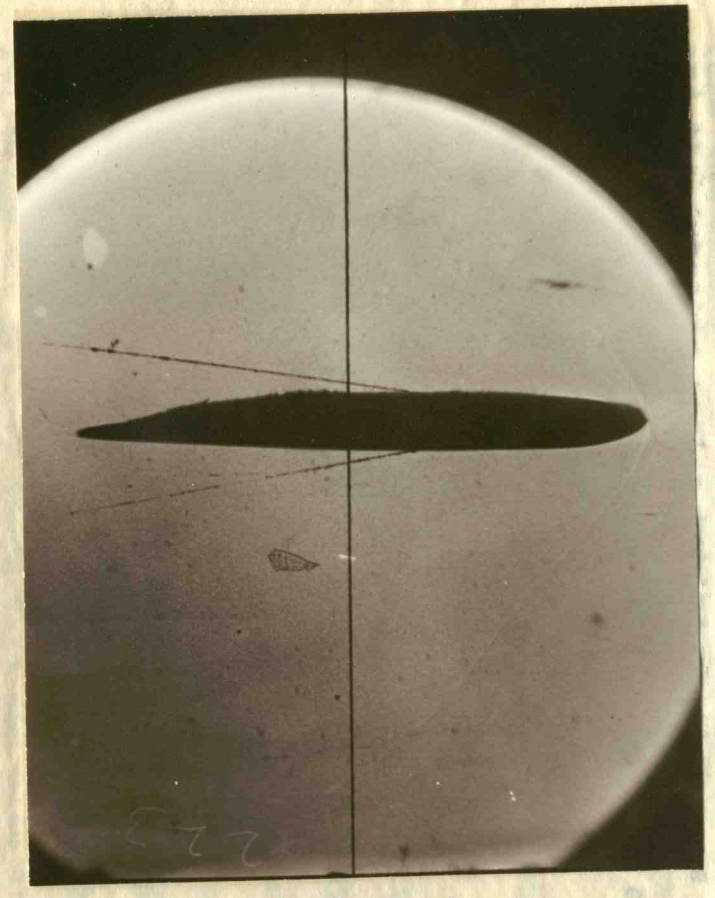

FIGURE 46
Round Number 222
Mach 1.02
Angle of Attack = 0°
Delay Time - 2540 Microseconds

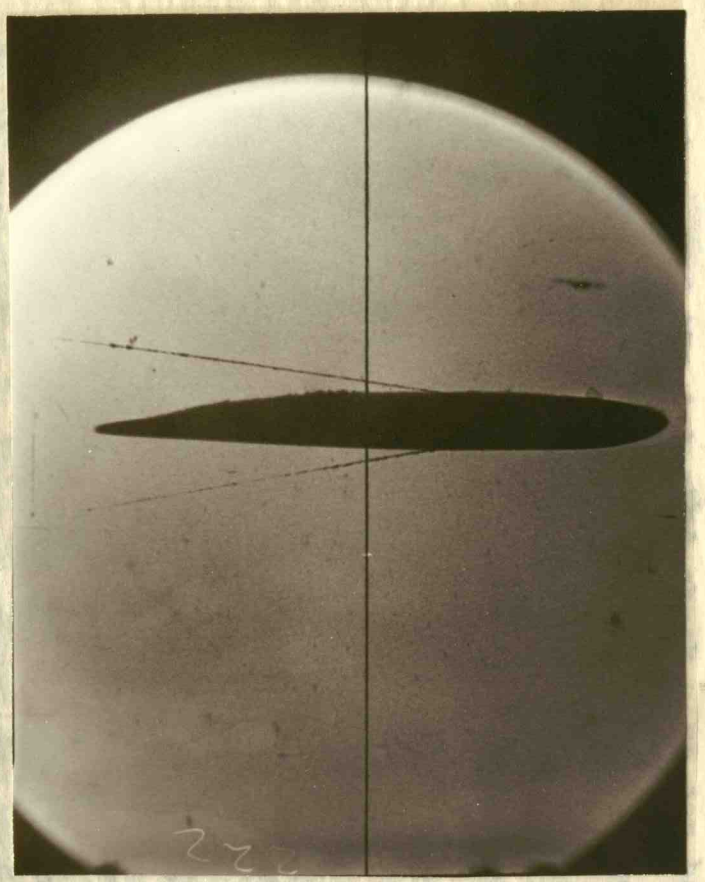

FIGURE 47
Round Number 223
Mach 1.14
Angle of Attack = 0°
Delay Time - 2540 Microseconds

FIGURE 46
Bound Number 555
Mod 1.05
Angle of Attack = 0°
Delay Time - 2540 Microseconds

FIGURE 47
Bound Number 553
Mod 1.14
Angle of Attack = 0°
Delay Time - 2540 Microseconds

mere trace of the detached shock wave can be seen while the shock fanning out from the trailing edge of the airfoil is clearly seen. There is a range behind the weak bow wave in which flow is subsonic. This range blends into a supersonic region over most of the airfoil to the trailing shock wave.

Figure 47 shows the flow at about Mach 1.14. At this Mach flow the bow wave approaches the leading edge of the airfoil, and the subsonic area following the bow wave is reduced. The position of the bow wave with respect to the leading edge and the extent of the subsonic region depend somewhat upon the shape of the leading edge. With a sharp leading edge, the bow wave may become attached and the subsonic region behind the bow wave may shrink to zero. The Mach number at which attachment occurs depends upon the wedge angle of the leading edge.

CHAPTER VII

SUMMARY OF RESULTS

In this investigation the flow in the cold gas behind the contact surface was found to follow the theory within 10 per cent up to Mach 2.00. Beginning at pressure ratios of 50 and above the flow became erratic. It appears possible that the test section was too close to the diaphragm for a full development of steady flow. No investigation of this phenomena was made.

The flow following the primary shock wave and before the contact surface had arrived was investigated. Over the range covered, the flow velocity was within 5 per cent of that predicted. This range was extremely limited, however, being between Mach 1.10 and 1.15. Above the Mach 1.15 no shadowgraph pictures could be obtained, probably because the density of the air in the channel section of the shock tube was not sufficient to show up in a shadowgraph study. The duration of the flow in this range of Mach 1.10 to 1.15 was found to be only about 300 microseconds instead of the predicted 800 microseconds.

A velocity calibration was made in the flow region following the primary shock wave and also in the flow region following the contact surface. A 3 degree wedge

made of hardened steel was used in both investigations. The difference between the predicted Mach flow and the actual measured flow in the region following the primary shock wave did not exceed 5 per cent. The variation was more pronounced in the flow region following the contact surface where the difference was as high as 10 per cent, but this region was usable only with flows up to Mach 1.75.

The measured Mach flow was always below the predicted Mach flow. This may have been caused by a failure of the diaphragm to burst instantaneously or by attenuation from the wall boundary layer of the shock tube. Either, or a combination of the two, could cause this reduction from the theoretical. No attempt was made to determine the cause. Following the contact surface the Mach flow was 16 per cent below the predicted Mach flow of 2.44, and seemed to attenuate rapidly as the delay time was increased. It is possible that this attenuation was due to lack of time for proper development of the flow at this pressure ratio of 100. Attenuation was slight at Mach 1.75 at a pressure ratio of 40. This will bear further investigation.

In tests made on the 3-degree steel wedge an agreement of 2 per cent was found in the measured bow wave angle and the Mach angle formed by a striation on the wedge. Local velocity is in agreement with the theory. A striation

formed by cellophane tape 1 1/2 thousandths thick was sufficient to give an excellent indication of local velocity.

Mach configurations over the NACA 0009 airfoil could be studied and its operation predicted. However, in the flow region following the primary shock wave there was apparently not enough density change of the air to make satisfactory measurements of the critical Mach number.

CHAPTER VIII

CONCLUSIONS AND RECOMMENDATIONS

The shadowgraph method of photography has definite limitations in high-speed velocity research. A change in density gradient causes the light rays to either converge or diverge, and hence produces either an increase or a decrease in light intensity on the screen. The method is not completely satisfactory unless the flow contains steep density gradients. Where weak shocks occur and density gradients are not steep enough no results may be observed. It was found that above Mach 1.18 in the flow following the primary shock wave, density was not sufficient to indicate any results.

Conclusions. The shock tube as presently available is a satisfactory test facility for limited experimentation. Flow velocities are available from sonic or Mach 1.00 to about Mach 1.75 with the shadowgraph method of observation in the flow region following the contact surface.

Triggering of the spark-delay system from the sound waves through the shock tube is satisfactory since the results were consistent and predictable.

CHAPTER VIII

CONCLUSIONS AND RECOMMENDATIONS

The spark source is satisfactory and should be usable for any shadowgraph work.

From the data taken it appears that local flow velocities may be measured on a model by use of an interrupting surface such as cellophane tape. This was used on a 3 degree wedge and satisfactory correlation resulted between readings of the bow wave and readings of the Mach wavelet angle.

Recommendations. The electronic delay, while satisfactory over the range it covered, does not have sufficient range for many of the lower pressure ratio studies and should probably be constructed for wider time coverage than from 300 to 3800 microseconds.

All other investigators studied used an optical method of triggering the delay circuits and it is possible that more consistent results might be obtained with an optical triggering system.

At all pressure ratios the mercurial manometer used for reading the pressure difference between the atmosphere and the channel was difficult to read accurately. Verniers might help but probably an oil manometer with its longer scale would be more satisfactory.

TABLE I

PRESSURE RATIO NECESSARY FOR VARIOUS SHOCK WAVE STRENGTHS

$$\frac{P_2}{P_0} = \frac{\gamma}{\left[1 - \frac{\gamma-1}{\sqrt{7(1+6\gamma)}}\right]^7} \qquad \gamma = 5 \quad \frac{P_2}{P_0} = \frac{5}{\left[1 - \frac{4}{\sqrt{7(1+30)}}\right]^7}$$

Shock Strength $\gamma = \frac{P_1}{P_0}$	Chamber Pressure / Channel Pressure $\frac{P_2}{P_0}$	Shock Strength $\gamma = \frac{P_1}{P_0}$	Chamber Pressure / Channel Pressure $\frac{P_2}{P_0}$
0.0	0.0	5.5	61.48
0.5	0.32	6.0	81.10
1.0	1.00	6.5	102.40
1.5	2.31	7.0	137.20
2.0	4.34	7.5	174.50
2.5	7.27	8.0	222.50
3.0	11.33	8.5	276.00
3.5	16.90	9.0	350.00
4.0	24.10	9.5	442.00
4.5	33.58	10.0	547.00
5.0	45.70		

TABLE II

PRESSURE RATIO NECESSARY FOR VARIOUS RATIOS OF SHOCK FRONT VELOCITIES TO THE SPEED OF SOUND IN THE GAS

$\frac{U}{a_0} = \sqrt{\frac{6\gamma+1}{7}}$ $\quad \gamma = 5 \quad \frac{P_2}{P_0} = 45.7 \quad \frac{U}{a_0} = \sqrt{\frac{30+1}{7}} = 2.105$

Chamber Pressure / Channel Pressure $\frac{P_2}{P_0}$	Primary Shock Velocity U / Velocity of Sound a_0	Chamber Pressure / Channel Pressure $\frac{P_2}{P_0}$	Primary Shock Velocity U / Velocity of Sound a_0
0.0	0.0	61.48	2.21
0.32	0.76	81.10	2.30
1.00	1.00	102.40	2.39
2.31	1.19	137.20	2.48
4.34	1.36	174.50	2.57
7.27	1.51	222.50	2.65
11.33	1.65	276.00	2.73
16.90	1.78	350.00	2.80
24.10	1.89	442.00	2.88
33.58	1.20	547.00	2.96
45.70	2.105		

TABLE II

PRESSURE RATIO NECESSARY FOR VARIOUS RATIOS OF SHOCK FRONT VELOCITIES TO THE SPEED OF SOUND IN THE GAS

Channel Pressure $\frac{P_2}{P_0}$	Velocity Behind Shock / Velocity of Sound $\frac{U_2}{a_0}$	Chamber Pressure Obtained $\frac{P_1}{P_2}$	Ratio Shock Velocity / Velocity of Sound $\frac{U_1}{a_0}$
0.0	0.0	61.49	2.21
0.32	0.76	81.10	2.36
1.00	1.00	102.40	2.59
2.71	1.25	137.20	2.86
4.54	1.36	174.50	2.97
7.27	1.51	222.30	3.09
11.33	1.65	276.00	3.25
16.90	1.78	350.00	3.36
24.10	1.89	446.00	3.48
33.50	2.00	547.00	3.56
45.70	2.105		

TABLE III

PRESSURE RATIO NECESSARY FOR VARIOUS SHOCK TUBE STRENGTHS AND PREDICTED MACH FLOWS FOLLOWING THE PRIMARY SHOCK FRONT

$$M_{PS} = \frac{5(\gamma - 1)}{\sqrt{7\gamma(\gamma+6)}} \qquad \gamma = 5 \quad M_{PS} = \frac{5 \times 4}{\sqrt{35 \times 11}} = 1.02$$

Shock Strength $\gamma = \frac{P_1}{P_0}$	Chamber Pressure / Channel Pressure $\frac{P_2}{P_0}$	Predicted Mach Flow M_{PS}	Shock Strength $\gamma = \frac{P_1}{P_0}$	Chamber Pressure / Channel Pressure $\frac{P_2}{P_0}$	Predicted Mach Flow M_{PS}
0.0	0.0	---	5.5	61.48	1.07
0.5	0.32	---	6.0	81.10	1.11
1.0	1.00	0.0	6.5	102.4	1.15
1.5	2.31	0.31	7.0	137.20	1.19
2.0	4.34	0.47	7.5	174.50	1.22
2.5	7.27	0.62	8.0	222.50	1.25
3.0	11.33	0.73	8.5	276.00	1.28
3.5	16.90	0.82	9.0	350.00	1.30
4.0	24.10	0.90	9.5	442.00	1.33
4.5	33.58	0.96	10.0	547.00	1.35
5.00	45.70	1.02			

TABLE III

PRESSURE RATIO NECESSARY FOR VARIOUS SHOCK TUBE STRENGTHS AND PREDICTED MACH FLOWS FOLLOWING THE PRIMARY SHOCK FRONT

$$M_{PS} = \frac{5(\gamma - 1)}{\sqrt{7\gamma(\gamma+6)}} \qquad \gamma = 5 \quad M_{PS} = \frac{5 \times 4}{\sqrt{35 \times 11}} = 1.02$$

Shock Strength $\gamma = \frac{P_1}{P_0}$	Chamber Pressure / Channel Pressure $\frac{P_2}{P_0}$	Predicted Mach Flow M_{PS}	Shock Strength $\gamma = \frac{P_1}{P_0}$	Chamber Pressure / Channel Pressure $\frac{P_2}{P_0}$	Predicted Mach Flow M_{PS}
0.0	0.0	---	5.5	61.48	1.07
0.5	0.32	---	6.0	81.10	1.11
1.0	1.00	0.0	6.5	102.4	1.15
1.5	2.31	0.31	7.0	137.20	1.19
2.0	4.34	0.47	7.5	174.50	1.22
2.5	7.27	0.62	8.0	222.50	1.25
3.0	11.33	0.73	8.5	276.00	1.28
3.5	16.90	0.82	9.0	350.00	1.30
4.0	24.10	0.90	9.5	442.00	1.33
4.5	33.58	0.96	10.0	547.00	1.35
5.00	45.70	1.02			

TABLE IV

PRESSURE RATIO NECESSARY FOR VARIOUS SHOCK TUBE STRENGTHS AND PREDICTED MACH FLOWS FOLLOWING THE CONTACT SURFACE

$$M_{PC} = \frac{5(\gamma-1)}{\sqrt{7(6\gamma+1)-(\gamma-1)}} \qquad \gamma = 5 \quad M_{PC} = \frac{5 \times 4}{\sqrt{7 \times 31} - 4} = 1.86$$

$$\frac{P_2}{P_0} = 45.7$$

Shock Strength $\gamma = \frac{P_1}{P_0}$	Chamber Pressure / Channel Pressure $\frac{P_2}{P_0}$	Predicted Mach Flow M_{PC}	Shock Strength $\gamma = \frac{P_1}{P_0}$	Chamber Pressure / Channel Pressure $\frac{P_2}{P_0}$	Predicted Mach Flow M_{PC}
0.0	0.0	--	5.5	61.48	2.04
0.5	0.32	--	6.0	81.10	2.25
1.0	1.00	0.0	6.5	102.40	2.45
1.5	2.31	0.28	7.0	137.20	2.65
2.0	4.34	0.59	7.5	174.50	2.84
2.5	7.27	0.75	8.0	222.50	3.04
3.0	11.33	1.05			
3.5	16.90	1.26			
4.0	24.10	1.47			
4.5	33.58	1.66			
5.0	45.70	1.86			

TABLE V

CALCULATED DATA FOR MEASURED MACH FLOW AS TAKEN FROM ONE-HALF BOW WAVE ANGLE MEASUREMENTS

$$M_m = \frac{1}{\sqrt{\sin^2\beta - \frac{0.0314 \sin\beta}{\cos(\beta - 1.5)}}} \qquad M_m = \frac{1}{\sqrt{(.866)^2 - \frac{0.0314 \times 0.866}{0.5225}}} = 1.16 \quad \beta = 60^\circ$$

One-half Bow Wave Angle β	Measured Mach Flow M_m	One-half Bow Wave Angle β	Measured Mach Flow M_m
10	6.33	50	1.35
15	4.11	55	1.26
20	3.07	60	1.19
25	2.46	65	1.16
30	2.07	70	1.11
35	1.80	75	1.10
40	1.60	80	1.10
45	1.46	85	1.17

NOTE: Fron 77 degrees on the shock wave will be detached and no measurements can be made below 1.098 Mach flow.

TABLE VI

PRESSURE RATIO -- VELOCITY CALIBRATION FOLLOWING THE PRIMARY SHOCK

Round Number	Air Temperature Deg. F.	Pressure Ratio P_2/P_0	Predicted Mach Number M_{PS}	Time After Triggering Microseconds	Bow Wave Angle Degrees	Measured Mach Number M_m	Remarks
196	95.5	39.9	1.00	2540	---	---	detached shock
201	95.0	39.8	1.00	3020	---	---	detached shock
202	95.0	39.8	1.00	2175	---	---	detached shock
206	88.5	40.0	1.00	3300	---	---	detached shock
239	89.0	135.0	1.18	2175	72	1.16	none
255	78.0	100.0	1.15	2175	70	1.13	none
270	68.0	142.0	1.19	2175	62.5	1.18	none
271	69.0	98.0	1.15	2350	69	1.13	none
280	69.0	102.0	1.17	1975	71	1.12	none

TABLE VII

VELOCITY CALIBRATION --- FOLLOWING THE CONTACT SURFACE

Round Number	Air Temperature Deg. F.	Pressure Ratio P_2/P_0	Predicted Mach Number M_{PC}	Time After Triggering Microseconds	Bow Wave Angle Degrees	Measured Mach Number M_m	Remarks
238	89.5	96	2.38	2175	32	1.90	none
239	89.0	191	2.92	2175	22	2.75	none
240	88.5	117	2.53	2175	28	2.20	none
241	89.0	130	2.60	2540	26.5	2.30	none
242	89.5	80	2.24	3100	29.0	2.05	none
243	91.0	53	1.94	3500	33.0	1.84	none
244	85.5	100	2.44	1980?	29.5	2.05	question time. appears short.
245	86.5	152	2.71	1980?	29	2.07	question time. appears short.
246	87.5	125	2.55	2360	34	1.81	none
247	89.0	70	2.13	2920	41	1.58	none
265	71.0	30	1.60	3500	46	1.46	none
266	63.0	62.3	2.05	3100	44	1.50	none

TABLE VII

VENOCAVAL OCCLUSION — FOLLOWING END CONTACT SURFACES

TABLE VII (continued)

VELOCITY CALIBRATION --- FOLLOWING THE CONTACT SURFACE

Round Number	Air Temperature Deg. F.	Pressure Ratio P_2/P_0	Predicted Mach Number M_{PC}	Time After Triggering Microseconds	Bow Wave Angle Degrees	Measured Mach Number M_m	Remarks
276	74.0	39.3	1.77	3400	36	1.74	none
277	73.5	39.3	1.77	3580	35.5	1.76	none
279	73.0	56.1	1.97	2175	32	1.92	none
288	77.0	54.4	1.96	3675	39	1.62	none
289	77.0	44.0	1.83	3675	40	1.60	none
290	77.0	24.5	1.48	3673	58	1.23	none

TABLE VII (continued)

VELOCITY CALIBRATION -- MOLDENKE FINE CONTACT DUSTACE

Run Number	Pressure Drop, P_d, in. H_2O	Velocity Head, P_v, in. H_2O	Coefficient, C	Reynolds Number, N_{Re}	Pitot Tube Assembly Type	Description
276	24.0	4.77	1.300	38	L-type	none
277	24.8	5.11	1.299	39.3	L-type	none
278	25.0	5.07	1.302	39.5	L-type	none
279	24.4	5.08	1.300	39.4	L-type	none
280	24.0	4.80	1.300	38	L-type	none
281	24.0	4.80	1.300	38	L-type	none
282	24.0	4.80	1.300	38	L-type	none
283	24.0	4.80	1.300	38	L-type	none
284	24.0	4.80	1.300	38	L-type	none
285	24.0	4.80	1.300	38	L-type	none

TABLE VIII

EARLY STRIATION FLOW MEASUREMENTS

Round Number	Air Temperature	Pressure Ratio	Predicted Mach Flow	One-half Bow Wave Angle	Measured Mach Flow	Striation Angles	Measured Mach Flow	Remarks
33	80	51.6	1.91	60	1.42	46 48 50	1.39 1.34 1.31	Flow following the contact surface.
34	80	46.7	1.86	---	---	60 56 52	1.15 1.21 1.27	Flow following the contact surface. Detached bow wave.
35	84	55.2	1.96	70	1.34	52 48 44	1.27 1.34 1.44	Flow following the contact surface.
36	84	49.7	1.90	---	---	52 48 44	1.27 1.34 1.44	Flow following the contact surface. Detached bow wave.

NOTE: Interference between Mach wavelets caused varying striation angle measurements. These results indicate the spread as measured.

TABLE VIII

BASIC STATISTICS FOR MOTIVATED WORK

| | | |

TABLE IX

EXPERIMENTAL DATA ON STRIATIONS

Round Number	Air Temperature Deg. F.	Pressure Ratio P_2/P_0	Time After Triggering Micro-seconds	Bow Wave Angle Degrees	Measured Mach Flow M_m	Mach Wavelet Angle (1/2")	Measured Mach Flow (1/2")	Mach Angle (1")	Measured Mach Flow (1")
252	72.0	167	3675	56.0	1.22	no data			
253	73.0	167	2925	58.0	1.21	no data			
254	77.0	98.2	3300	71.5	1.12	no data			
255	78.0	100.0	3850	70.0	1.13	no data			
256	79.0	24.0	3300	55.5	1.25	no data			
257	79.0	127.0	3850	27.0	2.28	no data		26.0	2.28
258	74.0	150.0	3300	30.0	2.02	no data			
259	75.0	43.0	3850	37.0	1.70	no data			
260	70.0	185	3300	33	1.86	no data			
261	71.0	185	3675	33	1.86	obscured		33.5	1.82
262	78.0	183	3300	30.5	2.03	29.5	2.03	30.0	2.00
263	77.0	183	3675	32.5	1.90	32	1.89	32.5	1.91
264	71.0	183	3675	distorted		34	1.82	not visible	
265	71.0	95.2	3500	distorted		32	1.89	32.0	1.89

TABLE IX

EXPERIMENTAL DATA ON STRIATIONS

TABLE IX (Continued)

EXPERIMENTAL DATA ON STRIATIONS

Round Number	Air Temperature Deg. F.	Pressure Ratio P_2/P_0	Time After Triggering Micro-seconds	Bow Wave Angle Degrees	Measured Mach Flow M_m	Mach Wavelet Angle (1/2")	Measured Mach Flow (1/2")	Mach Angle (1")	Measured Mach Flow (1")
266	63.0	62.3	3100	44	1.50	42	1.50	42.0	1.50
267	63.0	73.3	3100	none					
268	64.0	85.7	3100	obscured by cellophane		28.0	2.13	28.0	2.13
269	64.0	118.0	3100	27	2.25	26.0	2.28	26.0	2.28
270	68.0	142.0	2175	62.5	1.18	not enough density			
271	69.0	98.0	2350	69.0	1.13	not enough density			
272	74.0	79.8	2175	35.0	1.80	double exposure obscured			
273	74.0	91.5	1975	42.0	1.54	40.0	1.56	not enough intensity	
274	74.0	91.5	2360	44.5	1.48	42.0	1.49	42.0	1.49
275	74.0	91.5	3100	47.5	1.41	44.0	1.44	obscured	
276	74.0	39.3	3400	36.0	1.74	none			
277	73.5	39.3	3580	35.5	1.76	none			
278	73.5	56.1	1975	none					
279	73.0	56.1	2175	32.0	1.92	none			

TABLE IX (Continued)

EXPERIMENTAL DATA ON EVAPORATIONS

TABLE IX (Continued)

EXPERIMENTAL DATA ON STRIATIONS

Round Number	Air Temperature Deg. F.	Pressure Ratio P_2/P_0	Time After Triggering Micro-seconds	Bow Wave Angle Degrees	Measured Mach Flow M_m	Mach Wavelet Angle (1/2")	Measured Mach Flow (1/2")	Mach Angle (1")	Measured Mach Flow (1")
280	69.0	101.8	1975	69.0	1.13	not enough density			
281	70.0	101.8	2175	33.0	1.88	not enough density		32.0	1.89
282	71.0	101.8	2640	28.5	2.10	28.5	2.10	28.5	2.10
283	71.5	101.8	2830	34.0	1.80	not dense enough			
284	73.5	99.6	2260	32.0	1.90	not dense enough			
285	74.0	99.6	2360	32.0	1.90	32.0	1.90	not dense enough	
286	74.5	99.6	2450	32.0	1.90	not dense enough			
287	75.0	99.6	3500	35.0	1.78	35.0	1.74	not dense enough	
288	77.0	54.4	3675	39.0	1.62	not dense enough			
289	77.0	43.9	3675	40.0	1.60	40.0	1.60	40.0	1.60
290	77.0	24.5	3675	58.0	1.23	not dense enough			

TABLE IX (Continued)

EXPERIMENTAL DATA OF RUN 4

TABLE X

SHOCK TUBE CHOKING EXPERIMENTS

Round Number	Air Temperature Degrees F.	Pressure Ratio P_2/P_0	Shock Strength	Predicted Mach Number M_{PS}	Time After Triggering Microseconds	Remarks
31	89.0	77.8	5.90	1.12	695	none
32	89.0	77.8	5.90	1.12	900	none
33	89.0	77.8	5.90	1.12	300	none
34	89.0	77.8	5.90	1.12	500	none
3	79.5	60.2	5.50	1.07	0	pickup located in the center of the test window.
4	79.5	60.2	5.50	1.07	200	pickup located 6 inches behind the test window.

TABLE X

TABLE XI (Continued)

DATA ON NACA 0009 AIRFOIL EXPERIMENTS

Round Number	Air Temperature Deg. F.	Pressure Ratio P_2/P_0	Mach Flow Taken from Fig. 8	Time After Triggering Microseconds	Remarks	
207	93.5	167.0	1.20	2175	Detached shock	0 degree angle of attack
208	94.5	119.0	1.15	2175	Detached shock	0 degree angle of attack
209	94.5	96.4	1.13	2175	Detached shock	0 degree angle of attack
210	94.5	80.9	1.10	2175		0 degree angle of attack
211	95.5	159.0	1.19	2175		0 degree angle of attack
212	95.5	120.8	1.16	2540	Detached shock	0 degree angle of attack
213	98.0	97.7	1.13	2540	Detached shock	0 degree angle of attack
214	99.0	81.3	1.10	2540	Detached shock	0 degree angle of attack
215	89.0	61.1	1.05	2175	Flow some cellophane	0 degree angle of attack
216	89.0	49.1	1.01	2175	No flow indications	0 degree angle of attack
217	85.0	60.7	1.05	2175	No flow indications	0 degree angle of attack
218	86.0	55.4	1.03	2175		0 degree angle of attack
219	87.0	44.5	0.98	2175	No flow indications	0 degree angle of attack
220	88.5	50.9	1.02	2540		0 degree angle of attack

TABLE XI

DATA ON NAVY 6000 ATLAS MISSILES

TABLE XI (Continued)

DATA ON NACA 0009 AIRFOIL EXPERIMENTS

Round Number	Air Temperature Deg. F.	Pressure Ratio P_2/P_0	Mach Flow Taken from Figure 8	Time After Triggering Microseconds	Remarks
221	89.0	54.2	1.03	2540	Large cellophane 0 degree angle of attack
222	86.5	53.8	1.02	2540	None 0 degree angle of attack
223	86.5	109.0	1.14	2540	None 0 degree angle of attack
224	82.0	43.7	0.98	2540	None 0 degree angle of attack
225	82.0	37.2	0.95	2540	None 0 degree angle of attack
226	79.5	41.4	97.0	2540	Detached shock 4 degree angle of attack
227	79.5	52.7	1.02	2540	None 4 degree angle of attack
228	86.0	25.0	0.87	2540	None 4 degree angle of attack
229	86.0	25.0	0.87	3100	None 4 degree angle of attack
230	93.0	25.10	0.87	2440	Cellophane in flow stream 4 degree angle of attack
231	93.0	25.10	0.87	3675	Cellophane in flow stream 4 degree angle of attack
232	84.5	39.9	0.97	2540	Detached shock 4 degree angle of attack
233	84.0	39.9	0.97	2925	Detached shock 4 degree angle of attack
234	85.5	15.9	0.75	2540	No flow indication 4 degree angle of attack

TABLE XI (Continued)

DAYS OF MAXIMUM INTENSITY

TABLE XI (Continued)

DATA ON NACA 0009 AIRFOIL EXPERIMENTS

Round Number	Air Temperature Deg. F.	Pressure Ratio P_2/P_0	Mach Flow Taken from Figure 8	Time After Triggering Microseconds	Remarks
235	85.5	15.9	0.75	2925	No flow indication 4 degree angle of attack
236	85.5	15.9	0.75	2740	None 4 degree angle of attack
237	85.5	24.5	0.87	2920	None 4 degree angle of attack
238	89.5	96.0	1.12	2175	None 4 degree angle of attack

TABLE XI (Continued)

DATA ON MACA CODE AIRFOIL EXPERIMENTS

Round Jet Pressure Head Flow Time (Sec.)
Number Pressure Ratio Taken from Differential
Manometer Deg. P_1/P_0 Figure 8 Micromanometer
Readings

252	83.2	25.9	0.75	252	No flow interruption
254	85.3	25.8	0.75	2740	" "
257	82.2	25.8	0.81	2750	" "
258	86.0	25.8	0.75	2775	" "

BIBLIOGRAPHY

BIBLIOGRAPHY

Bleakney, Walker, D. K. Weimer, and C. H. Fletcher, "Shock Tube: A facility for investigations in fluid dynamics," Review of Scientific Instruments, 20:807-815, November, 1949.

Brinkley, S. R. Jr., and J. G. Kirkwood, "Theory of the Propagation of Shock Waves," Physical Review, 71: 606-611, May 15, 1947

Cowan, G. R. and D. F. Hornig, "The Thickness of a Shock Front in a Gas," Physical Review, 75:1294, April 15, 1949.

Dwinnell, J. H., Principles of Aerodynamics. New York: McGraw-Hill Book Company, Inc., 1949. 391 pp.

Emrich, R. J., and C. W. Curtis, "Dissipation of a Shock Traveling in a Tube," Physical Review, 77:573, February 15, 1950.

Emrich, R. J., and F. B. Harrison, "Measurements of Velocity Loss of Shocks Traveling in a Shock Tube," Physical Review, 73:1255, May 15, 1948.

Finklestein, R., "Normal Reflection of Shock Waves," Physical Review, 71:42-48, January 1, 1947.

Geiger, F. W., and C. W. Mautz, "The Shock Tube as an Instrument for the Investigation of Transonic and Supersonic Flow Patterns," Engineering Research Institute, University of Michigan, Ann Arbor, June, 1949.

Geiger, F. W., "The Shock Tube as a Tool for the Investigation of Flow Phenomena," Physical Review, 76:881, September 15, 1949.

Hollyer, R. N., "A Study of Attenuation in the Shock Tube," Engineering Research Institute, University of Michigan, Ann Arbor, July, 1953.

Lampson, C. W., "Resume' of the Theory of Plane Shock and Adiabatic Waves with Applications to the Theory of the Shock Tube," Ballistics Research Laboratory, Technical Note No. 139, Aberdeen, Maryland (1950).

Liepmann, H. W., and A. E. Puckett, Introduction of Aerodynamics of a Compressible Fluid. New York: John Wiley & Sons, Inc., 1947, 262 pp.

Lukasiewicz, J., "Shock Tube Theory and Applications," National Aeronautical Establishment, Canada, Report 15,1952.

Mautz, C. W., "Factors Affecting the Production of Steady Flow Past Models in the Shock Tube," Physical Review, 76:172, July 1, 1949.

Mautz, C. W., P. W. Geiger, and H. T. Epstein, "On the Investigation of Supersonic Flow Patterns by Means of the Shock Tube," Physical Review, 74:1872-1873, December 15, 1948.

Payman, W. and W. C. F. Sheppard, "Explosion and Shock Waves, VI," The disturbance produced by bursting diaphragms with compressed air. Proceedings Royal Society, A-186:293-321, June to September, 1946.

Rudinger, G., Note on the use of the shock tube as an intermittent supersonic wind tunnel. Physical Review, 75:1948-1949, June 15, 1949.

Sibert, H. W., High-Speed Aerodynamics. New York: Prentice-Hall, Inc., 1948, 283 pp.

Taylor, G. I., "The Air Wave Surrounding an Expanding Sphere," Proceedings Royal Society, A-186:273-292, June to September, 1946.

Weimer, D. K, C. H. Fletcher, and W. Bleakney, "Transonic Flow in a Shock Tube," Journal of Applied Physics, 20:418, April, 1949.

Witmer, E. A., V. L. Beals, Jr., and W. Herrmann, Massachusetts Institute of Technology, Aero Elastic and Structures Research, June, 1954. A summary of diaphragm test results obtained in the shock tube laboratory.

APPENDICES

The following definitions will be used whenever it is convenient:

$y \equiv \frac{P}{P_o}$ where P_o and P are the pressures ahead of and behind a shock front, respectively.

$\nu \equiv \frac{\gamma+1}{\gamma-1}$, where $\gamma \equiv \frac{C_p}{C_v}$

The numerical values of γ and ν are very nearly 1.4 and 6, respectively, when the gas under consideration is air, and these values will often be substituted into the final formula.

APPENDIX I

DEVIATION OF THE RANKINE-HUGONIOT RELATION FOR AN IDEAL GAS

The conservation laws of mass, momentum and energy, applied to the gas contained in a cylinder of unit cross section which passes through a plane, stationary shock front are:

mass: $$\rho_0 V_0 = \rho_1 V_1 \qquad \text{(AI-1)}$$

momentum: $$P_0 + \rho_0 V_0^2 = P_1 + \rho_1 V_1^2 \qquad \text{(AI-2)}$$

energy: $$\frac{1}{2} V_0^2 + C_p T_0 = \frac{1}{2} V_1^2 + C_p T_1$$

or $$V_0^2 + \frac{2\gamma}{\gamma-1}\frac{P_0}{\rho_0} = V_1^2 + \frac{2\gamma}{\gamma-1}\frac{P_1}{\rho_1} \qquad \text{(AI-3)}$$

where ρ is density, V is velocity, P is pressure, γ is the ratio of specific heats (assumed constant), and the subscripts 0 and 1 apply to the states on the upstream and downstream sides of the shock, respectively.

Division of the momentum equation by the mass or continuity equation gives

$$\frac{P_0}{\rho_0 V_0} + V_0 = \frac{P_1}{\rho_1 V_1} + V_1$$

or

$$V_0 - V_1 = \frac{P_1}{\rho_1 V_1} - \frac{P_0}{\rho_0 V_0} \qquad \text{(AI-4)}$$

and multiplication of (AI-4) by $V_0 + V_1$ gives

$$V_0^2 - V_1^2 = (V_0 + V_1)\left(\frac{P_1}{\rho_1 V_1} - \frac{P_0}{\rho_0 V_0}\right) \qquad \text{(AI-5)}$$

Equating this value of $V_0^2 - V_1^2$ to that obtained directly from the energy equation gives

$$(V_0 - V_1)\left(\frac{P_1}{\rho_1 V_1} - \frac{P_0}{\rho_0 V_0}\right) = \frac{2\gamma}{\gamma - 1}\left(\frac{P_1}{\rho_1} - \frac{P_0}{\rho_0}\right) \qquad \text{(AI-6)}$$

Making use of the continuity equation, this may be written

$$\frac{P_1}{\rho_0} - \frac{P_0}{\rho_0} + \frac{P_1}{\rho_1} - \frac{P_0}{\rho_1} = \frac{2\gamma}{\gamma - 1}\left(\frac{P_1}{\rho_1} - \frac{P_0}{\rho_0}\right)$$

or

$$\frac{1}{\rho_0}\left(P_1 - P_0 + \frac{2P_0\gamma}{\gamma - 1}\right) = \frac{1}{\rho_1}\left(P_0 - P_1 + \frac{2P_1\gamma}{\gamma - 1}\right) \qquad \text{(AI-7)}$$

from which

$$\frac{\rho_1}{\rho_0} = \frac{V_0}{V_1} = \frac{P_0 + \left(\frac{2\gamma}{\gamma-1} - 1\right)P_1}{P_1 + \left(\frac{2\gamma}{\gamma-1} - 1\right)P_0} = \frac{P_0 + \frac{\gamma+1}{\gamma-1}P_1}{P_1 + \frac{\gamma+1}{\gamma-1}P_0} = \frac{\mu\gamma + 1}{\gamma + \mu}$$

$$\frac{\rho_1}{\rho_0} = \frac{V_0}{V_1} = \frac{6\gamma + 1}{\gamma + 6} \qquad \text{(AI-8)}$$

which is the Rankine-Hugoniot relation for air.

V_0 and V_1 are velocities of flow relative to the shock front. For later reference, the transformation to a coordinate system in which the gas ahead of the shock front is stationary is affected by

$$\left.\begin{aligned} V_0 &= U \\ V_1 &= U - u \end{aligned}\right\} \qquad \text{(AI-9)}$$

where U is the velocity of the shock front and u is the velocity of flow behind the shock front. (AI-8) is then

$$\frac{U}{U\ \ u} = \frac{\mu\gamma + 1}{\gamma + \mu} = \frac{6\gamma + 1}{\gamma + 6} \qquad \text{(AI-10)}$$

from which

$$u = U\left(1 - \frac{\gamma + \mu}{\mu\gamma + 1}\right) = U\frac{(\gamma - 1)(\mu - 1)}{\mu\gamma + 1} = U\frac{(\gamma - 1)\,5}{6\gamma + 1} \qquad \text{(AI-11)}$$

APPENDIX II

DERIVATION OF PRANDTL'S RELATION $V_0 V_1 = a_{cr}^2$

If a_{cr} is the critical sound speed, defined as the value at which the sound speed and the flow speed become equal in an expansion from a reservoir, the energy equation (AI-3) may be written

$$\left.\begin{aligned} \frac{\gamma}{\gamma-1}\frac{P_0}{\rho_0} &= -\frac{1}{2}\frac{\gamma+1}{\gamma-1}a_{cr}^2 - \frac{1}{2}V_0^2 \\ \frac{\gamma}{\gamma-1}\frac{P_1}{\rho_1} &= -\frac{1}{2}\frac{\gamma+1}{\gamma-1}a_{cr}^2 - \frac{1}{2}V_1^2 \end{aligned}\right\} \qquad \text{(AII-1)}$$

from which

$$P_0 = \rho_0\left(-\frac{\gamma+1}{2\gamma}a_{cr}^2 - \frac{\gamma-1}{2\gamma}\right)$$

$$P_1 = \rho_1\left(-\frac{\gamma+1}{2\gamma}a_{cr}^2 - \frac{\gamma-1}{2\gamma}\right)$$

Putting these values for P_0, P_1 into the momentum equation (AI-2),

$$\rho_0\left(\frac{\gamma+1}{2\gamma}V_0^2 + \frac{\gamma+1}{2\gamma}a_{cr}^2\right) =$$

$$\rho_1\left(\frac{\gamma+1}{2\gamma}V_1^2 + \frac{\gamma+1}{2\gamma}a_{cr}^2\right)$$

$$\rho_0\left(V_0^2 + a_{cr}^2\right) = \rho_1\left(V_1^2 + a_{cr}^2\right)$$

APPENDIX II

DERIVATION OF PRANDTL'S RELATION $V_0 V_1 = a_{cr}^2$

If a_{cr} is the critical sound speed, defined as the value at which the sound speed and the flow speed become equal in an expansion from a reservoir, the energy equation (AII-3) may be written

$$\begin{cases} \dfrac{\gamma}{\gamma-1}\dfrac{p_0}{\rho_0} = \dfrac{1}{2}\dfrac{\gamma+1}{\gamma-1}a_{cr}^2 - \dfrac{1}{2}V_0^2 \\ \dfrac{\gamma}{\gamma-1}\dfrac{p_1}{\rho_1} = \dfrac{1}{2}\dfrac{\gamma+1}{\gamma-1}a_{cr}^2 - \dfrac{1}{2}V_1^2 \end{cases} \qquad \text{(AII-3)}$$

From which

$$p_0 = \rho_0\left(\frac{\gamma+1}{2\gamma}a_{cr}^2 - \frac{\gamma-1}{2\gamma}V_0^2\right)$$

$$p_1 = \rho_1\left(\frac{\gamma+1}{2\gamma}a_{cr}^2 - \frac{\gamma-1}{2\gamma}V_1^2\right)$$

Putting these values for p_0, p_1 into the momentum equation (AII-2),

$$\rho_0\left(\frac{\gamma+1}{2\gamma}V_0^2 + \frac{\gamma+1}{2\gamma}a_{cr}^2\right) =$$

$$\rho_1\left(\frac{\gamma+1}{2\gamma}V_1^2 + \frac{\gamma+1}{2\gamma}a_{cr}^2\right)$$

$$\rho_0\left(V_0^2 + a_{cr}^2\right) = \rho_1\left(V_1^2 + a_{cr}^2\right)$$

or, using the continuity equation (AI-1),

$$V_1\left(V_0^2 + a_{cr}^2\right) = V_0\left(V_1^2 + a_{cr}^2\right) \qquad \text{(AII-2)}$$

Solving (AII-2) for a_{cr}^2,

$$a_{cr}^2 = \frac{V_0 V_1^2 - V_0^2 V_1}{V_1 - V_0} = V_0 V_1 \qquad \text{(AII-3)}$$

APPENDIX III

DERIVATION OF THE FORMULAE FOR THE SPEED OF A SHOCK OF PRESSURE RATIO y, PROCEEDING INTO A STATIONARY GAS, AND FOR THE FLOW SPEED BEHIND THE SHOCK

The energy equation,

$$\frac{1}{2} V^2 + \frac{1}{\gamma-1} a^2 = \frac{\gamma+1}{2(\gamma-1)}$$

on division by 1/2 v^2, becomes

$$1 + \frac{2}{\gamma-1} \left(\frac{a}{V}\right)^2 \quad \frac{\gamma+1}{\gamma-1} \left(\frac{a_{cr}}{V}\right)^2 \qquad \text{(AIII-1)}$$

If v is considered the flow speed upstream of a stationary shock, as in Appendix I, this is

$$1 + \frac{2}{\gamma-1} \left(\frac{a_0}{V_0}\right)^2 = \frac{\gamma+1}{\gamma-1} \left(\frac{a_{cr}}{V_0}\right)^2$$

or

$$\left(\frac{a_{cr}}{V_0}\right)^2 = \frac{\gamma-1}{\gamma+1} \left[1 + \frac{2}{\gamma-1} \left(\frac{a_0}{V_0}\right)^2\right] = \frac{1}{\mu}\left[1 + (\mu-1)\left(\frac{a_0}{V_0}\right)^2\right] \text{(AIII-2)}$$

An alternate expression for $(a_{cr}/v_0)^2$ is obtained from the Rankine-Hugoniot relation (AI-7), and Prandtl's Relation (AII-3):

$$\frac{V_1}{V_0} = \frac{V_0 V_1}{V_0^2} = \left(\frac{a_{cr}}{V_0}\right)^2 = \frac{y+\mu}{y\mu+1} \qquad \text{(AIII-3)}$$

setting these expressions for $(a_{cr}/v_0)^2$ equal,

$$\frac{\gamma+\mu}{\gamma\mu+1} = \frac{1}{\mu}\left[1+(\mu-1)\left(\frac{a_0}{V_0}\right)^2\right] \qquad \text{(AIII-4)}$$

from which

$$\left(\frac{V_0}{a_0}\right)^2 = \frac{\gamma\mu+1}{\mu+1}$$

or, transforming to coordinates in which the medium ahead of the shock front is at rest,

$$U = a_0\sqrt{\frac{\gamma\mu+1}{\mu+1}} = a_0\sqrt{\frac{6\gamma+1}{7}} \qquad \text{(AIII-5)}$$

(AIII-5) with (AI-11) gives, for the flow speed behind the shock wave

$$u = a_0\frac{(\mu-1)(\gamma-1)}{\sqrt{(\mu+1)(\gamma\mu+1)}} \qquad \text{(AIII-6)}$$

APPENDIX IV

DERIVATION OF THE EXPRESSION FOR THE MACH NUMBER OF THE FLOW BEHIND A SHOCK WAVE WHICH MOVES INTO A STATIONARY MEDIUM

The ratio of the sound speed ahead of a shock front to that behind it is given by

$$\frac{a_0}{a_1} = \sqrt{\frac{T_0}{T_1}} = \sqrt{\frac{P_0}{P_1}\frac{\rho_1}{\rho_0}} \qquad \text{(AIV-1)}$$

By means of Equation (AI-7) this may be written

$$\frac{a_0}{a_1} = \sqrt{\frac{\gamma\mu+1}{\gamma(\gamma+\mu)}} \qquad \text{(AIV-2)}$$

With the flow speed given by Equation (AIII-6), the Mach Number is given by

$$M = \frac{u}{a_1} = \frac{u}{a_0}\frac{a_0}{a_1} = \frac{(\mu-1)(\gamma-1)}{\sqrt{(\mu+1)(\gamma\mu+1)}} \cdot \sqrt{\frac{\gamma\mu+1}{\gamma(\gamma+\mu)}}$$

$$= \frac{(\mu-1)(\gamma-1)}{(\mu+1)\gamma(\gamma+\mu)} = \frac{5(\gamma-1)}{\sqrt{7\gamma(\gamma+6)}} \qquad \text{(AIV-3)}$$

APPENDIX V

DERIVATION OF THE EXPRESSION FOR THE MACH NUMBER IN THE FLOW BEHIND THE CONTACT SURFACE IN THE SHOCK TUBE, WHEN AIR IS USED IN BOTH CHAMBERS

The sound speed in the air behind the contact surface is given by

$$a_{1c} = a_0 \left(\frac{P_1}{P_2}\right)^{\frac{\gamma-1}{2\gamma}} = a_0 \left(\frac{P_1}{P_2}\right)^{\frac{1}{\mu+1}} \qquad \text{(AV-1)}$$

From Equation (AIII-6)

$$\frac{P_0}{P_2} = \frac{1}{\gamma}\left[1 - \frac{\gamma-1}{\sqrt{(\mu+1)(\gamma\mu+1)}}\right]^{\mu+1}$$

or

$$\frac{P_0}{P_2}\gamma = \frac{P_0}{P_2}\frac{P_1}{P_0} = \frac{P_1}{P_2} = \left[1 - \frac{\gamma-1}{\sqrt{(\mu+1)(\gamma\mu+1)}}\right] \qquad \text{(AV-2)}$$

with (AV-1), this gives

$$\frac{a_{1c}}{a_0} = 1 - \frac{\gamma-1}{\sqrt{(\mu+1)(\gamma\mu+1)}} \qquad \text{(AV-3)}$$

Therefore the Mach number is given by

$$M_{\substack{\text{Predicted}\\ \text{Contact}\\ \text{Surface}}} = \frac{u}{a_{1c}} = \frac{\sqrt{\frac{(\mu-1)(\gamma-1)}{(\mu+1)(\gamma\mu+1)}}}{1 - \frac{\gamma-1}{\sqrt{(\mu+1)(\gamma\mu+1)}}} = \frac{(\mu-1)(\gamma-1)}{\sqrt{(\mu+1)(\gamma\mu+1)} - (\gamma-1)}$$

$$= \frac{5(\gamma-1)}{\sqrt{7(6\gamma+1)} - (\gamma-1)} \qquad \text{(AV-4)}$$

APPENDIX VI

DERIVATION OF THE EXPRESSION FOR THE CHOKING MACH NUMBER IN THE FLOW IN THE SHOCK

Sibert[1] developes the following equation stating that A_1 is for the flow in the tube and A_2 is for the flow at the model.

$$\frac{A_2}{A_1} = \frac{M_1}{M_2}\left(\frac{1+\frac{\gamma-1}{2}M_2^2}{1+\frac{\gamma-1}{2}M_1^2}\right)^{\frac{\gamma+1}{2(\gamma-1)}} \qquad \text{(AVI-1)}$$

for $\gamma = 1.4$

$$\frac{A_2}{A_1} = \frac{M_1}{M_2}\left(\frac{1+0.2M_2^2}{1+0.2M_1^2}\right)^3 \qquad \text{(AVI-2)}$$

M_1 becomes M_{ch} and M_2 becomes unity since the flow at the model will become unity Mach.

$$\frac{A_2}{A_1} = \frac{1.728 M_{CH}}{(1+0.2M_{CH}^2)^3} \qquad \text{(AVI-3)}$$

since the area of the model, A_m, taken from the area of the tube is equal to the area at the model

$$A_2 = A_1 - A_m$$

$$\frac{A_1 - A_m}{A_1} = \frac{1.728 M_{CH}}{(1+0.2M_{CH}^2)^3} \qquad \text{(AVI-4)}$$

$$\frac{A_m}{A_1} = 1 - \frac{1.728 M_{CH}}{(1+0.2M_{CH}^2)^3}$$

---

[1] Sibert, loc. cit., pp. 85-86.

IMPORTANT!

Special care should be taken to prevent loss or damage of this volume. If lost or damaged, it must be paid for at the current rate of typing.

Date Due

DEC 19 1956			
DEC 1 8 RECD ps		JAN 9 1968	
		JAN 7 RECD	
OCT 16'57			
OCT 25'57			
semester used		FEB 29 1968	
OCT 21 RECD		FEB 2 5 RECD	
APR 6 - 1962			
MAR - 9 RECD AB			
MAR 18 1968		JUL 1 '70	
		JUN 30 70	
MAR 14 RECD			
AUG 6 1964			
JUL 28 RECD			

PRINTED IN U. S. A.

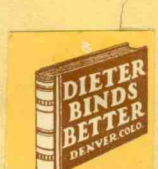
DIETER
BINDS
BETTER
DENVER, COLO.